THE EFFECTS OF NA^+/H^+ EXCHANGER REGULATORY FACTOR 1 AND TRYPSIN ON PANCREATIC DUCTAL BICARBONATE SECRETION

Petra Pallagi

Ph.D. Thesis

Supervisors: Zoltán Rakonczay Jr., M.D., Ph.D., D.Sc.
Péter Hegyi, M.D., Ph.D., D.Sc

First Department of Medicine
University of Szeged
Szeged, Hungary
2013

Articles closely related to the subject of the thesis

I. **Pallagi P**, Venglovecz V, Rakonczay Z Jr, Borka K, Korompay A, Ózsvári B, Judák L, Sahin-Tóth M, Geisz A, Schnúr A, Maléth J, Takács T, Gray MA, Argent BE, Mayerle J, Lerch MM, Wittman T, Hegyi P. Trypsin reduces pancreatic ductal bicarbonate secretion by inhibiting CFTR Cl^- channels and luminal anion exchangers. *Gastroenterology* 141:2228–2239.e6 (2011). **[IF: 11.675]**

II. **Pallagi P***, Balla Zs*, Singh AK*, Dósa S, Iványi B, Kukor Z, Tóth A, Riederer B, Liu Y, Engelhardt R, Jármay K, Szabó A, Janovszky Á, Perides G, Venglovecz V, Maléth J, Wittmann T, Takács T, Gray MA, Gácser A, Hegyi P, Seidler U, Rakonczay Z Jr. The role of pancreatic ductal secretion in protecting against acute pancreatitis in mice. *Crit Care Med* (2013). Accepted. **[IF_{2012}: 6.124].** *The first three authors contributed equally.

Articles related to the subject of the thesis

III. Hegyi P, Venglovecz V, **Pallagi P**, Maleth J, Takács T, Rakonczay Z. Galanin - a potent inhibitor of pancreatic bicarbonate secretion - is involved in the induction and progression of cerulein-induced experimental acute pancreatitis. *Pancreas* 2011, 40(1):155-6.

Number of full publications:	3
Cumulative impact factor:	17.799

TABLE OF CONTENTS

LIST OF ABBREVIATIONS

AQP	aquaporin
BAPTA-AM	1,2-bis(o-aminophenoxy)ethane-N,N,N',N'-tetraacetic acid
BCECF-AM	2'7'-bis(carboxyethyl)-5(6)-carboxyfluorescein acetoxymethyl ester
$[Ca^{2+}]_i$	intracellular Ca^{2+} concentration
cAMP	cyclic AMP
CFTR	cystic fibrosis transmembrane conductance regulator Cl^- channel
CFTRinh-172	CFTR inhibitor-172
DAPI	4',6-diamidino-2-phenylindole
DRA	down-regulated in adenoma
FURA-2-AM	5-Oxazolecarboxylic acid, 2-(6-(bis(carboxymethyl)amino)-5-(2-(2-(bis(carboxymethyl)amino)-5-methylphenoxy)ethoxy)-2-benzofuranyl)-5-oxazolecarboxylic acetoxymethyl ester
H_2DIDS	dihydro-4,4'-diisothiocyanostilbene-2,2'-disulfonic acid
$J(B^-)$	transmembrane base flux
KO	knock-out
NBC	Na^+/HCO_3^- contransporter
NHE	Na^+/H^+ exchanger
NHERF-1	NHE regulatory factor-1
PAR-2	proteinase-activated receptor-2
PAR-2-AP	PAR-2 activating peptide
PAR-2-ANT	PAR-2 antagonist
PAT-1	putative anion transporter 1
PBS	phosphate-buffered saline
PDEC	pancreatic ductal epithelial cells
PDZ	postsynaptic density-95/disc-large/zonula occludens-1
pH_i	intracellular pH
pH_L	luminal pH
RT-PCR	real-time reverse transcription polymerase chain reaction
SBTI	soybean trypsin inhibitor
SLC26	solute carrier family 26
WT	wild-type

1. INTRODUCTION

The pancreas is a unique exocrine and endocrine organ located in the retroperitoneal region of the upper abdominal cavity. The exocrine pancreas consists of two main types of cells: acinar and ductal cells. Acinar cells secrete an isotonic, NaCl-rich fluid containing a multitude of enzymes and precursor enzymes (Petersen, 2008). The protease precursors are trypsinogen, chymotrypsinogen, and procarboxypeptidases. These precursors are activated in the small intestine, initiated by conversion of trypsinogen to trypsin by the intestinal enzyme enteropeptidase. Trypsin then activates trypsinogen autocatalytically and also consequently activates other precursors (Petersen, 2008).

It was believed for a long time that the main function of pancreatic ductal epithelial cells (PDEC) is to insure mechanical frame for acinar cells. Barry Argent and his co-workers have worked out a method, which made it possible to isolate intact pancreatic ducts and PDEC (Argent et al., 1986). Thereafter, a number of publications proved, that PDEC are not only responsible for the formation a mechanical frame for the acini, but also for the HCO_3^- and fluid secretion of the pancreatic juice (Ishiguro et al., 2012). The human pancreatic ductal epithelium secretes 1-2 L of alkaline fluid daily that may contain up to 140 mM $NaHCO_3$ (Lee and Muallem, 2008; Ishiguro et al., 2012). The physiological function of this alkaline secretion is to wash toxic agents down the pancreatic ductal tree into the duodenum, and to neutralise acidic chyme entering the duodenum.

1.1. Physiology of pancreatic ductal HCO_3^- and fluid secretion

The first step of HCO_3^- secretion is the accumulation of HCO_3^- inside the cell across the basolateral membrane of the duct cell by Na^+/HCO_3^- co-transporters (NBC) and by the backward transport of protons via the Na^+/H^+ exchanger (NHE) and an H^+-ATPase (Ishiguro et al., 2012). HCO_3^- secretion across the apical membrane of PDEC is thought to be mediated by anion channels and transporters such as cystic fibrosis transmembrane conductance regulator (CFTR) and solute carrier family 26 (SLC26) anion exchangers (Ishiguro et al., 2012) (Figure 1.).

How these transporters act in concert to produce a high HCO_3^- secretion is controversial. One hypothesis is that HCO_3^- is secreted via the anion exchanger until the luminal concentration reaches about 70 mM, after which the additional HCO_3^- required to raise the luminal concentration to 140 mM is transported by CFTR (Sohma et al., 2000; Ishiguro et al., 2002). Another hypothesis is that all the HCO_3^- is secreted via the apical

SLC26 anion exchangers and CFTR functions only to activate the exchangers and to provide the luminal Cl^- required for anion exchange to occur (Ko et al., 2004).

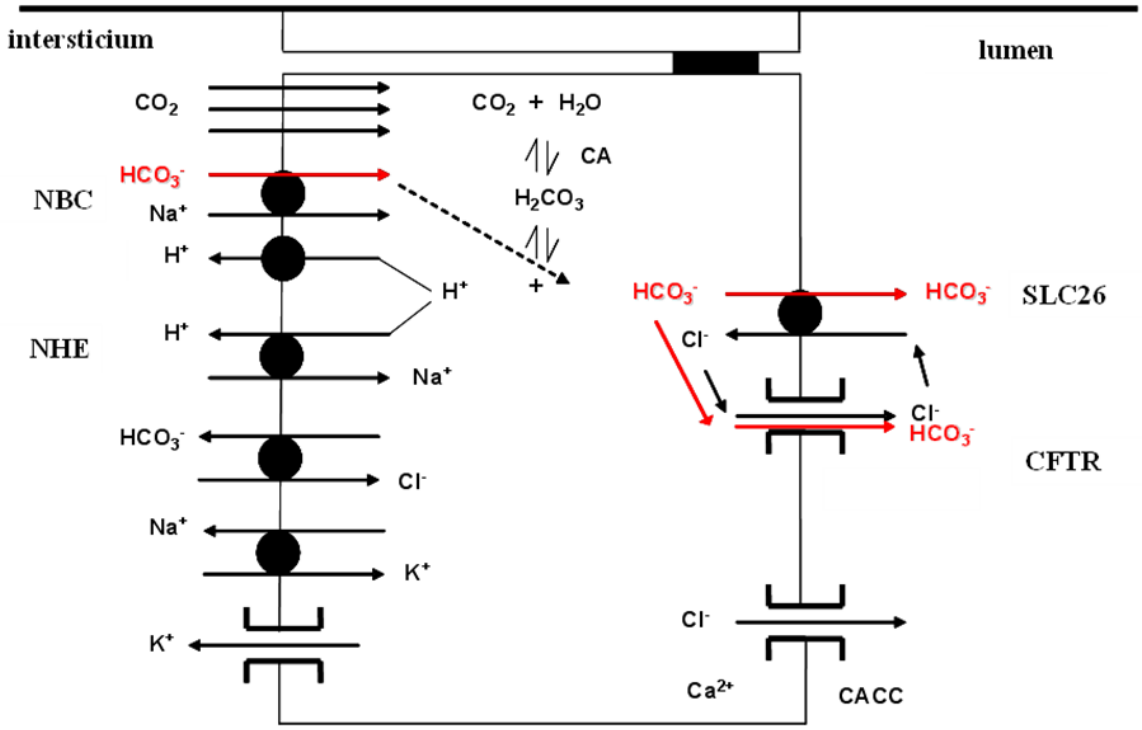

Figure 1. Schematic diagram of the ion transport systems in pancreatic ductal epihelial cells. NBC: sodium-bicarbonate contransporter; NHE: sodium-hydrogen exchanger; SLC26: solute linked carrier 26; CFTR: cystic fibrosis transmembrane conductance regulator; CACC: Ca^{2+}-activated chloride channel.

In the past it was assumed that water followed the osmotic gradient and flowed from the basolateral to the luminal side via the paracellular pathway. However, it is now clear that water transport is also mediated by the water channel aquaporins (AQP) and is a regulated process (Lee and Muallem, 2008). AQP water channels, first discovered in 1992 (Preston et al., 1992), are known to enhance the water permeabilities of a wide range of epithelia. The aquaporins are small integral membrane proteins whose six α-helical membrane spanning domains surround a highly selective aqueous pore (Verkman & Mitra, 2000). Currently, at least 10 mammalian members of the family have been identified and many show very specific tissue localisation. Immunolocalization indicates expression of AQP1 at both the basolateral and the luminal membranes and AQP5 at the luminal membrane of pancreatic duct cells (Burghardt et al., 2003).

1.1.1. Major proteins involved in pancreatic ductal HCO_3^- secretion

1.1.1.1. Cystic fibrosis transmembrane conductance regulator

CFTR, a plasma-membrane cAMP-activated Cl^- channel, is a member of the ATP binding cassette transporter superfamily. CFTR is expressed in numerous functionally diverse tissues, including the pancreas, kidney, intestine, sweat duct, heart and lung. In epithelial cells, CFTR mediates the secretion of Cl^-. In addition to its role as a secretory Cl^- channel, CFTR also regulates several transport proteins, including the epithelial sodium channel, K^+ channels, ATP-release mechanisms, anion exchangers, sodium-bicarbonate transporters, and aquaporin water channels (Guggino & Stanton, 2006).

ATP binding cassette transporters usually contain two nucleotide-binding domains, two transmembrane domains, which contain several membrane-spanning α-helices and a regulatory (R) domain that is phosphorylated by protein kinase A and C (Riordan, 2005). CFTR contains several other domains that mediate protein–protein interactions, including postsynaptic density-95/disc-large/zonula occludens-1 (PDZ)-interacting domains in the C terminus. PDZ domains consist of an 80–100 amino-acid sequence that mediates protein–protein interactions by binding to short peptide sequences, most often in the C termini of target proteins. Proteins that contain PDZ domains often contain other protein-interacting modules (such as, ezrin, radixin, moesin-binding domains and coiled-coil domains) and therefore can promote homotypic and heterotypic protein–protein interactions (Shenolikar et al., 2004). The PDZ-interacting domain of human CFTR mediates the binding of CFTR to several PDZ domain-containing proteins, including Na^+/H^+ exchanger regulatory factor isoform-1 (NHERF-1) NHERF-2, NHERF-3, NHERF-4 and CFTR-associated ligand (Brone & Eggermont, 2005; Guggino, 2004; Li & Naren, 2005). NHERF-1 is involved in numerous physiological processes, but the role of NHERF-1 in the pancreas has not yet been investigated, despite the fact that CFTR, a key regulator of epithelial functions, is controlled by this scaffolding protein (Lamprecht & Seidler, 2006).

NHERF-1 (also known as ezrin binding protein of 50 kDa, EBP50) is a scaffolding protein that is involved in the apical targeting and trafficking of several membrane proteins and anchors them to the cytoskeleton via ezrin (Lamprecht & Seidler, 2006). NHERF-1 also facilitates the association of multiprotein complexes via PDZ and ezrin, radixin, moesin-binding domains, a process that is essential for the adequate transport and function of transporters, channels, and receptors (Brone & Eggermont, 2005). The adapter protein has been shown to bind to the PDZ-binding motifs of CFTR, NHE3, as well as a number of

other proteins that functionally interact with CFTR or NHE3, such as the β_2-adrenoreceptor (Hall et al., 1998; Singh et al., 2009), or the SLC26 family anion exchanger down-regulated in adenoma (DRA, SLC26A3) (Rossmann et al., 2005). The role of NHERF-1 in the pancreas has not yet been investigated, despite the fact that CFTR, a key regulator of epithelial functions, is controlled by this scaffolding protein.

1.1.1.2. Solute carrier family 26

SLC26 isoforms are members of a large, conserved family of anion exchangers, many of which display highly restricted and distinct tissue distribution. To date, ten SLC26 genes or isoforms (SLC26A1–11) have been cloned (SLC26A10 is a pseudogene) (Ishiguro et al., 2007). These genes encode polypeptides with cytoplasmic N- and C-termini flanking a transmembrane domain of unknown structure. The C-terminal cytoplasmic region of all SLC26 proteins includes a ‘‘sulfate transporter and anti-sigma factor antagonist (STAS) domain’’, which includes the PDZ recognition motif (Aravind & Koonin, 2000). Several SLC26 isoforms function as Cl^-/HCO_3^- exchangers. These include DRA, SLC26A6 (PAT-1), SLC26A7 (PAT-2), and SLC26A9 (PAT-4). Out of these isoforms PAT-1 and DRA were detected on the apical membrane of pancreatic ducts cells and play important role in the mechanism of pancreatic ductal HCO_3^- secretion (Ishiguro et al., 2007; Ko et al., 2004).

DRA was first identified as a candidate tumor suppressor gene (Schweinfest et al., 1993). However, DRA functions as an electrogenic $2Cl^-/1HCO_3^-$ exchanger. The C-terminal PDZ recognition motif in DRA binds to PDZ domain adaptor proteins NHERF-1, NHERF-3 and NHERF-4 in lipid rafts. DRA interacts directly and functionally with CFTR. Combined overexpression of DRA and CFTR in heterologous systems revealed that each protein stimulated activity of the other through direct interaction of the DRA STAS domain with the R domain of CFTR, as well as indirectly through mediation of PDZ domain proteins (Ko et al., 2002; Ko et al., 2004).

PAT-1 was identified as a mouse kidney protein with Cl^-/formate exchange activity (Knauf et al., 2001). PAT-1 is a major apical Cl^-/HCO_3^- exchanger in the small intestine and mediates majority of prostaglandin E-stimulated HCO_3^- secretion in the duodenum (Tuo et al., 2006). On the basis of its localization in the apical membrane of the pancreatic duct and its function as a $1Cl^-/2HCO_3^-$ exchanger (Ko et al., 2002), PAT-1 has been proposed to be a major contributor to apical HCO_3^- secretion in the pancreatic duct (Greeley et al., 2001).

1.2. Pathophysiological role of pancreatic HCO_3^- secretion

Pancreatic ducts not only have prominent roles physiologically, but also pathophysiologically. Most studies of acute pancreatitis focus on the damage to acinar cells since they are assumed to be the primary target of multiple stressors affecting the pancreas. However, increasing evidence suggest that the ductal tree may have a crucial role in induction of the disease and is the primary target of stressors (Hegyi et al., 2011). Our hypothesis is that ductal secretion serves to defend the pancreas by washing out toxic agents such as bile acids, ethanol or activated trypsin. If this ductal defence mechanism is insufficient, ductal secretion will be inhibited and the harmful agents cannot leave the pancreas.

1.2.1. Toxic factors inducing pancreatitis

1.2.1.1. Bile acids

The effects of bile acids on the pancreatic ductal tree depend on the bile concentration. Non-conjugated bile acids at a concentration of 100 μM stimulate pancreatic ductal HCO_3^- secretion in a Ca^{2+} dependent manner, whereas at 1 mM concentration they damage the mitochondria, deplete intracellular ATP levels and block both the basolateral and apical ion transport mechanisms (Ignáth et al., 2009; Maléth et al., 2011; Venglovecz et al., 2008). In contrast, the conjugated glycochenodeoxycholate has a significantly smaller effect than the non-conjugated form (Venglovecz et al., 2008), suggesting that while non-conjugated bile salts (as weak acids) can pass through the cell membranes by passive diffusion, conjugated bile acids are impermeable to cell membranes and require active transport mechanisms for cellular uptake (Meier, 1995).

1.2.1.2. Ethanol

Ethanol administration itself does not induce experimental acute pancreatitis (Apte et al., 2006; Petersen & Sutton, 2006). Ethanol itself mostly only exerts modest effects on acinar cell Ca^{2+} homeostasis, even in very high concentrations, whereas a combination of alcohol and fatty acids causes massive intracellular Ca^{2+} release and intracellular trypsin activation (Criddle et al., 2004 and 2006; Gerasimenko et al., 2009; Petersen & Sutton, 2006). There is much less data available concerning the effects of ethanol and their metabolites on

pancreatic ductal cells. Interestingly, similarly to the non-conjugated bile acids, ethanol has a dual effect on pancreatic HCO_3^- secretion (Yamamoto et al., 2003). Yamamoto et al. (2003) showed that ethanol in low concentration augmented the stimulatory effect of secretin, whereas, in high concentration it inhibited the secretory rate.

1.2.1.3. Trypsin

Trypsinogen is the most abundant digestive protease in the pancreas. Under physiological conditions, trypsinogen is synthesised and secreted by acinar cells, transferred to the duodenum via the pancreatic ducts and then activated by enteropeptidase in the small intestine (Petersen, 2008). There is substantial evidence that early intra-acinar (Lerch & Gorelick, 2000; Thrower et al., 2010) or luminal (Geokas & Rinderknecht, 1974; Renner et al., 1978) activation of trypsinogen to trypsin is a key and common event in the development of acute and chronic pancreatitis. Therefore, it is crucially important to understand the effects of trypsin on PDEC.

Several studies have demonstrated that trypsin stimulates enzyme secretion from acinar cells via protease-activated receptor 2 (PAR-2) (Kawabata et al., 2006; Singh et al., 2007), whereas the effect of trypsin on PDEC is somewhat controversial. Trypsin activates ion channels in dog PDEC (Nguyen et al., 1999) and stimulates HCO_3^- secretion in the CAPAN-1 human pancreatic adenocarcinoma cell line (Namkung et al., 2003). On the other hand, the protease dose-dependently inhibits HCO_3^- efflux from bovine PDEC (Alvarez et al., 2004). The effect of trypsin differs not only among species, but also with respect to the localization of PAR-2. When PAR-2 is localized to the basolateral membrane and activated by trypsin, the result is stimulation of HCO_3^- secretion (Namkung et al., 2003; Nguyen et al., 1999). In contrast, when the receptor is localised to the luminal membrane, the effect is inhibition (Alvarez et al., 2004). Interestingly, there are no data available concerning the effects of trypsin on guinea pig PDEC which, in terms of HCO_3^- secretion, are an excellent model of human PDEC (Lee & Muallem, 2008).

2. AIMS

The main aims of this work were to investigate the physiology and pathophysiology of HCO_3^- and fluid secretion of PDEC.

Our **specific aims** were:

1. To evaluate the role of NHERF-1 in pancreatic ductal localization of CFTR, and in HCO_3^- and fluid secretion.

2. To investigate the effects of trypsin on pancreatic ductal HCO_3^- secretion.

3. MATERIALS AND METHODS

3.1. Materials

All laboratory chemicals were obtained from Sigma-Aldrich (Munich, Germany) unless indicated otherwise. Forskolin was from Tocris Bioscience (Bristol, UK), purified CLSPA collagenase was from Worthington Biochemical Corporation (Lakewood, NJ, USA). 2,7-bis-(2-carboxyethyl)-5-(and-6-)carboxyfluorescein, acetoxymethyl ester (BCECF-AM), 2-(6-(bis(carboxymethyl)amino)-5-(2-(2-(bis(carboxymethyl)amino)-5-methylphenoxy)ethoxy)-2-benzofuranyl)-5-oxazolecarboxylic acetoxymethyl ester (FURA 2-AM), dihydro-4,4'-diisothiocyanostilbene-2,2'-disulfonic acid (H_2DIDS), 1,2-bis(o-aminophenoxy)ethane-N,N,N',N'-tetraacetic acid (BAPTA-AM), Superscript III RT, Alexa Fluor 488-labelled goat anti-rabbit IgG, phalloidin-633 and SlowFade Gold antifade reagent were purchased from Invitrogen Corporation (Carlsbad, CA, USA). NucleoSpin RNA XS Total RNA Isolation Kit was from Machery & Nagel (Düren, Germany). RNeasy FFPE Kit was from QIAGEN (Hilden, Germany). High Capacity RNA-to-cDNA Kit and Power SYBR Green PCR Master Mix were from Applied Biosystems (Carlsbad, CA, USA). DirectPCR (Tail) reagent was obtained from Viagen Biotech Inc. (Los Angeles, CA, USA). MesaGreen was from Eurogentec (Seraing, Liège, Belgium). CellTak was purchased from Becton Dickinson Labware (Bedford, MA, USA). Background reducing buffer was from DAKO (Glostrup, Denmark). Tissue-freezing medium was from TissueTec O.C.T. (Sakura). Rabbit anti-NHERF-1 antibody provided by C. Yun, Emory University (Atlanta, GA, USA). Mr Pink rabbit polyclonal antibody against human CFTR provided by W.E. Balch, Scripps Research Institute (La Jolla, CA, USA). Rabbit PAR-2 polyclonal antibody was purchased from Santa Cruz Biotechnology (Heidelberg, Germany). Secondary anti-rabbit IgG antibody was purchased from Vector Laboratories (Burlingame, CA, USA). Anti- glyceraldehyde 3-phosphate dehydrogenase **(**GAPDH) antibody and secondary anti-mouse GAPDH antibody were from AbDSerotec (Düsseldorf, Germany). Laboratory chow was from Biofarm (Zagyvaszántó, Hungary). Concentrated stock solutions of forskolin (100 mM) and amiloride (50 mM) were prepared in dimethylsulfoxide. 2% stock solution of dextran was dissolved in physiological saline. PAR-2 antagonist (PAR-2-ANT, H-Phe-Ser-Leu-Leu-Arg-Tyr-NH_2) and PAR-2 activating peptide (PAR-2-AP, H-Ser-Leu-Ile-Gly-Arg-Leu-amid trifluoroacetate salt) were from

Peptides International (Louisville, Kentucky, USA). Primers were ordered from Biobasic Canada Inc (Markham, Ontario, Canada).

3.2. Ethics

All experiments were conducted in compliance with the *Guide for the Care and Use of Laboratory Animals* (National Academies Press, Eight Edition, 2011), and were approved by Committees on investigations involving animals at the University of Szeged and at the Hannover Medical School and also by independent committees assembled by local authorities.

3.3. Maintenance and genotyping of animals

The mice and guinea pigs were housed in a standard animal care facility with a 12-h light/12-h dark cycle and were allowed free access to water and standard laboratory chow. NHERF-1-deficient mice were originally generated and described at Duke University Medical Center (Shenolikar et al., 2002). NHERF-1 mutation was congenic for the FVB/N background for at least 15 generations. Genotyping of mice was performed after DNA extraction from tail samples using the DirectPCR (Tail) reagent supplemented with proteinase K. The primer sequences for genotyping NHERF-1 mice were as follows: wild-type forward, 5'-TCGGGGTTGTTGGCTGGAGAC-3'; common reverse, 5'-AGCCCAACCCGCACTTACCA-3'; knock-out (KO) forward, 5'-AGGGCTGGCACTCTGTCG-3'. Amplicons generated by PCR were 294 bp for the wild-type (WT) gene and 242 bp for the KO gene.

PAR-2 KO mice (B6.Cg-F2rl1$^{tm1Mslb/J}$) were previously generated by Schmidlin et al. (2002) and were a kind gift from Ashok Saluja.

3.4. Isolation and culture of pancreatic ducts

Mice and guinea pigs were humanly killed by cervical dislocation, the pancreas was removed and intra-/interlobular pancreatic ducts were isolated by enzymatic digestion, microdissection, and then they were cultured overnight at 37 °C in a humidified atmosphere containing 5% CO_2 as described previously (Gray et al., 1994). During overnight incubation, both ends of the isolated ducts seal and the ducts swell due to fluid secretion into the lumen.

3.5. Real-time reverse transcription polymerase chain reaction

3.5.1. mRNA expression of CFTR, PAT-1, DRA and NHERFs in mouse pancreatic ducts

Pancreatic ducts from WT and NHERF-1 KO mice were homogenized by sonication in lysis-buffer and RNA was isolated with a NucleoSpin RNA XS Total RNA Isolation Kit. Reverse transcription was performed using Superscript III RT. The primer sequences were designed with "Primer Express" (Applied Biosystems, Foster City, CA, USA). The primer sequences were:

Gene name	Primer sequence (5'- 3')	Product lenght (bp)
CFTR	TTCTTCACGCCCCTATGTCGA (forward) GCTCCAATCACAATGAACACCA (reverse)	145
DRA	TTCCCCTCAACATCACCATCC (forward) GTAAAATCGTTCTGAGGCCCC (reverse)	110
PAT-1	GGCTCCTGGGTGATCTGTTA (forward) CCAAACATAGGAGGCAATCC (reverse)	100
NHERF-1	AGATCTGCCTCCAGCGATAC (forward) TTCATTTTTCTTGCTCCAGTCC (reverse)	206
NHERF-2	TAGTCGATCCTGAGACTGATG (forward) ATTGTCCTTCTCTGAGCCTG (reverse)	173
NHERF-3	TGACGGTGTGGTGGAAATG (forward) TGGCAGTAAAGAAGTGGAGAC (reverse)	117
ß-actin	AGA GGG AAA TCG TGC GTG AC (forward) CAA TAG TGA TGA CCT GGC CGT (reverse)	138

Real-time polymerase chain reactions were carried out using MesaGreen in the Applied Biosystems 7300 Real-time PCR System. PCR extension was performed at 60 °C with 40 repeats. Data were analyzed using Sequence Detection Software 1.2.3 (Applied Biosystems) and exported to Microsoft Excel. Relative quantification was carried out using

β-actin as a reference gene.

3.5.2. mRNA expression of PAR-2 in human pancreatic tissue

RNA extraction: 15 formalin-fixed, paraffin-embedded normal pancreatic tissue samples and 15 samples of chronic pancreatitic tissue were selected for real time RT-PCR analysis. Total RNA was isolated from five 5-10 μm macrodissected sections (connective tissue excluded) using RNeasy FFPE Kit in accordance with the manufacturer's instructions. RNA concentrations were determined using NanoDrop Spectrophotometer ND-1000 (Thermo Fisher Scientific Inc., Waltham, MA, USA).

Reverse Transcription of RNA: cDNA samples were prepared from 1 μg total RNA using High Capacity RNA-to-cDNA Kit as specified by the manufacturer. Gene-specific primers were designed by AlleleID 6.01 primer design software (Premier Biosoft International, CA, USA) for real-time RT-PCR. Isoform specificity and primer sizes were checked by BioEdit biological sequence alignment editor software (Tom Hall Ibis Therapeutics, Carlsbad, CA, USA). Primer specificity was checked by BiSearch software (Hungarian Academy of Sciences, Institute of Enzymology, Budapest, Hungary). Primer specific amplification degree (58 °C) was optimized by gradient PCR. The used primer sequences:

Gene name	Primer sequence (5'- 3')	Product length (bp)	Annealing temperature (°C)
β-actin	GTACGCCAACACAGTGCTG (forward) CTTCATTGTGCTGGGTGCC (reverse)	100	55
PAR-2	GGCACCATCCAAGGAACCAATAG (forward) GCAGAAAACTCATCCACAGAAAAGAC (reverse)	128	58

RT-PCR: Real-time RT-PCR analysis was performed using SYBR Green technology on ABI Prism 7000 Sequence Detection System (Applied Biosystems), according to manufacturer's instructions. β-actin was used as the internal control gene. Primer specific amplification was controlled by 2% agarose gel electrophoresis, as well as by melting temperature analysis. The final 20 μl reaction mixture contained Power SYBR Green PCR Master Mix, 10 pM of forward and reverse primers and 100 ng cDNA as template. Amplification conditions were as follows: incubation at 95 °C for 10 min,

followed by 45 cycles at 95 °C for 15 sec, 60 °C for 60 sec and 72 °C for 15 sec, with subsequent melting analysis: heating to 95 °C for 20 sec, cooling to 45 °C for 10 sec, then reheating to 95 °C.

3.6. Immunohistochemistry

3.6.1. Localization of NHERF-1 and CFTR proteins in WT and NHERF-1 KO mice

Immunohistochemistry of the mouse pancreas was performed as described by Cinar et al. (2007) using rabbit polyclonal antibodies against NHERF-1 and CFTR. Briefly, for NHERF-1 staining, paraformaldehyde-fixed, paraffin-embedded tissue sections (5 μm) from mice of different genotypes were prepared on the same slide. After deparaffinization with xylene, sections were treated with 0.01 M sodium citrate solution at 100 °C for 10 min. For CFTR staining, pancreata were fixed in 2% paraformaldehyde in phosphate buffered saline (PBS). Fixed tissue was rinsed with PBS and transferred to 30% sucrose in PBS overnight. The tissue was embedded in tissue-freezing medium. Cryosectioning was done with a microtome cryostat at −20 °C and 10 μm thick sections were collected on microscope slides (SuperFrost Plus, Menzel-Gläser, Germany).

Pancreatic sections were incubated sequentially with PBS for 5 min, washing buffer of PBS with 50 mM NH_4Cl twice for 10 min each, background reducing buffer for 20 min and 5-10% goat serum for 30 min for blocking and incubated with rabbit anti-NHERF-1 (1:500) (Weinman et al., 1998) antibody or Mr. Pink rabbit polyclonal antibody against human CFTR (1:100) in background reducing buffer overnight at 4 °C. Washing 4 times for 5 min in the washing buffer was followed by secondary antibody (Alexa Fluor 488-labelled goat anti-rabbit IgG) incubation for 1 h at room temperature at a dilution of 1:300-1:500 in background reducing buffer. After 2-4 washes for 5 min each, in case of NHERF-1 staining, the sections were treated with 5U/ml phalloidin-633 in PBS with 1% bovine serum albumin, 0.2% Triton X-100 for 30 min which was followed by washes with washing buffer (six times). After washing, each cover slide was mounted with SlowFade Gold antifade reagent with 4',6-diamidino-2-phenylindole (DAPI), and slides were imaged on a confocal microscope (TCS SP2; Leica, Wetzlar, Germany). Excitation wavelengths used were 405, 488, and 633 nm, and emission was taken at 415–450, 490–540, and 560–700 nm for detection of DAPI, Alexa Fluor 488, and phalloidin 633, respectively.

3.6.2. Localization of PAR-2 protein in guinea pig, human and WT and PAR-2 KO mice

Pancreatic tissue from guinea pig, patients without pancreatic disease near neuroendocrine tumor (average age: 59.5, female:male: 7:8) and WT and PAR-2 KO mice were investigated. The human samples were obtained with the permission of the Regional Ethical Committee of Semmelweis University (#172/2003).

The pancreatic tissues were fixed in 10% neutral buffered formalin for 24 hours, followed by paraffin embedding, then cut and stained with hematoxylin eosin (HE) to establish the diagnosis. Paraffin embedded, 3-4 μm thick sections were used for immunohistochemistry to detect PAR-2 expression. The slides were treated for 30 minutes with target retrieval solution in a microwave oven, followed by incubation with the primary rabbit polyclonal antibody in 1:100 dilution overnight at 4 °C. Signal detection was achieved by ImPRESS reagent with secondary anti-rabbit IgG antibody (20 min). Diaminobenzidine was used to visualize immune complexes and nuclear counterstaining was performed with haematoxylin. For negative controls, the appropriate antibody was omitted and either the antibody diluent alone or isotype matched IgG serum was used. The negative controls exhibited no signal. Normal skin epithelial cells were used as positive controls to confirm correct immunohistochemical staining for PAR-2.

The immunohistochemical reactions were digitalized with a Mirax MIDI slide scanner (3DHistech Ltd., Budapest, Hungary). Relative optical (RO) density was calculated using Image J program (National Institutes of Health, Bethesda, USA). Pixel values (PV) were normalized to erythrocyte density ($PV_{Norm} = PV_{Measured} - PV_{Erythrocyte}$) in all sections. RO-density values were calculated from the RO-Density = $\log_{10}(255/PV_{Norm})$ equation assuming that the brightest value in the image equals 255.

3.7. Western blot analysis

Western blot analysis were used to determine the specificity of the PAR-2 antibody. Proteins were extracted from fresh-frozen guinea pig (n=3) and human (n=3) pancreatic tissue stored at -80 °C. Isolation was performed by using lysis buffer (20 mM TRIS pH 7.5, 150 mM NaCl, 2 mM EDTA, 1% Triton X-100 containing protease-inhibitor complex). Samples (50 mg) were homogenized, followed by centrifugation at 13,200 rpm at 4 °C for 5 min. Measurements of protein concentration were performed using Bradford-analysis (Bradford, 1976). 30 μg of protein samples were loaded in each lane, run on 10%

sodium dodecyl sulphate (SDS)-polyacrylamide electrophoresis at 200V for 35 min, then transferred to nitrocellulose membranes at 100V, 4 °C for 75 min. For aspecific protein-blocking, non-fat dry milk (5%, PBS) was used for 30 min. Blots were incubated with polyclonal PAR-2 rabbit antibody (1:300) and anti-GAPDH antibody (1:5000) at 4 °C overnight. After washing with 0.1% TRIS, horseradish peroxidise-conjugated anti-rabbit antibody (1:2000) was applied at room temperature for 90 min. Following three series of washings in Tris-Buffered Saline Tween-20, signals were visualized by enhanced chemiluninescent detection.

3.8. Solutions used for the determination of pancreatic ductal secretion in vitro

The HEPES-buffered solution contained (in mM): 130 NaCl, 5 KCl, 1 $CaCl_2$, 1 $MgCl_2$, 10 Glucose and 10 Na-HEPES and its pH was set to 7.4 with HCl at 37 °C. The standard HCO_3^--buffered solution contained (in mM): 115 NaCl, 25 $NaHCO_3$, 5 KCl, 1 $CaCl_2$, 1 $MgCl_2$, 10 Glucose. In the NH_4^+ pulse experiments in HCO_3^--buffered soultion, 20 mM NaCl was replaced with NH_4Cl. The Cl^--free HCO_3^- solution contained (in mM): 25 $NaHCO_3$, 115 Na-gluconate, 1 Mg-gluconate, 6 Ca-gluconate, 2.5 K_2-sulfate and 10 glucose. The HCO_3^--containing solutions were equilibrated with 95% O_2 and 5% CO_2 to maintain pH at 7.4 at 37 °C.

3.9. Microperfusion and measurement of intracellular pH, Ca^{2+} concentration

The microperfusion of the cultured pancreatic ducts was performed as described previously (Venglovecz et al., 2008). Briefly, two concentric pipettes were used. One end of a sealed duct was cut off and the other end was aspirated into the outer, holding pipette. Then the inner, perfusion pipette, was gently inserted into the lumen of the holding pipette while a negative pressure was applied to the holding pipette using a syringe. The duct was then perfused at a rate of 10-30 µl/min, the luminal perfusate left the duct at the open end. The high rate of the bath perfusion (5-6 ml/min), which was in the same direction as the flow of luminal perfusate, ensured that the outgoing luminal perfusate did not gain access to the basolateral surface of the duct cells. Replacement of the luminal perfusate took up to 2 min.

Intacellular pH (pH_i) was estimated using the pH-sensitive fluorescent dye 2'7'-bis(carboxyethyl)-5(6)-carboxyfluorescein acetoxymethyl ester (BCECF-AM) (Hegyi et al., 2004). Briefly, ducts were loaded with the membrane permeable acetoxymethyl derivative of BCECF (2 μmol/l) for 20-30 min. After loading, the ducts were continuously perfused with solutions at a rate of 5-6 ml/min. pH_i was measured using a Cell^R imaging system (Olympus, Budapest, Hungary). 4-5 small areas (Region of interests – ROIs) of 5-10 cells in each intact duct were excited with light at wavelengths of 490 and 440 nm, and the 490/440 fluorescence emission ratio was measured at 535 nm. One pH_i measurement was obtained per second. *In situ* calibration of the fluorescence signal was performed using the high K^+-nigericin technique (Hegyi et al., 2004).

Measurement of $[Ca^{2+}]_i$ was performed using the same method except that the cells were loaded with the Ca^{2+}-sensitive fluorescent dye 5-Oxazolecarboxylic acid, 2-(6-(bis(carboxymethyl)amino)-5-(2-(2-(bis(carboxymethyl)amino)-5-methylphenoxy)ethoxy)-2-benzofuranyl)-5-oxazolecarboxylic acetoxymethyl ester (FURA 2-AM) (5 μmol/l) for 60 min. For excitation, 340 and 380 nm filters were used, and the changes in $[Ca^{2+}]_i$ were calculated from the fluorescence ratio (F_{340}/F_{380}) measured at 510 nm.

3.10. Determination of HCO_3^- efflux in WT and NHERF-1 KO mice

To determine the HCO_3^- efflux across the apical membrane of the pancreatic ductal epithelia, we used three methods: inhibitory stop, alkali load and luminal Cl^- withdrawal. The measured rates of pH_i change (dpH/dt) were converted to transmembrane base flux [J(B^-)] using the equation: J(B^-)=(dpH/dt)xβ_{total} where β_{total} is the total buffering capacity of the cells. J(B^-) reflects the rate of HCO_3^- efflux (i.e. secretion) on luminal Cl^-/HCO_3^- exchangers (Hegyi et al., 2005).

3.11. Measurement of fluid secretion

In vitro

Fluid secretion into the closed luminal space of the cultured pancreatic ducts was analysed using a swelling method developed by Fernandez-Salazar et al. (2004). Briefly, the ducts were transferred to a perfusion chamber (0.45 ml) and were attached to a coverslip precoated with CellTak in the base of the chamber. Bright-field images were acquired at 1 min intervals using a CCD camera (CFW 1308C, Scion Corporation, Frederick, MD, USA). The integrity of the duct wall was checked at the end of each

experiment by perfusing the chamber with a hypotonic solution (HEPES-buffered solution diluted 1:1 with distilled water). Digital images of the ducts were analysed using Scion Image software (Scion Corporation, Frederick, MD, USA) to obtain values for the area corresponding to the luminal space in each image.

In vivo

Mice were anesthetized with 1.5 g/kg urethane by i.p. injection. The body temperature of mice was maintained by placing the animals on a warm pad (37 °C) during the experiments. The abdomen was opened, and the lumen of the common biliopancreatic duct was cannulated with a blunt-end 30-gauge needle. Then the proximal end of the common duct was occluded with a microvessel clip to prevent contamination with bile, and the pancreatic juice was collected in PE-10 tube for 30 min. Using an operating microscope, the jugular vein was cannulated for administration of secretin (0.75 CU/kg) and the pancreatic juice was collected for an additional 120 min.

3.12. Intravital video microscopy and data analysis

A separate experimental series was performed to assess the possible consequences of secretin treatment on the microcirculation of the pancreas in mice anaesthetized with 1.5 g/kg urethane i.p. (n=3-4 in each group). Using an operating microscope, the right jugular vein was cannulated (with polyethylene tubing ID: 0.28 mm, OD: 0.61 mm, Smiths Medical International Ltd, Kent, UK) for i.v. administration of secretin and the fluorescence marker used for the intravital microscopic examination. The animals were placed in a supine position on a heating pad to maintain the body temperature between 36 and 37 ^{o}C, and a midline laparotomy performed. The majority of the intestines were exteriorized to gain good assess to the pancreas which was carefully placed on a specially designed stage and covered with a microscopic cover slip. The rest of the exteriorized abdominal organs were also covered with Saran wrap to minimize the fluid and heat loss.

The microcirculation of the pancreas was visualized by intravital fluorescence microscopy (Zeiss Axiotech Vario 100HD microscope, 100 W HBO mercury lamp, Acroplan 20x water immersion objective) using a single i.v. bolus of fluorescein isothiocyanate-labeled dextran (150 kDa; 75 µl/animal for plasma labeling). The microscopic images were recorded with a charge-coupled device video camera (AVT HORN-BC 12; Aalen, Germany) attached to an S-VHS video recorder (Panasonic AG-MD

830, Budapest, Hungary) and a personal computer. Video images of the microcirculatory network of the pancreatic tail were recorded at baseline and 20 min after the i.v. application of secretin.

Plasma velocity in the pancreatic capillaries was assessed off-line by frame-to-frame analysis of the videotaped images, using image analysis software (IVM, Pictron Ltd., Budapest, Hungary). Average velocity values were measured in 3-5 separate capillaries per 3-5 microscopic fields in each animal.

3.13. Statistical analysis

Statistical analysis was performed by SigmaPlot (Systat Software Inc., Chicago, IL, USA). Data are presented as means ± SEM. Both parametric (one– or two-way analysis of variance) and non-parametric (Kruskal-Wallis) tests were used based on the normality of data distribution (analyzed by the Shapiro-Wilk test). Post-hoc analysis (either Dunn's or Bonferroni's test) was performed according to the recommendations made by SigmaPlot. Statistical analysis of the immunohistochemical data was performed using the Mann-Whitney U test. Probability values of $P<0.05$ were accepted as being significant.

4. RESULTS

4.1. Role of NHERF-1 in pancreatic ductal HCO_3^- and fluid secretion

4.1.1 mRNA expression of CFTR, DRA, PAT-1 and NHERFs in mouse pancreatic ducts

CFTR, DRA, PAT-1, NHERF-1 and NHERF-2, but not NHERF-3 mRNA were expressed in isolated pancreatic ducts of WT mice (Figure 2). Notably, quantitative RT-PCR indicated that NHERF-1 was expressed more abundantly than the other two CFTR-binding NHERFs (NHERF-2 and NHERF-3).

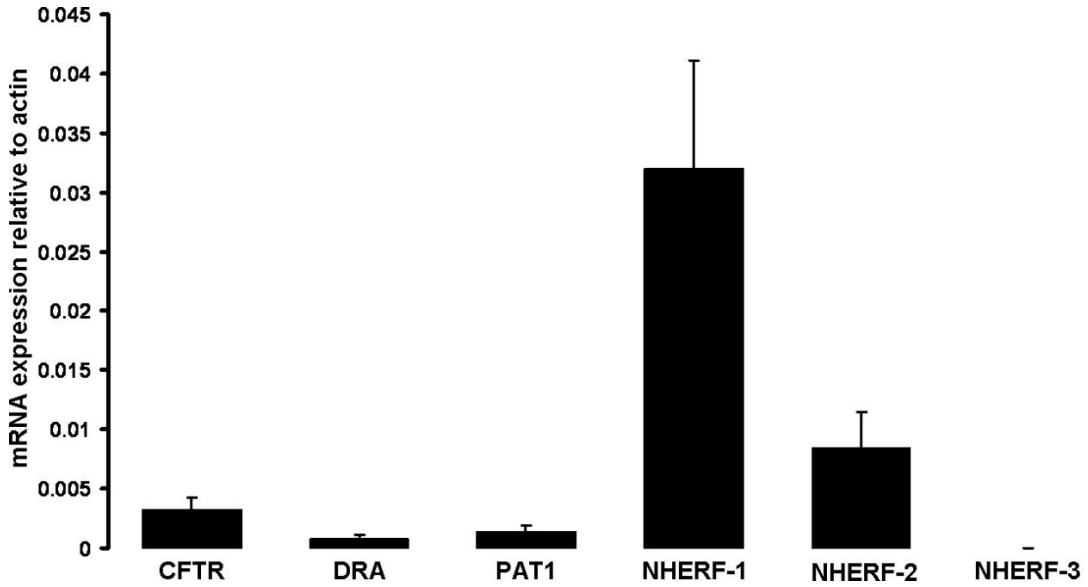

Figure 2. mRNA expression of CFTR, DRA, PAT-1, NHERF-1, NHERF-2 and NHERF-3 in isolated mouse pancreatic ducts. Total RNA was prepared from isolated interlobular pancreatic ducts of wild-type (WT) mice (n=6) after overnight culture and mRNA expression of transporters/NHERF-1-3 was measured by real-time RT-PCR. Data are shown as means ± SEM.

4.1.2. Apical NHERF-1 and CFTR localization in pancreatic ducts is reduced in NHERF-1-knock-out mice

NHERF-1 was highly expressed in the apical membrane of pancreatic duct cells, but only weakly expressed in some acinar cells of WT mice (Figure 3A, B). No or weak staining was detected in NHERF-1-KO mice (Figure 3G, H). The weak staining is non-specific and was not localized to the luminal membrane.

Next, we determined whether NHERF-1 affects the localization of CFTR. The Cl^- channel was expressed in both pancreatic acinar and ductal cells of WT and NHERF-1-KO

mice. Compared to WT animals (Figure 3C), apical CFTR staining in pancreatic ducts was markedly reduced and overall CFTR staining in the pancreas appeared more diffuse in the absence of NHERF-1 (Figure 3I). The strong cytoplasmic staining by the CFTR antibody correlates with the high CFTR mRNA expression levels in murine pancreas as compared to other gastrointestinal tissues [i.e. some cytoplasmic and basolateral staining in the duodenum (Singh et al., 2009), but not the ileum or colon of this mouse strain - unpublished observations]. Expression of pancreatic ductal CFTR mRNA was not significantly different in WT and NHERF-1-KO mice (results not shown).

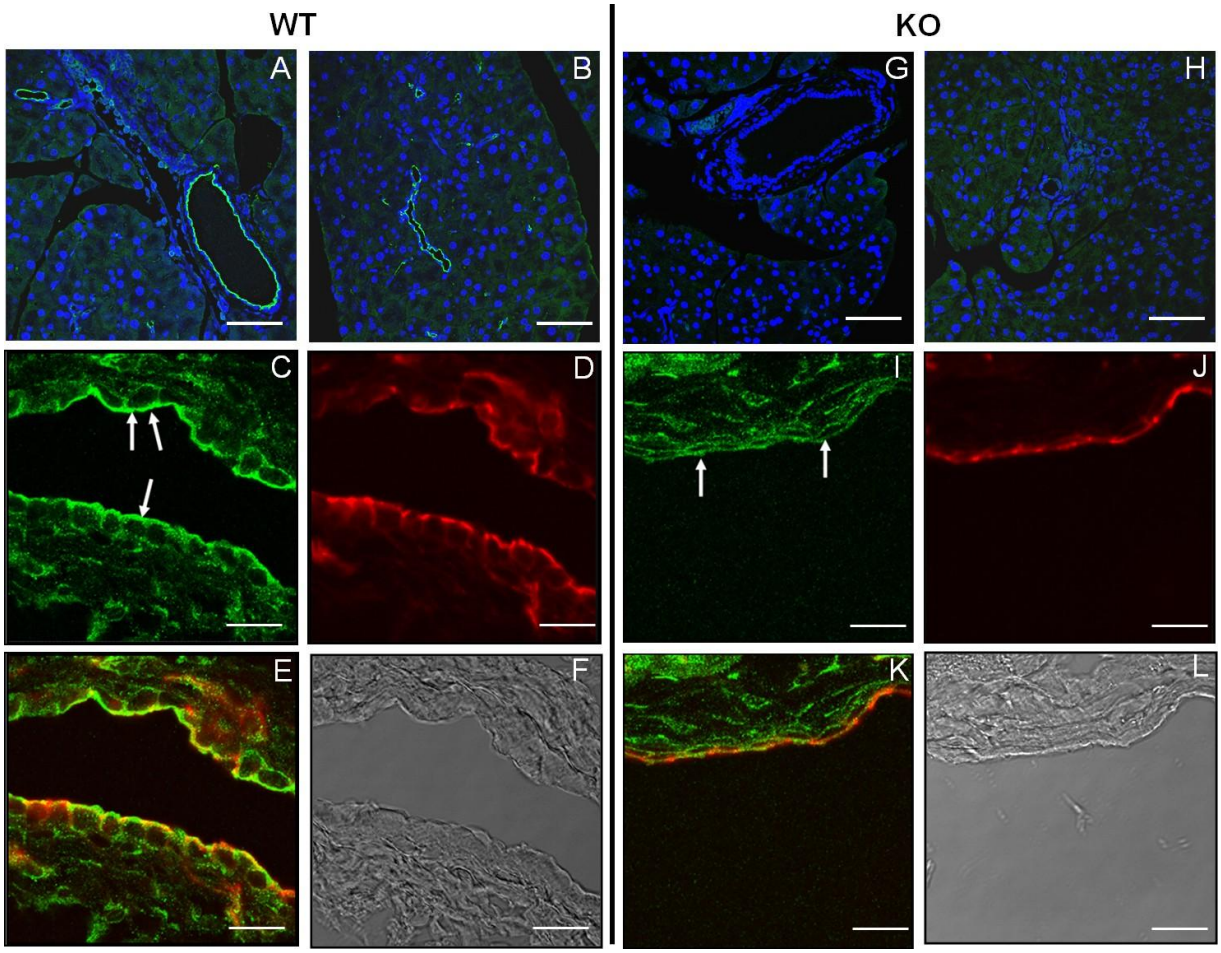

Figure 3. NHERF-1 and CFTR staining in wild-type and NHERF-1-knock-out pancreata. Representative immunohistochemical staining of NHERF-1 (**A, B, G, H**) and CFTR (**C, I**) in the pancreas of WT and NHERF-1-knock-out (KO) mice. NHERF-1 was localized in the apical membrane of intra- and interlobular duct cells; only weak staining was noted in some acinar cells of WT mice (**A, B**). No or weak staining was detected in NHERF-1-KO mice (**G, H**). CFTR staining in the pancreas of WT and NHERF-1-KO mice showed that apical (white arrow) CFTR localization (green) was reduced in NHERF-1-KO (**I**) vs. WT (**C**) ducts. Red staining shows F-actin expression (**D, J**). **E, K** show merged images of CFTR and F-actin (yellow color indicates co-localization). **F, L** are phase contrast pictures. Scale bar=50 µm.

4.1.3. Pancreatic ductal HCO_3^- secretion is decreased in NHERF-1-knock-out mice

To determine if mislocalization of CFTR affects pancreatic ductal function, we investigated HCO_3^- secretion in isolated ducts using three different, but complementary, methods that measure the rate at which HCO_3^- is secreted across the luminal membrane via Cl^-/HCO_3^- exchangers and/or CFTR (Hegyi et al., 2005).

(1) Inhibitor stop. With this method the initial rate of pH_i acidification is measured after the basolateral membrane is exposed to H_2DIDS (0.2 mM) and amiloride (0.2 mM) which block HCO_3^- accumulation into the cell by the NBC and NHE (Venglovecz et al., 2008). Using this approach the rate of $J(B^-)$ was more than 4-fold lower in NHERF-1-KO compared to WT mice (Figures 4A, D).

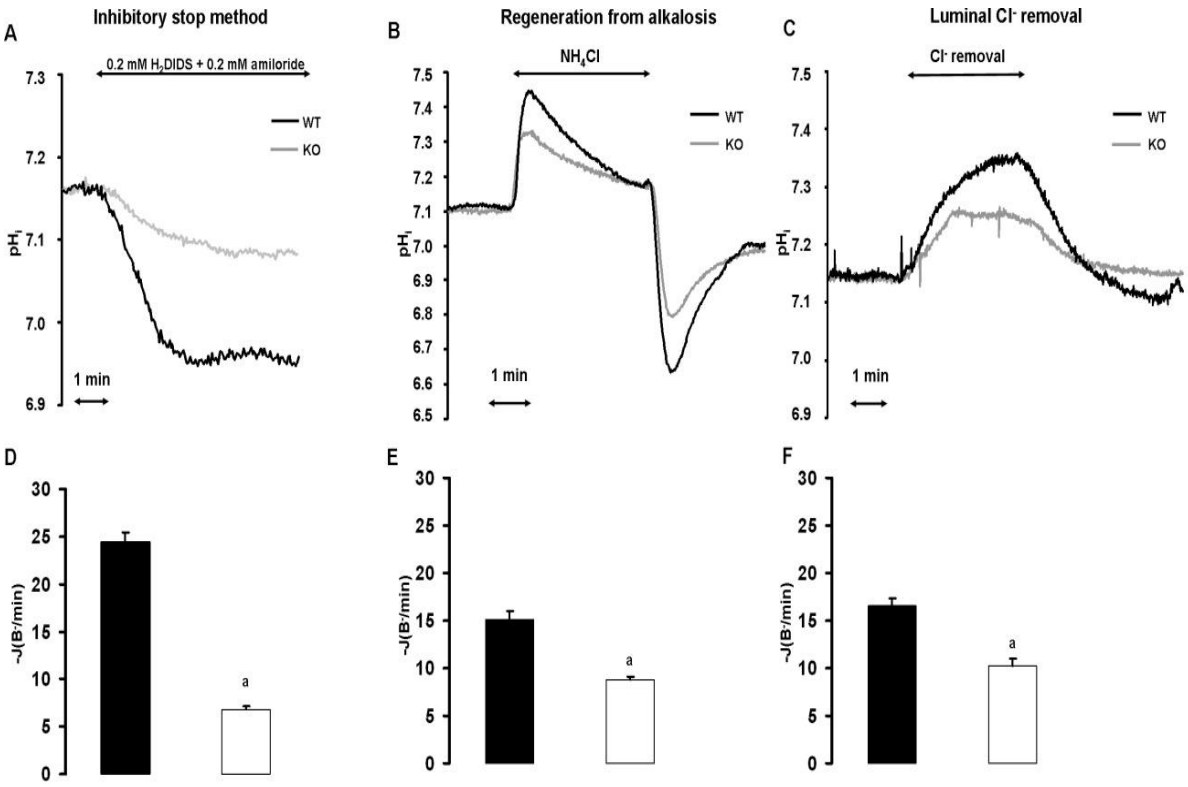

Figure 4. Pancreatic ductal HCO_3^- secretion is decreased in NHERF-1-knock-out mice. Panels **A-C** show representative intracellular pH (pH_i) traces of isolated pancreatic ducts bathed in standard HCO_3^-/CO_2 solution demonstrating the effects of 0.2 mM amiloride and 0.2 mM H_2DIDS administered from the basolateral membrane (**A**), the recovery from alkalosis via administration of 20 mM NH_4Cl (**B**), or after luminal Cl^- removal (**C**). Bar charts show summary data for the base fluxes [$-J(B^-/min)$] after exposure of the transport inhibitors (**D**), 20 mM NH_4Cl (**E**) or luminal Cl^- removal (**F**) in WT (closed columns) and NHERF-1-KO (open columns) mice. Means ± SEM are from 30-50 regions of interest from 5-8 ducts. a: $P<0.05$ vs. the respective WT group.

(2) Alkali load. Here the recovery of pH_i from an alkali load induced by exposure to 20 mM NH_4Cl in a HCO_3^-/CO_2-containing solution reflects the rate of HCO_3^- secretion (Venglovecz et al., 2008). Figures 4B and 4E show that the recovery from alkali load was about 2-fold lower in NHERF-1-KO vs. WT animals.

(3) Chloride removal. Figures 4C and 4F show that pH_i alkalinisation induced by removal of luminal Cl^- was significantly reduced in NHERF-1-KO compared to WT mice.

These data show that pancreatic ductal HCO_3^- secretion was significantly reduced in NHERF-1-KO compared to WT mice.

4.1.4. Fluid secretion is decreased in NHERF-1-knock-out mice

To investigate if fluid secretion was also compromised in KO mice, the rate of fluid secretion was measured using sealed ducts and the swelling technique. In the absence of secretagogue, we could not detect any significant changes in the volume of WT and NHERF-1-KO ducts (Figure 5A). Stimulation of WT ducts with 5 μM forskolin caused dynamic swelling of the ducts as a result of fluid secretion into the closed luminal space. In contrast, ducts from NHERF-1-KO mice had a blunted response to forskolin (Figure 5B).

We also examined the rate of pancreatic juice secretion *in vivo* in anesthetized mice. Under basal conditions, WT animals secreted pancreatic juice at a rate of 0.12 ± 0.02 μl/hour/g body weight (Figure 5C). In contrast, we could not detect any basal secretion in NHERF-1-KO animals. In response to secretin stimulation, we observed about 4-fold higher rates of pancreatic juice secretion in WT mice, values significantly higher than from NHERF-1-KO mice. These results demonstrate that pancreatic fluid secretion was significantly reduced in NHERF-1-KO compared to WT animals under both basal and secretin-stimulated conditions.

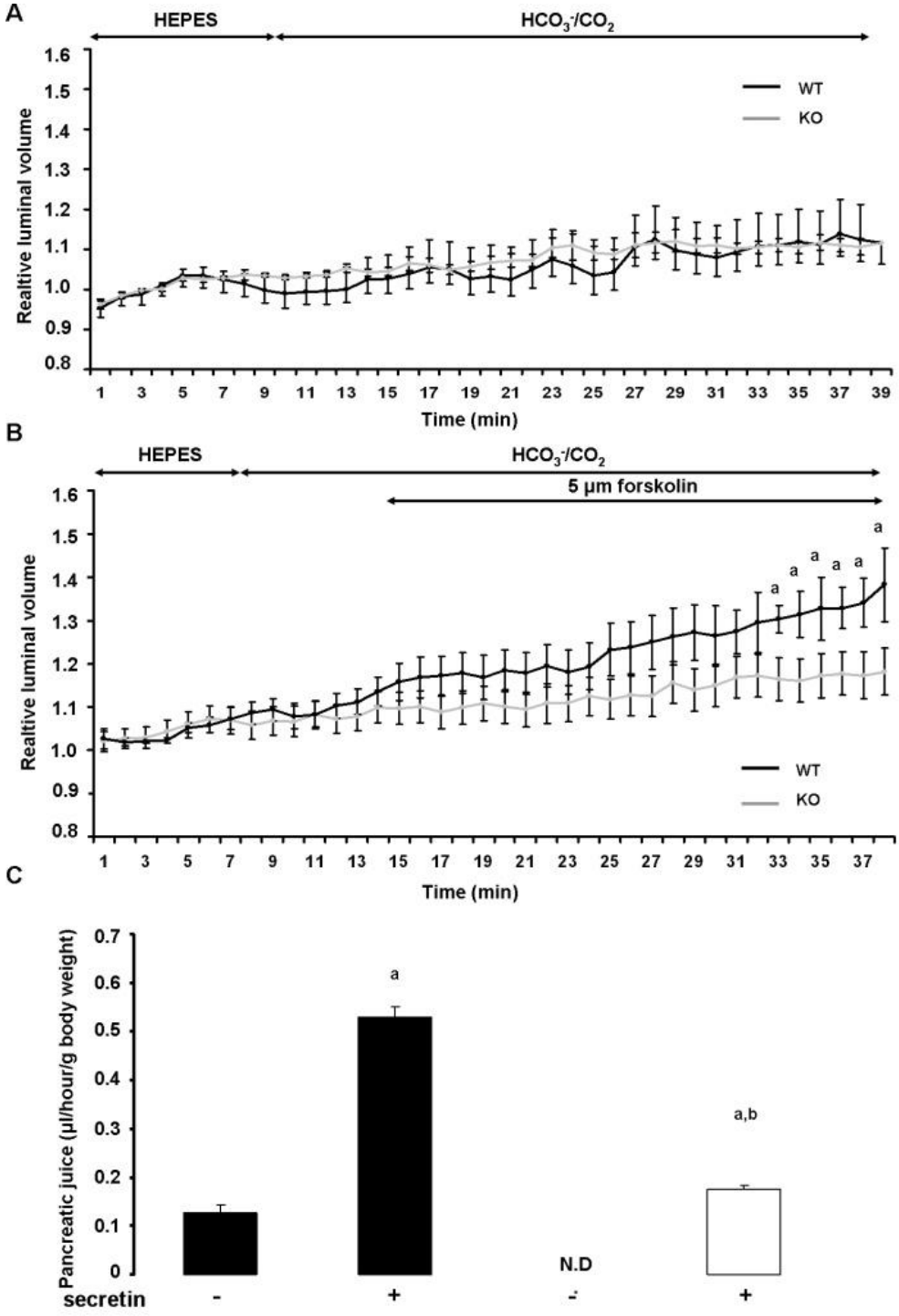

Figure 5. Fluid secretion is decreased in NHERF-1-knock-out vs. wild-type mice. A and **B** show changes in the relative luminal volume of pancreatic ducts from WT (black line, n=8 from 3 animals) and NHERF-1-KO (gray line, n=8 from 3 animals) mice. Initially, ducts were perfused with HEPES-buffered solution, then perfusion was switched to standard HCO_3^-/CO_2-buffered solution (**A**). In some cases the ductal secretion was stimulated with 5 µM forskolin (**B**). Panel **C** shows the volume of pancreatic juice collected *in vivo* under basal (secretin -) and secretin-stimulated (secretin +, 0.75 CU/kg i.v.) conditions from WT (closed columns) and NHERF-1-KO (open column) mice anesthetized with urethane. Means ± SEM are from 5-6 animals. $P<0.05$ vs. a: the respective secretin– group or b: vs. the WT secretin+ group. N.D.: not detected in case of NHERF-1-KO mice.

To rule out secondary alterations in pancreatic fluid secretion by changes in microcirculation due to loss of NHERF-1, we measured baseline microcirculatory plasma velocities in the capillaries of the pancreas, which were similar in WT and NHERF-1-KO animals under both basal and secretin-stimulated conditions (Figure 6).

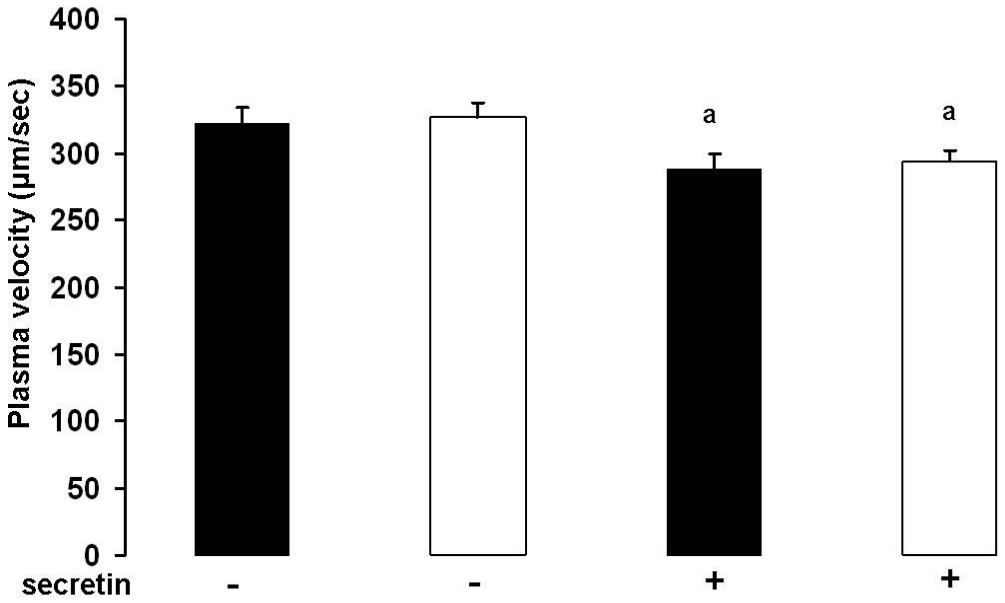

Figure 6. Pancreatic microcirculation shows similar changes in wild-type and NHERF-1-knock-out mice. The microcirculation of the pancreatic tail was visualized by intravital fluorescence microscopy using a single i.v. bolus of fluorescein isothiocyanate-labelled dextran for plasma labeling in WT (closed columns) or NHERF-1-KO (open columns) mice anesthetized with urethane (1.5 g/kg i.p.). Video images were recorded at baseline (secretin -) and 20 min after the i.v. administration of secretin (0.75 CU/kg, secretin +). 20 min after the i.v. injection of secretin, significantly lower plasma velocity values were observed in both experimental groups. These reduced microcirculatory velocities, however, were not due to the effect of secretin, but most likely resulted from the 20-min exteriorization period of the pancreas, since a similar degree of reduction (by about 10%) in plasma velocities was also observed in time-matched pilot studies where mice were treated with PS vehicle (data not shown). a: $P<0.05$ vs. the respective secretin – group.

4.2. Role of trypsin in pancreatic ductal HCO_3^- secretion

4.2.1. Expression of PAR-2 in guinea pig and human pancreata

PAR-2 was highly expressed in the luminal membrane of small intra- and interlobular ducts (Figure 7A.i; cuboidal epithelial cells forming the proximal pancreatic ducts), but was almost undetectable in the larger interlobular ducts (Figure 7A.ii; columnar epithelial cells forming the distal pancreatic ducts). The localization of PAR-2 in the human pancreas was identical to that in the guinea pig gland (Figure 7A.iv-vi). Measurements of relative optical density confirmed the significant differences between the

expression of PAR-2 in small intra- and interlobular ducts and the larger interlobular ducts in both species (Figure 7C).

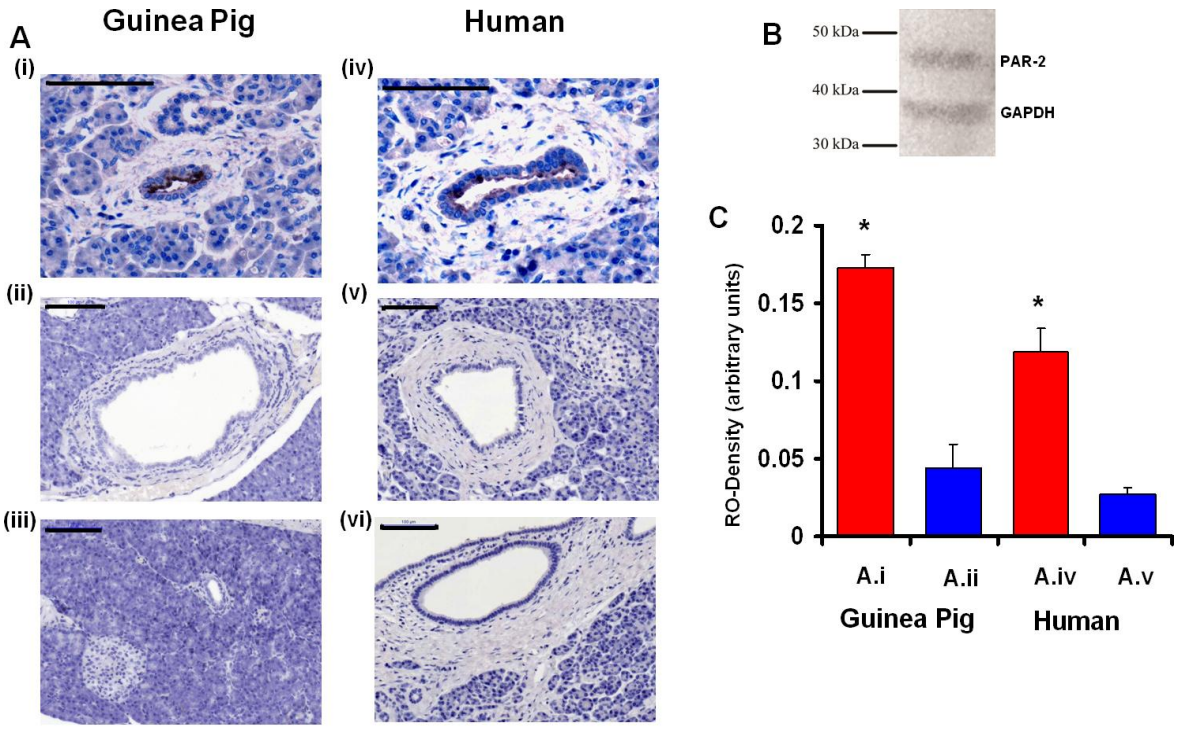

Figure 7. Localization of PAR-2 on human and guinea pig pancreatic ducts. Representative light micrographs of guinea pig (Ai-iii) and human (Aiv-vi) pancreas are shown. **i)** PAR-2 is localized to the luminal membrane of PDEC in small intra- and interlobular ducts. **ii)** Large interlobular ducts do not express PAR-2. **iii)** No primary antiserum. **iv-v)** Sections from human pancreas exhibit a similar localization of PAR-2 compared to the guinea pig gland. **vi)** No primary antiserum. **B)** Western blot analysis was used to determine the specificity of the PAR-2 antibody. Polyclonal anti-PAR-2 demonstrated a single 44kDa band. **C)** Quantitative measurement of relative optical densities (RO-Density) of small intra- and interlobular ducts (A.i, iv), and large interlobular ducts (A.ii, v) are shown. n=12.*: P<0.05 *vs.* A.ii or A.v, respectively. Scale bar=100 µm on A.i, iv; 100 µm on A.ii-iii and A.v-vi.

4.2.2. Luminal administration of PAR-2-AP and trypsin induces dose-dependent intracellular calcium signaling

Since PAR-2 expression was detected only on the luminal membrane of intralobular duct cells, we used the microperfusion technique to see whether these receptors can be activated by PAR-2 agonists. First, the experiments were performed at pH 7.4, in order to understand the effects of trypsin and PAR-2 under *quasi* physiological conditions (Figure 8). The fluorescent images in Figure 8A clearly show that luminal administration of PAR-2-AP increased $[Ca^{2+}]_i$ in perfused pancreatic ducts. The $[Ca^{2+}]_i$ response was dose-dependent, and consisted of a peak which decayed in the continued

presence of the agonist, possibly reflecting PAR-2 inactivation or depletion of intracellular Ca^{2+} stores (Figure 8B). Pre-treatment of PDEC with 10 µM PAR-2-ANT for 10 min completely blocked the effects of 10 µM PAR-2-AP on $[Ca^{2+}]_i$ (Figure 8A,C). Removal of extracellular Ca^{2+} had no effect on the $[Ca^{2+}]_i$ rise evoked by luminal administration of 10 µM PAR-2-AP; however, pre-loading ducts with the Ca^{2+} chelator BAPTA-AM at 40 µM totally blocked the response (Figure 8A,C).

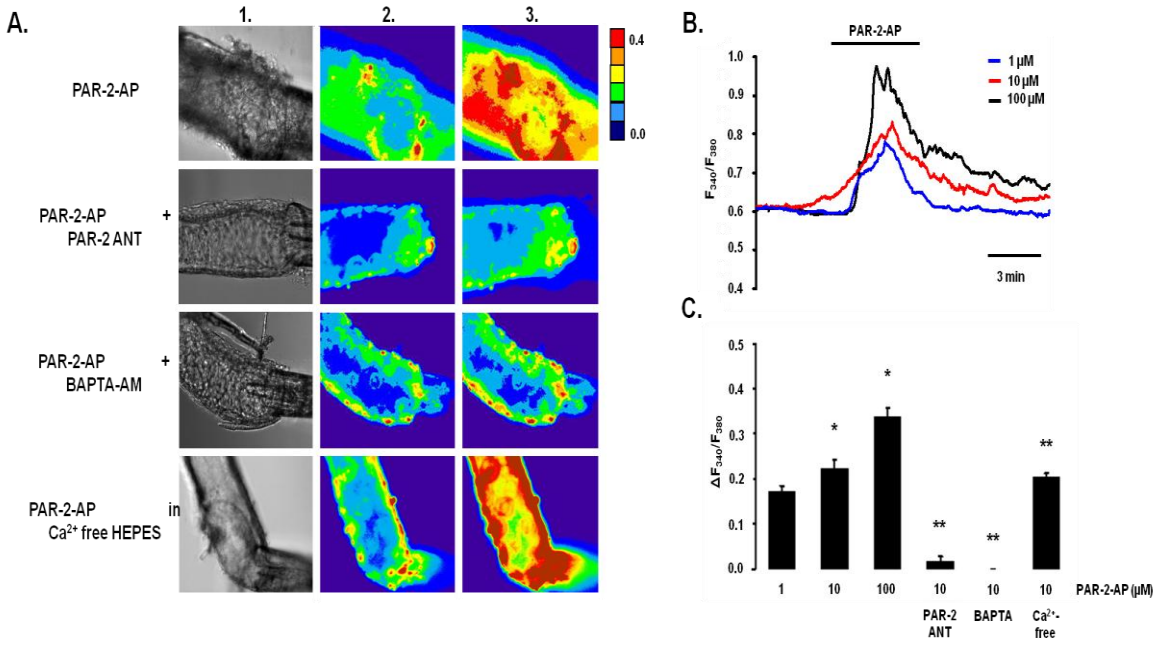

Figure 8. Effects of PAR-2-AP on $[Ca^{2+}]_i$ in microperfused guinea pig pancreatic ducts at pH 7.4. A) Light (1) and fluorescent ratio images (2 and 3) of microperfused pancreatic ducts showing the effects of luminal administration of 10 µM PAR-2 activating peptide (PAR-2-AP), 10 µM PAR-2 antagonist (PAR-2-ANT), or 40 µM BAPTA-AM on $[Ca^{2+}]_i$. Images were taken before (1 and 2) and after (3) exposure of the ducts to PAR-2-AP. **B-C)** Representative experimental traces and summary data of the changes in $[Ca^{2+}]_i$. n=5 for all groups,*: P<0.05 *vs.* 1 µM PAR-2-AP. **: P<0.001 *vs.* 10 µM PAR-2-AP.

Trypsin also induced a dose-dependent $[Ca^{2+}]_i$ elevation similar to that evoked by PAR-2-AP (Figure 9B,C). 5 µM soybean trypsin inhibitor (SBTI), 10 µM PAR-2-ANT and 40 µM BAPTA-AM totally blocked the rise in $[Ca^{2+}]_i$ (Figure 9A,C). These data show that trypsin activates PAR-2 on the luminal membrane of the duct cell which leads to release of Ca^{2+} from intracellular stores and an elevation of $[Ca^{2+}]_i$.

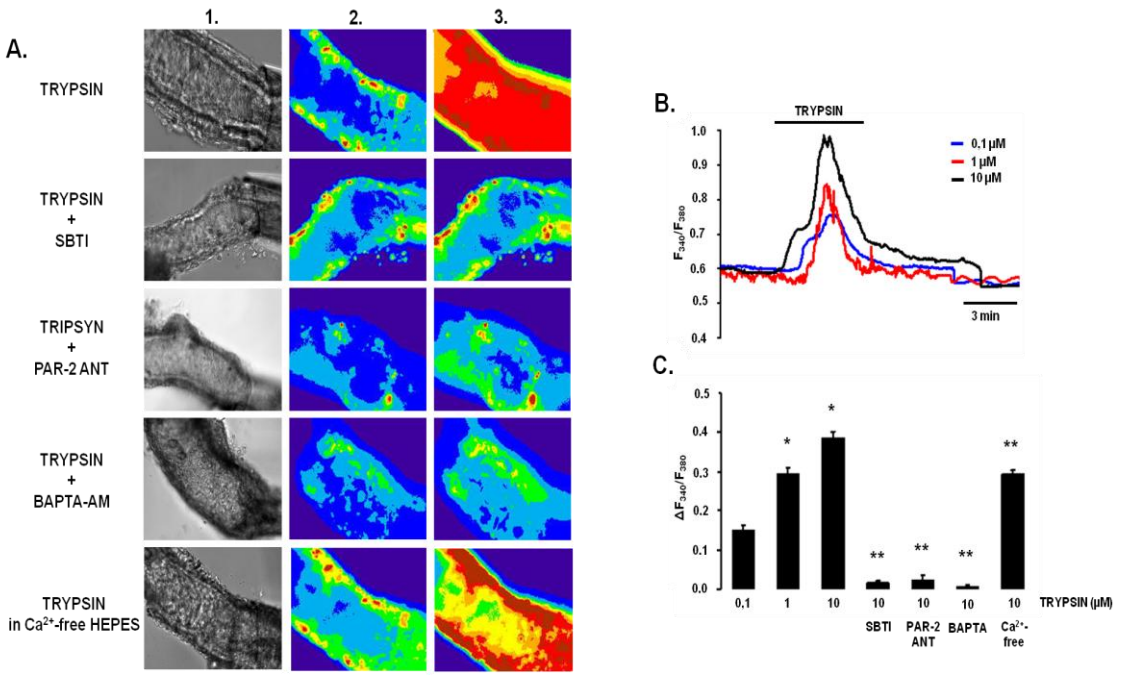

Figure 9. Effects of trypsin on $[Ca^{2+}]_i$ in microperfused guinea pig pancreatic ducts at pH 7.4. A) Light (1) and fluorescent ratio images (2 and 3) of microperfused pancreatic ducts showing the effects of luminal administration of 10 µM trypsin, 5 µM soybean trypsin inhibitor (SBTI) , 10 µM PAR-2-ANT, or 40 µM BAPTA-AM on $[Ca^{2+}]_i$. Images were taken before (1 and 2) and after (3) exposure of the ducts to trypsin. **B-C)** Representative experimental traces and summary data of the changes in $[Ca^{2+}]_i$. n=5 for all groups,*: P<0.05 *vs.* 0.1 µM trypsin. **: P<0.001 *vs.* 10 µM trypsin.

Since the pH of pancreatic juice can vary between approximately 6.8 and 8.0 (Behrendorf et al., 2010; Ishiguro et al., 1996), we also checked the effects of trypsin and PAR-2-AP on $[Ca^{2+}]_i$ at these pH values (Figures 10 and 11, respectively). The elevations of $[Ca^{2+}]_i$ at pH 6.8 and 8.0 were generally very similar to the changes observed at pH 7.4. However, the $[Ca^{2+}]_i$ rises evoked by 1 µM PAR-2-AP and 0.1 µM trypsin were significantly lower at pH 6.8 compared to either pH 7.4 or 8.0 (Figure 12).

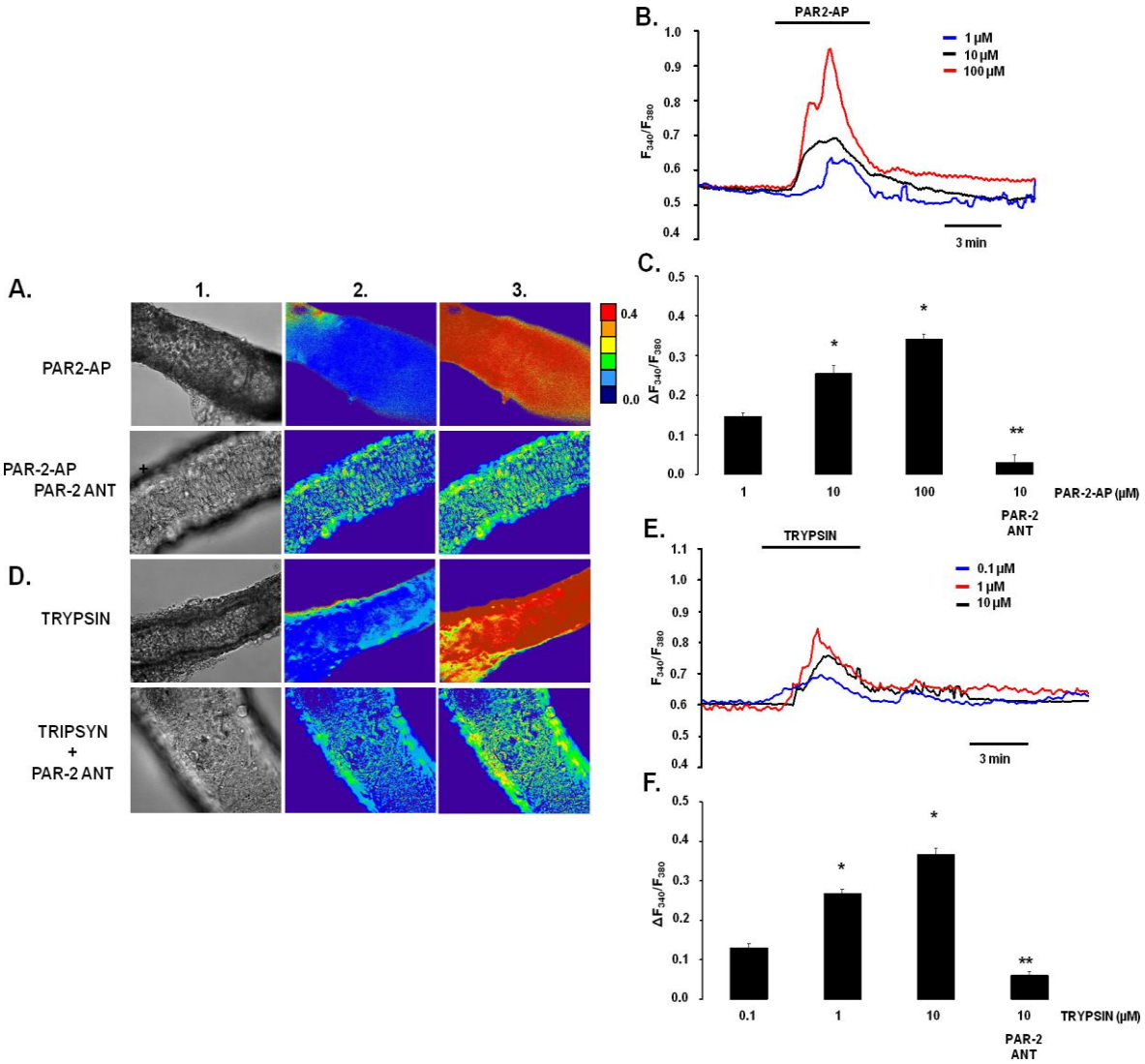

Figure 10. Effects of PAR-2-AP and trypsin on $[Ca^{2+}]_i$ in microperfused guinea pig pancreatic ducts at pH 6.8. **A)** Light (1) and fluorescent ratio images (2 and 3) of microperfused pancreatic ducts showing the effects of luminal administration of 10 µM PAR-2-AP and 10 µM PAR-2-ANT on $[Ca^{2+}]_i$ at pH 6.8. Images were taken before (1 and 2) and after (3) exposure of the ducts to either PAR-2-AP or trypsin. An increase in $[Ca^{2+}]_i$ is denoted by a change from a ‘‘cold’’ colour (blue) to a ‘‘warmer’’ colour (yellow to red); see scale on the right. **B-C)** Representative experimental traces and summary data of the changes in $[Ca^{2+}]_i$ at pH 6.8. **D)** The same protocol was used to evaluate the effects of trypsin. **E-F)** Representative experimental traces and summary data of the changes in $[Ca^{2+}]_i$ at pH 6.8. n=3-4, *: P<0.05 *vs.* 1 µM PAR-2-AP or 0.1 µM trypsin, respectively. **: P<0.001 *vs.* 10 µM PAR-2-AP or 10 µM trypsin, respectively.

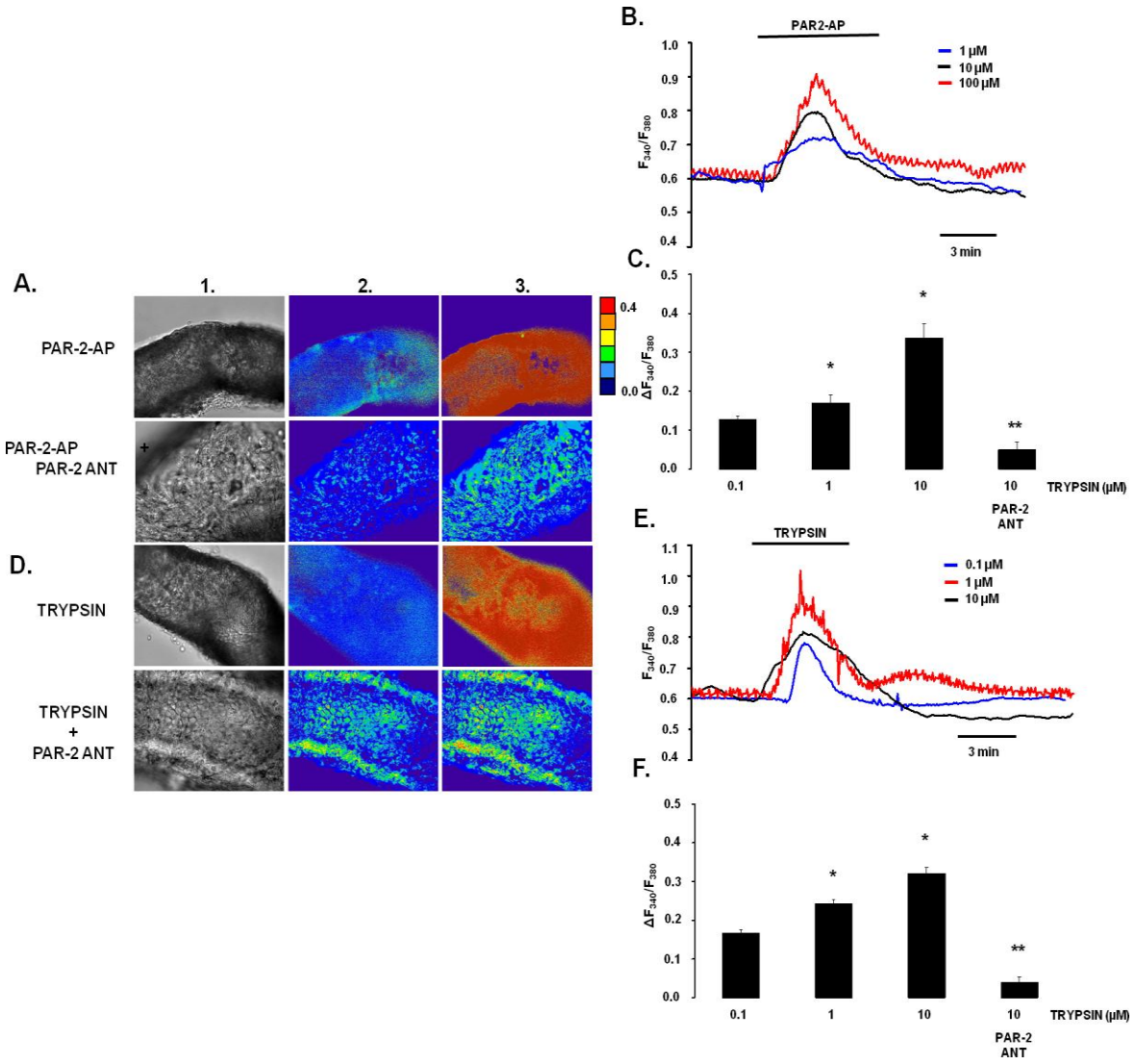

Figure 11. Effects of PAR-2-AP and trypsin on $[Ca^{2+}]_i$ in microperfused guinea pig pancreatic ducts at pH 8.0. A) Light (1) and fluorescent ratio images (2 and 3) of microperfused pancreatic ducts showing the effects of luminal administration of 10 µM PAR-2-AP and 10 µM PAR-2-ANT on $[Ca^{2+}]_i$ at pH 8.0. Images were taken before (1 and 2) and after (3) exposure of the ducts to PAR-2-AP or trypsin. The colors are described in figure 10; see scale on the right. **B-C)** Representative experimental traces and summary data of the changes in $[Ca^{2+}]_i$ at pH 8.0. **D)** The same protocol was used to evaluate the effects of trypsin. **E-F)** Representative experimental traces and summary data of the changes in $[Ca^{2+}]_i$. n=3-4, *: P<0.05 *vs.* 1 µM PAR-2-AP or 0.1µM trypsin, respectively. **: P<0.001 *vs.* 10 µM PAR-2-AP or 10 µM trypsin, respectively.

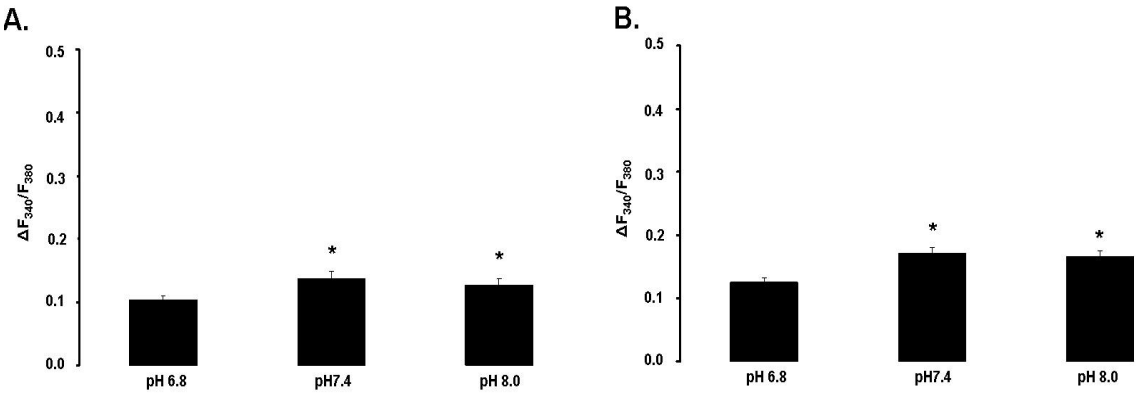

Figure 12. Summary of the effects of PAR-2-AP and trypsin on $[Ca^{2+}]_i$ in microperfused guinea pig pancreatic ducts at different extracellular pH values. A) The $[Ca^{2+}]_i$ elevation evoked by 1 μM PAR-2-AP and **B)** 0.1 μM trypsin at different extracellular pH values (6.8; 7.4; 8.0). n=3-4, *: P<0.05 vs. at pH 6.8.

4.2.3. Luminal exposure to PAR-2-AP and trypsin evoke intracellular alkalosis in guinea pig PDEC

Figure 13 shows pH_i recordings from microperfused pancreatic ducts. Luminal application of the CFTR inhibitor-172 (CFTRinh-172, 10 μM) and the anion exchanger inhibitor H_2DIDS (500 μM) induced an intracellular alkalization in PDEC (Figure 13A). These data indicate that when HCO_3^- efflux across the luminal membrane of PDEC (i.e. HCO_3^- secretion) is blocked an elevation of duct cell pH_i occurs, presumably because the basolateral transporters continue to move HCO_3^- into the duct cell. Note also that the rise in pH_i evoked by the inhibitors is not sustained and begins to reverse before the inhibitors are withdrawn (Figure 13A), which might be explained by the regulation of pH_i by basolateral acid/base transporters.

Both luminal PAR-2-AP and trypsin induced a dose-dependent elevation of pH_i (Figure 13B, C), suggesting that activation of PAR-2 inhibits HCO_3^- efflux across the apical membrane of the duct cell. Pre-incubation of PDEC with either 10 μM PAR-2-ANT or 5 μM SBTI or 40 μM BAPTA-AM for 30 min totally blocked the effect of trypsin on pH_i (Figure 13D). The inhibitory effect of the Ca^{2+} chelator, BAPTA-AM, suggests that the actions of trypsin and PAR-2-AP on pH_i are mediated by the rise in $[Ca^{2+}]_i$ that they evoke (Figures 8, 9). Therefore, in this case, the transient nature of the pH_i response may reflect the transient effect that PAR-2 activators have on $[Ca^{2+}]_i$ (Figures 8B, 9B), as well as pH_i regulation by basolateral acid/base transporters.

Next we tested the effects of trypsin on pH_i in Cl^--free conditions and during pharmacological inhibition of the luminal anion exchangers and/or CFTR (Figure 13E-H). Luminal Cl^--free conditions increased the pH_i of PDEC presumably by driving HCO_3^- influx on the apical anion exchangers (Figure 13E). Note that luminal administration of trypsin further elevated pH_i in Cl^- free conditions (Figure 13E), and also in the presence of H_2DIDS (Figure 13F) and CFTRinh-127 (Figure 13G). However, pre-treatment of ducts with a combination of H_2DIDS and CFTRinh-172 markedly reduced the effect of trypsin on pH_i (Figure 13H).

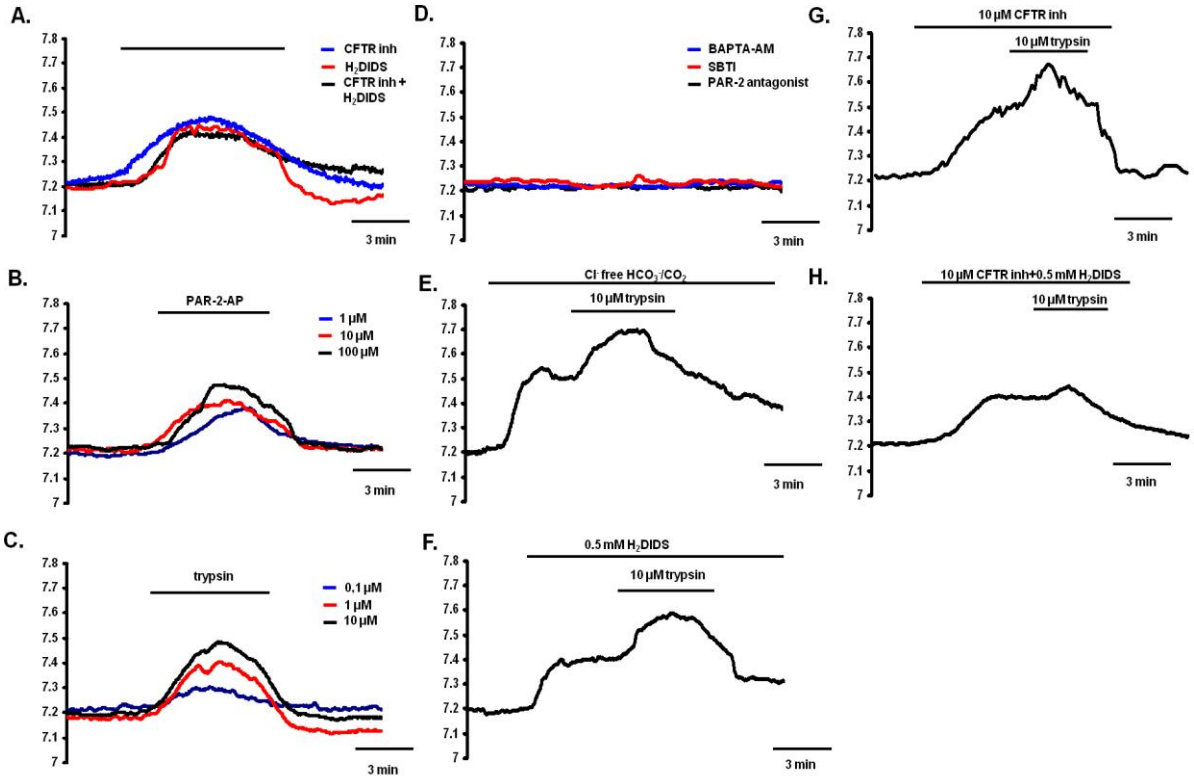

Figure 13. Effects of PAR-2-AP and trypsin on pH_i in microperfused guinea pig pancreatic ducts. Representative pH_i traces showing the effects of luminal administration of different agents in microperfused pancreatic ducts. **A)** 10 µM CFTRinh-172 and/or 500 µM H_2DIDS caused alkalization of pH_i. **B)** PAR-2-AP and **C)** trypsin induced a dose-dependent pH_i elevation, **D)** Preincubation of ductal cells with 10 µM PAR-2-ANT or 5 µM SBTI or 40 µM BAPTA-AM totally blocked the alkalization caused by 10 µM trypsin. **E)** Removal of luminal Cl^- or **F)** administration of H_2DIDS (500 µM) decreased, but did not totally abolish, the effects of 10 µM trypsin on pH_i. **G)** Pretreatment with 10 µM CFTRinh-172 also decreased the effects of trypsin (10 µM) on pH_i. **H)** Simultaneous administration of H_2DIDS and CFTRinh-172 strongly inhibited the effect of 10 µM trypsin.

Figure 14A-C is a summary of the pH_i experiments. Trypsin (Figure 14A) and PAR-2- AP (Figure 14B) both induced statistically significant, dose-dependent rises in pH_i and these effects were blocked by PAR-2-ANT, SBTI and BAPTA-AM. Exposure of the ducts to luminal Cl^- free conditions, H_2DIDS, CFTRinh-172 or a combination of the

inhibitors also induced an intracellular alkalosis (Figure 14C). Also shown in Figure 14C is the additional, statistically significant, rise in pH_i caused by trypsin in ducts exposed to Cl^--free conditions and the individual inhibitors. However, when ducts were exposed to both CFTRinh-172 and H_2DIDS simultaneously, the effect of trypsin on pH_i was markedly reduced although it remained statistically significant (Figure 14 C). We interpret these results as indicating that trypsin inhibits both Cl^- dependent (i.e. anion exchanger mediated; revealed when CFTR is blocked by CFTRinh-172) and Cl^- independent (i.e. CFTR mediated; revealed in Cl^--free conditions and when the luminal exchangers are blocked by H_2DIDS) HCO_3^- secretory mechanisms in PDEC. Reduced HCO_3^- secretion will lead to a decrease in intraductal pH.

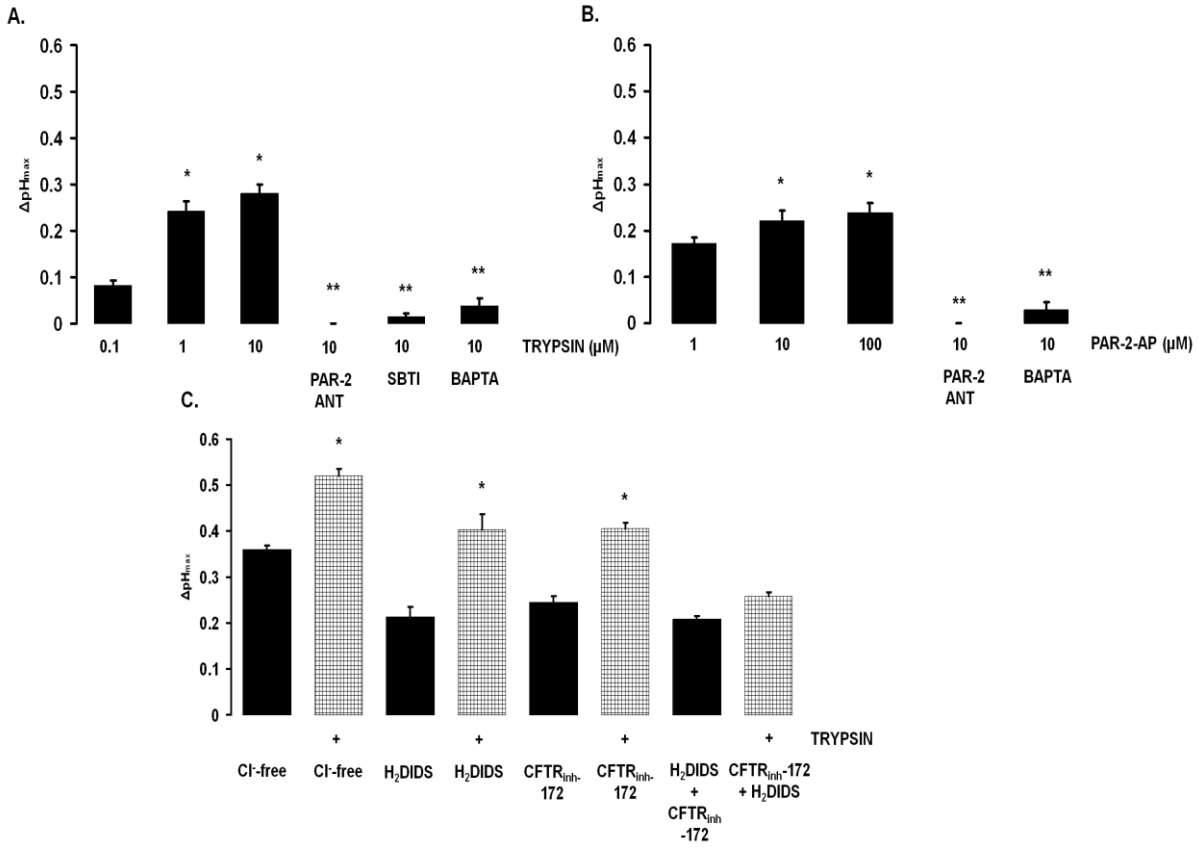

Figure 14. A-B) Summary of the effects of PAR-2-AP and trypsin on pH_i changes. ΔpH_{max} was calculated from the experiments shown in Figure 13. **C) Effects of Cl^--free conditions**. Cl^--free conditions, H_2DIDS, CFTRinh-172 and a combination of the inhibitors all induced an intracellular alkalosis. Trypsin further increased the alkalinisation of pH_i although the effect was markedly reduced when both H_2DIDS and CFTRinh-172 were present. n=4-5 for all groups. **A)***: P<0.05 *vs.* 0.1 μM trypsin; **: P<0.001 *vs.* 10 μM trypsin, **B)***: P<0.05 *vs.* 0.1 μM PAR-2-AP; **: P<0.001 *vs.* 10 μM PAR-2-AP, **C)***: P<0.05 *vs.* the respective filled column.

To gain insight into the mechanism by which trypsin inhibits HCO_3^- secretion, we next investigated the effects of trypsin and PAR-2-AP on basal and forskolin-activated CFTR currents using the whole cell configuration of the patch clamp technique. Exposure

of PDEC to 10 µM trypsin did not affect the basal currents; however, administration of either 10 µM PAR-2-AP or 10 µM trypsin inhibited forskolin-stimulated CFTR currents (data not shown).

4.2.4. PAR-2 is down-regulated in patients suffering from chronic pancreatitis

It has been documented that there is activated trypsin in the pancreatic ductal lumen in chronic pancreatitis in human (Fedail et al., 1979; Kukor et al., 2002; Tympner, 1981; Tympner & Rosch, 1978). If trypsin activity is elevated in the duct lumen, PAR-2 down-regulation should occur, which could be due either: (i) to changes in PAR-2 mRNA transcription and/or (ii) due to receptor internalization and translocation to the cytoplasm.

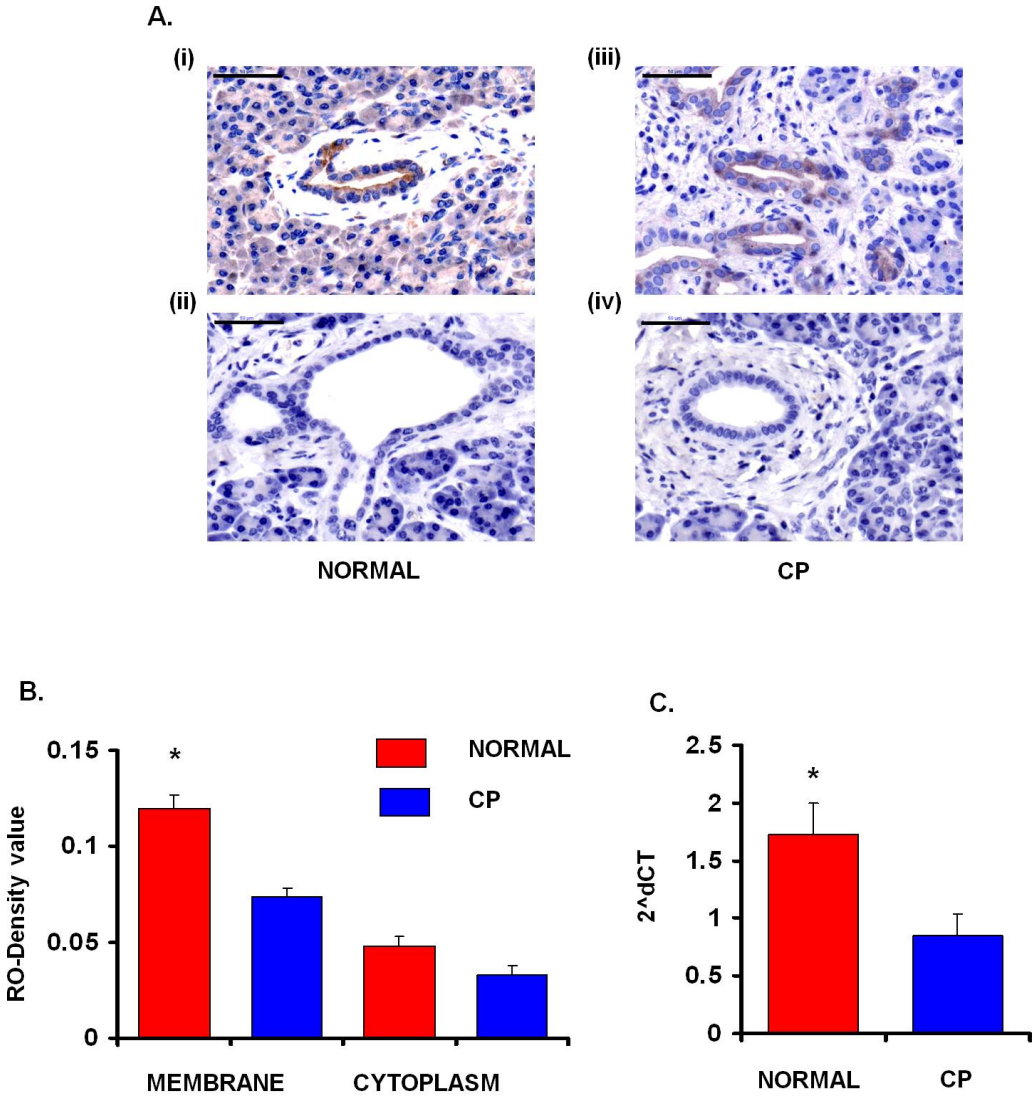

Figure 15. Analyses of PAR-2 expression in human pancreatic samples. A. i-iv) PAR-2 expressing cells were visualized by immunohistochemistry. **i)** Representative section of normal human pancreas. **ii)** No primary antiserum. **iii)** Representative section of human pancreas from a

patient suffering from chronic pancreatitis (CP). **iv)** No primary antiserum. **B)** Relative optical density of immunohistochemistry. n=15,*: P<0.05 *vs.* CP membrane. **C)** Real-time RT-PCR analysis of PAR-2 mRNA expression of human pancreas. Data are given in 2^dCT. n=15,*: P<0.05 *vs.* CP. Scale bar=50 μm.

Our data show a marked reduction in membranous PAR-2 protein level, but no significant changes in cytoplasmic PAR-2 protein in chronic pancreatitis (Figure 15A. i-iv, B). Furthermore, PAR-2 mRNA level was markedly reduced in chronic pancreatitis (Figure 15C), suggesting that reduced PAR-2 mRNA transcription may cause PAR-2 down-regulation in chronic pancreatitis.

4.2.5. Luminal exposure to R122H mutant cationic trypsin induces elevation of intracellular calcium concentration and evokes alkalosis in PDEC

It has been demonstrated that mutations in cationic trypsinogen increase the risk of chronic pancreatitis, most likely because of the enhanced autoactivation exhibited by the mutant trypsinogens (Sahin-Tóth & Tóth, 2000). Here we tested whether the most common mutation in cationic trypsin, R122H, affected the protease's ability to interact with PAR-2. Figure 16 A-B shows that 1 μm of R122H cationic trypsin causes comparable changes in pH_i and $[Ca^{2+}]_i$ to 0.4 μM wild-type trypsin, suggesting that a trypsin-mediated inhibition of HCO_3^- secretion could play a role in the pathogenesis of hereditary as well as chronic pancreatitis.

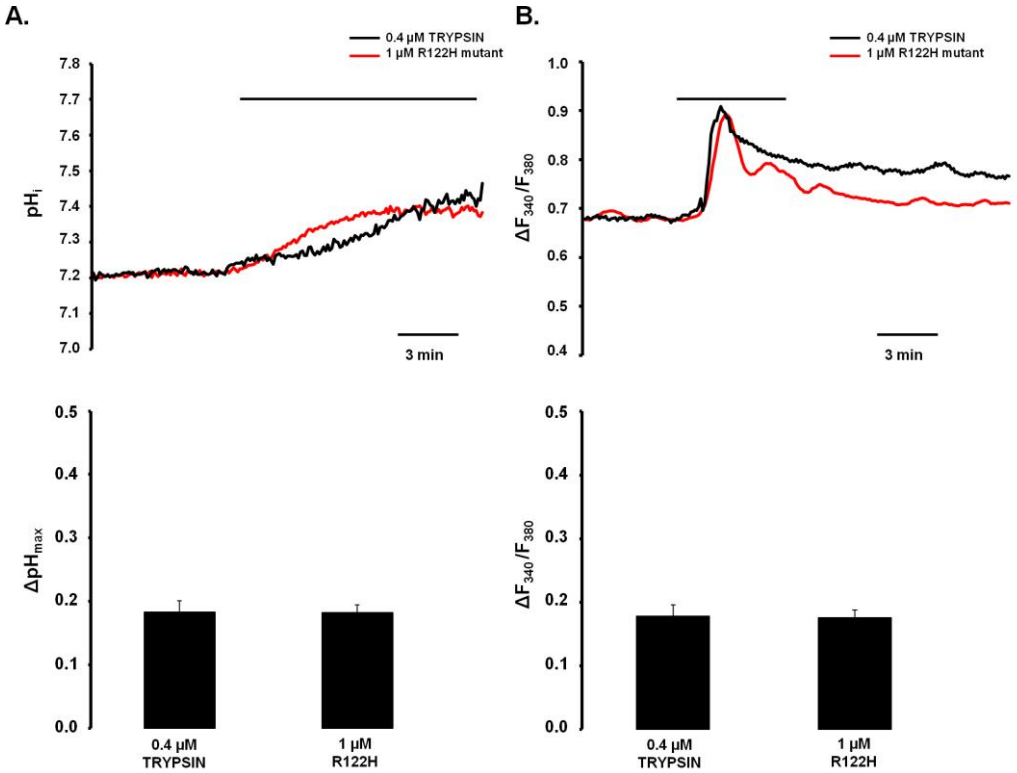

Figure 16. R122H cationic trypsin causes comparable changes in pH_i and $[Ca^{2+}]_i$ to wild-type trypsin. Representative **A)** pH_i and **B)** $[Ca^{2+}]_i$. measurements using luminal administration of normal and R122H mutant cationic trypsin in microperfused guinea pig pancreatic ducts. n=5 for all experiments.

4.2.6. Activation of PAR-2 is diminished in PAR-2 KO mice

Finally, we investigated the effects of both PAR-2-AP and trypsin on PDEC isolated from WT and PAR-2 KO mice (Figure 18A-B). First we confirmed using immunohistochemistry that WT mice do, whereas PAR-2 KO mice do not express PAR-2 in their PDEC (Figure 17A-D). Accordingly, our functional data clearly show that the pH_i and $[Ca^{2+}]_i$ responses to luminal administration of either trypsin or PAR-2-AP were markedly diminished in PAR-2 KO PDEC (Figure 18A-B).

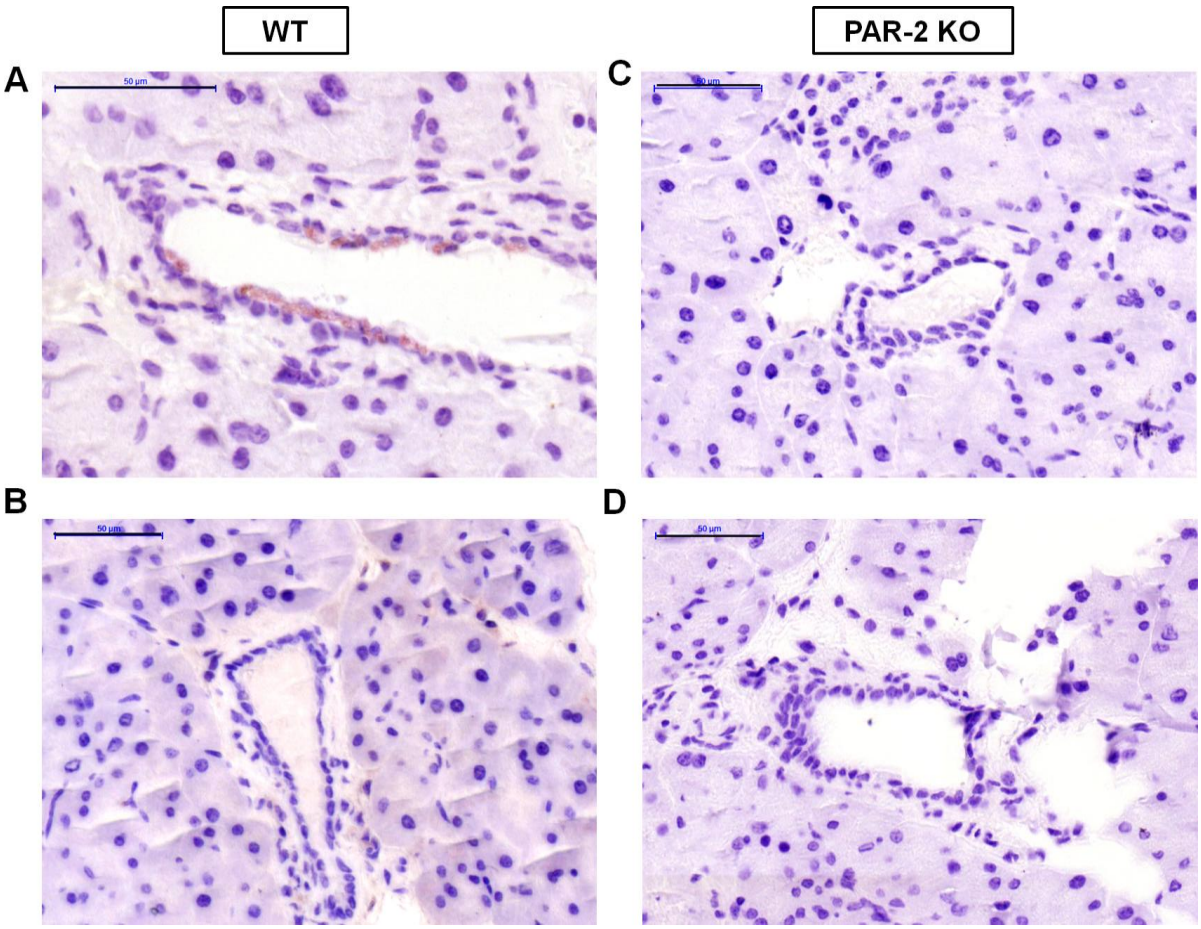

Figure 17. Expression of PAR-2 on pancreatic ductal cells of WT and PAR-2 KO mice. PAR-2 expressing cells were visualized by immunohistochemistry as described in Figure 7. **A)** Representative section of the pancreas removed from WT mice. **B)** Section without primary antiserum. **C)** Pancreas removed from PAR-2 KO mice. **D)** Section without primary antiserum. Scale bar=50 µm.

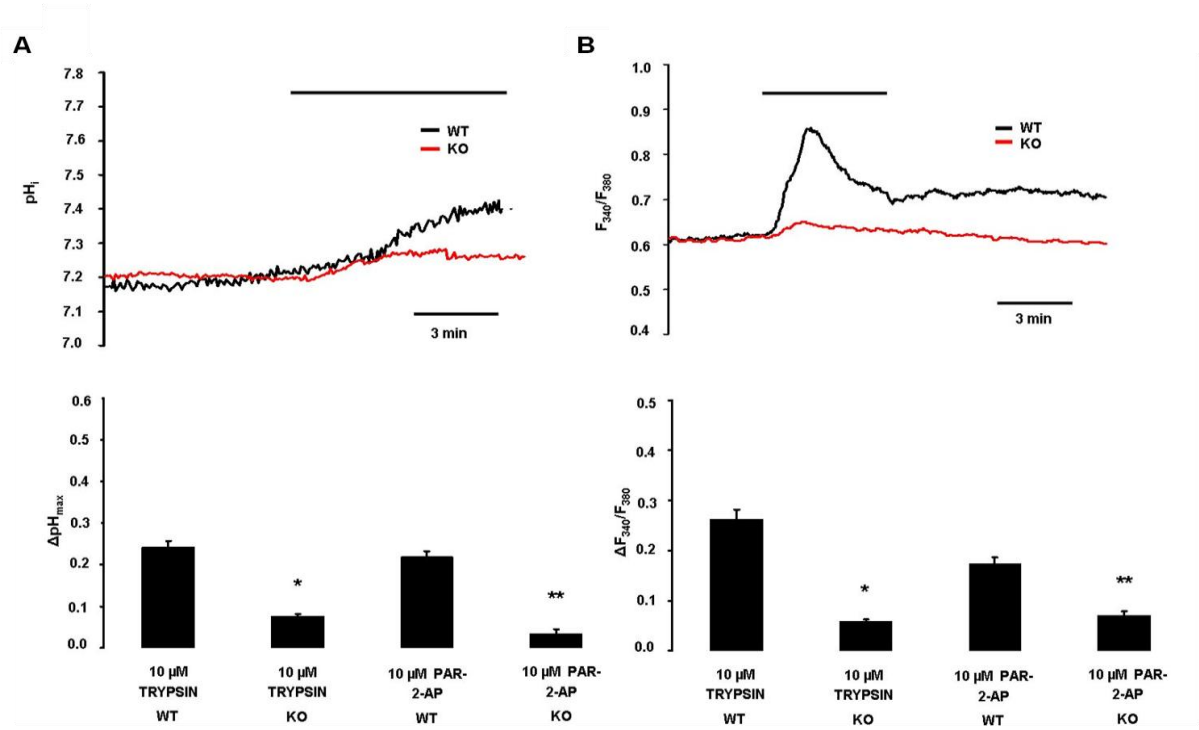

Figure 18. Effects of PAR-2-AP and trypsin on pH_i and $[Ca^{2+}]_i$ in microperfused pancreatic ducts isolated from WT and PAR-2 KO mice. A) pH_i and **B)** $[Ca^{2+}]_i$. measurements using luminal administration of trypsin in microperfused pancreatic ducts isolated from PAR-2 KO (red curve) and PAR-2 WT mice (black curve). n=5 for all experiments,*: P<0.05 *vs.* 10 µM trypsin PAR-2 WT;
**: P<0.05 *vs.* 10 µM PAR-2-AP PAR-2 WT.

5. DISCUSSION

In the present work we described the roles of NHERF-1 and trypsin in the regulation of pancreatic ductal HCO_3^- secretion.

5.1. The effect of NHERF-1 on pancreatic ductal HCO_3^- and fuid secretion

We have demonstrated that NHERF-1 mRNA is highly expressed in mouse pancreatic ducts. Furthermore, the genetic deletion of NHERF-1 greatly reduced the translocation of CFTR to the luminal ductal cell membrane and also decreased both *in vitro* and *in vivo* pancreatic HCO_3^- and fluid secretion. Both basal and cAMP-stimulated (by forskolin or secretin) secretion were affected in the transgenic animals, but this effect was not caused by alterations in pancreatic blood flow.

Localization of CFTR to the apical plasma membrane of epithelial cells is critical for vectorial transport of chloride in a variety of epithelia, including the airway, pancreas, intestine, and kidney (Moyer et al., 1999). NHERF-1 has been shown to play an important role in the apical trafficking, targeting, membrane retention and activation of several membrane proteins such as CFTR (Raghuram et al., 2001). These effects on CFTR were shown to require PDZ domain interactions with NHERF-1 in several studies (Milewski et al., 2001; Moyer et al., 1999; Swiatecka-Urban et al., 2002), although other similar studies failed to confirm these results (Benharouga et al., 2003; Ostedgaard et al., 2003). Moyer et al. (1999) identified the last 3 amino acids in the C-terminus of CFTR (T-R-L) comprise a PDZ-interacting domain that is required for the polarization of CFTR to the apical plasma membrane in human airway and kidney epithelial cells. Milewski et al. (2001) also demonstrated that the cytoplasmic C-terminal tail (PDZ-interacting sequence) of CFTR contains signals sufficient for its localization to the apical membrane in polarized epithelial cells. The C-terminal amino acids of several other integral membrane proteins are suspected of being an essential part of a multi-component signal that mediates apical or basolateral localization in epithelial cells. In contrast, Benharouga et al. (2003) showed that the inhibition of NHERF binding has no discernible effect on the apical localization of CFTR in polarized tracheal, pancreatic, intestinal, and kidney epithelia and did not influence the metabolic stability or the cAMP-dependent protein kinase-activated Cl^- channel conductance in polarized pancreatic epithelia. These results indicate that apical

localization of CFTR involves sorting signals other than the C-terminal 26 amino acid residues and the PDZ-binding motif in differentiated epithelia (Benharouga et al., 2003). In accordance with our findings, CFTR mutations causing cystic fibrosis that impair the stability of the Cl^- channel in the plasma membrane also result in markedly reduced HCO_3^- and fluid secretion (Lukács & Verkman, 2012). Of course we cannot exclude the direct or indirect (e.g. via CFTR) effects of NHERF-1 deletion on other transporters involved in pancreatic HCO_3^- and fluid secretion, such as anion exchangers DRA and PAT-1. Of note, both DRA and PAT-1 are known to have PDZ domain binding motifs (Lamprecht & Seidler, 2006), and to bind to NHERF-1 (Lamprecht et al., 2002; Lohi et al., 2003; Rossmann et al., 2005). In addition, activation of CFTR by SLC26 transporters was shown to be facilitated by PDZ ligands (Ko et al., 2004). We could not test the expression of PAT-1 and DRA in the apical membrane of pancreatic ducts, because the antibodies that we have available also stain the apical membranes in PAT-1 KO and DRA-KO pancreatic ducts, respectively. Nevertheless, the reduced expression of CFTR in the apical membrane in NHERF-1 KO pancreatic ducts will likely decrease the activities of PAT-1 and DRA (Chernova et al., 2003; Rakonczay et al., 2008).

Several studies have shown that binding of CFTR to NHERF proteins may also be important for the regulation of CFTR activity. Broere et al. (2007) and Singh et al. (2009) have demonstrated that NHERF-1 is required for full activation of transepithelial Cl^- and HCO_3^- secretion by cAMP- and cGMP-linked agonists in the duodenum and jejunum. This reduced activation of anion currents in NHERF-1 KO mice seemed to be independent of the total amount of CFTR protein expression in epithelial cells, but did appear to be due to a defect in apical targeting and/or apical retention of CFTR (Broere et al., 2007). In addition, the NHERF-1 assisted formation of receptor-transporter signalling complexes in the apical membrane were disrupted (Singh et al., 2009). Interestingly, NHERF-1 deletion did not cause a generalized CFTR dysfunction, because in the NHERF-1 deficient ileum where CFTR is strongly crypt located (Jakab et al., 2011), whereas NHERF-1 expression shows a gradient with high expression in the villi, CFTR-mediated I_{sc} response to forskolin was not different in NHERF-1 KO and WT mucosa (Broere et al., 2007). A recent study has shown that CFTR activity is also dependent on NHERF-1 regulated cAMP compartmentalization and local protein kinase A activity in human airway epithelial cells (Monterisi et al., 2012). The particularly high expression of NHERF-1, as well as CFTR in pancreatic ducts, compared to other NHERFs and SLC26 anion transporters is quite different from the relative expression levels of these transporters and the NHERFs in the

small intestine (Hillesheim et al., 2007; Singh et al., 2010). These findings suggested to us that CFTR-NHERF-1 interaction may be crucial to pancreatic ductal secretion.

5.2. The effect of trypsin on pancreatic ductal HCO_3^- secretion

Until quite recently, the pathophysiological relevance of pancreatic ducts in acute pancreatitis has been neglected. However, there are important lines of evidence supporting the idea that pancreatic ducts play a role in the pathogenesis of pancreatitis: i) ductal fluid and HCO_3^- secretion are compromised in acute and chronic pancreatitis (Cavestro et al., 2010; Hegyi & Rakonczay, 2010), ii) one of the main endpoints of chronic pancreatitis is the destruction of the ductal system (Ectors et al., 1997; Kloppel et al., 2005), iii) mutations in CFTR may increase the risk of pancreatitis (Cavestro et al., 2010; Hegyi et al., 2011; Hegyi & Rakonczay, 2010; Nousia-Arvanitakis, 1999; Weiss et al., 2009), and iv) etiological factors for pancreatitis, such as bile acids or ethanol in high concentration, inhibit pancreatic ductal HCO_3^- secretion (Maléth et al., 2011; Venglovecz et al., 2008; Yamamoto et al., 2003) Despite the above mentioned data, the role of PDEC in the development of pancreatitis has received relatively little attention (Lee & Muallem, 2008).

There are important species differences regarding the localization of PAR-2 in pancreatic ducts and in the effect of PAR-2 activation on HCO_3^- secretion. For example, CAPAN-1 cells (Namkung et al., 2003) and dog PDEC (Nguyen et al., 1999) express PAR-2 only on the basolateral membrane, whereas bovine PDEC express PAR-2 on the luminal membrane (Alvarez et al., 2004). Therefore, one of our aims was to determine which animal model best mimics human PAR-2 expression and thus would be the best for studying the effects of trypsin on PDEC function. Our results showed that in the human pancreas PAR-2 is localized to the luminal membrane of small proximal pancreatic ducts, which are probably the major site of HCO_3^- and fluid secretion. Since CAPAN-1 cells and dog PDEC express PAR-2 only on the basolateral membrane, they do not mimic the human situation. Rats or mice are also not good models for the human gland because they secrete only 70-80 mM HCO_3^- (Padfield et al., 1989; Steward et al., 2005). However, the guinea pig pancreas secretes ~140 mM HCO_3^-, as does the human gland, and the regulation of HCO_3^- secretion is similar in both species (Padfield et al., 1989; Stewart et al., 2009). Since PAR-2 expression in the guinea pig pancreas was localized to the luminal membrane of duct cells, we performed our experiments on isolated guinea pig ducts.

First we characterized the effects of PAR-2 activation by trypsin and PAR-2-AP on PDEC. Previously, it has been shown that activation of the G-protein-coupled PAR-2 by proteinases requires proteolytic cleavage of the receptor, which is followed by an elevation of $[Ca^{2+}]_i$ (Bohm et al., 1996; Hoxie et al., 1993; Vergnolle, 2000). As expected, luminal trypsin and PAR2-AP caused a dose-dependent elevation of $[Ca^{2+}]_i$ in guinea pig ducts. Importantly, the trypsin inhibitor SBTI, PAR-2-ANT and the intracellular Ca^{2+} chelator BAPTA-AM all completely blocked the elevation of $[Ca^{2+}]_i$, whereas removal of extracellular Ca^{2+} had no effect. Acidosis (pH 6.8) also slightly reduced the changes in $[Ca^{2+}]_i$ evoked by trypsin, most probably due to reduced cleavage activity of trypsin at an acidic pH. Next we characterized the effects of PAR-2 activation on pH_i. Luminal application of trypsin and PAR-2-AP both caused a dose-dependent intracellular alkalosis in PDEC. This alkalosis is most likely explained either by a reduction in the rate of HCO_3^- efflux (i.e. secretion) across the apical membrane of PDEC or by an increase in the rate of HCO_3^- influx at the basolateral side of the cell. We favour the former explanation as luminal application of the anion exchange inhibitor, H_2DIDS, or the CFTR inhibitor, CFTRinh-172, produced a similar intracellular alkalization (Hegyi et al., 2005; Stewart et al., 2009). Thus, PAR-2 activation inhibits HCO_3^- secretion in PDEC by inhibiting SLC26 anion exchangers and CFTR expressed on the apical membrane of the duct cell. In similarity with the $[Ca^{2+}]_i$ signals, the effect of PAR-2 activation on pH_i was blocked by SBTI, PAR-2-ANT and BAPTA-AM; the action of BAPTA-AM suggesting that the inhibition of HCO_3^- secretion follows from the rise in $[Ca^{2+}]_i$. Interestingly, an elevation of $[Ca^{2+}]_i$ is crucial for both stimulatory [(e.g. acetylcholine (Argent, 2006), low concentrations of bile acids (Venglovecz et al., 2008) and ethanol (Yamamoto et al., 2003)] and inhibitory pathways (e.g. basolateral ATP, arginine vasopressin and high concentrations of ethanol) that control HCO_3^- secretion by PDEC. Such marked differences in the outcome of $[Ca^{2+}]_i$ signals in PDEC probably reflect differences in the source of Ca^{2+} and/or in the intracellular compartmentalisation of $[Ca^{2+}]_i$ signals generated by different secretory agonists and antagonists.

Remarkably, trypsin was still able to evoke an elevation of pH_i when Cl^- was removed from the duct lumen and when PDEC were pre-treated with H_2DIDS, conditions that should inhibit HCO_3^- efflux on the exchanger. These results suggested the involvement of CFTR, the only other known HCO_3^- efflux pathway on the apical membrane, in the inhibitory effect of trypsin. This hypothesis was confirmed by patch clamp experiments in which trypsin decreased CFTR whole cell currents in isolated guinea pig PDEC by 50-

60%. Finally, the fact that the trypsin-induced alkalinisation was completely blocked by a combination of CFTRinh-172 and H_2DIDS confirms the involvement of both CFTR and SLC26 anion exchangers. Our conclusion from these pH_i and patch clamp data is that PAR-2 activation inhibits both the SLC26 anion exchanger (probably PAT-1, Ko et al., 2002) as DRA is only weakly inhibited by disulfonic stilbenes (Chernova et al., 2003, Ko et al., 2002) and CFTR expressed on the apical membrane of the duct cell.

The pH of pancreatic juice [and therefore the luminal pH (pH_L) in the duct] can vary between approximately 6.8 and 8.0. It has recently been shown that protons co-released during exocytosis cause significant acidosis (up to 1 pH unit) in the lumen of the acini (Behrendorff et al., 2010). However, Ishiguro et al. (1998) have clearly shown that the pH_L in pancreatic ducts is dependent on the rate of HCO_3^- secretion. pH_L can be elevated from 7.2 to 8.5 by stimulation with secretin or forskolin and this effect was strictly dependent on the presence of HCO_3^- (Ishiguro et al., 1999; Ishiguro et al., 1998; Ishiguro et al., 1996). Also, inhibition of ductal HCO_3^- secretion with H_2DIDS can decrease the pH_L to below 8.0 (Ishiguro et al., 1998). In view of these results, we tested whether trypsinogen autoactivation was affected by pH over the range 6.0 to 8.5. Autoactivation of trypsinogen was relatively slow at pH 8.5, but decreasing the pH from 8.5 to 7 progressively stimulated autoactivation (data not shown). These results suggest that under physiological conditions HCO_3^- secretion by PDEC is not only important for elevating the pH in the duodenum, but also for keeping pancreatic enzymes in an inactive state in the ductal system of the gland.

Receptor down-regulation is a phenomenon that occurs in the continued presence of an agonist and leads to a reduction in the cell's sensitivity to the agonist. Potentially, there are two mechanisms that could underlie receptor down-regulation of PAR-2: i) after proteolytic activation, the PAR-2 is internalized by a clathrin-mediated mechanism and then targeted to lysosomes (Hoxie et al., 1993), and ii) if trypsin is present for a longer time in the lumen, PAR-2 may be down-regulated at the transcriptional level. In this study, we provide evidence that the second mechanism, transcriptional down-regulation, explains the reduced expression of PAR-2 seen in chronic pancreatitis.

Conflicting data can be found in the literature concerning the role of PAR-2 in acute pancreatitis. Namkung et al. (2004) concluded that PAR-2 might play a protective role in pancreatitis when they found that PAR-2 activation reduces the severity of rat secretagogue-induced pancreatitis. In contrast to these data, Singh et al. (2007) showed that in secretagogue-induced experimental pancreatitis, PAR-2 deletion is associated with a

more severe pancreatitis. Although Laukkarinen et al. (2008) confirmed these results of Singh in cerulein-induced pancreatitis, they also clearly showed that in taurocholate-induced pancreatitis, PAR-2 deletion markedly reduced the severity of the disease. There is no evidence to suggest that clinical pancreatitis is evoked by supramaximal secretagoge stimulation; however, the taurocholate-induced pancreatitis model may mimic the clinical situation. Therefore, Laukkarinen et al. (2008) speculated that PAR-2 activation promotes the worsening of clinical pancreatitis and our data are consistent with that hypothesis.

Besides the clear pathophysiological role of the trypsin-PAR-2 interaction in chronic pancreatitis, there is still a debate as to why PAR-2 is localized to the luminal membrane of PDEC in small ducts close to the acinar cells. What could the physiological role of this PAR-2 be? A number of agents have been shown to have dual effects on PDEC at different concentrations. For example, bile acids in low concentrations stimulate, but in high concentrations inhibit HCO_3^- secretion (Venglovecz et al., 2008). The same applies to ethanol (Yamamoto et al., 2003). Under physiological conditions, trypsin inhibitors are co-released from acinar cells with trypsinogen and should block the activity of any trypsin that is generated spontaneously. Therefore, only very small amounts of active trypsin, if any, will be present in the duct lumen under normal conditions. However, there remains a possibility that very small amounts of active trypsin (i.e. concentrations below 0.1 μM that would not cause a $[Ca^{2+}]_i$ elevation or pH change) could bind to PAR-2 on the luminal membrane of the ducts and augment other stimulatory mechanisms so as to enhance flushing of digestive enzymes down the ductal tree.

In conclusion, we suggest for the first time that one of the physiological roles of HCO_3^- secretion by PDEC is to curtail trypsinogen autoactivation within the pancreatic ductal system. However, if trypsin is present in the duct lumen (as may occur during the early stages of pancreatitis due to leakage from acinar cells), PAR-2 on the duct cell will be activated leading to Ca^{2+} release from intracellular stores and a rise in cytosolic Ca^{2+} concentration. This causes inhibition of the luminal anion exchangers and CFTR reducing HCO_3^- secretion by the duct cell. The fall in HCO_3^- secretion will increase the transit time of zymogens down the duct tree and decrease $pH_{L,}$ both of which will promote the autoactivation of trypsinogen. The trypsin so formed will further inhibit HCO_3^- transport leading to a vicious cycle generating further falls in pH_L and enhanced trypsinogen activation, which will favour development of the pancreatitis. Finally, the R122H mutant cationic trypsin also elevated $[Ca^{2+}]_i$ and pH_i in duct cells, suggesting that this mechanism

may be particularly important in hereditary pancreatitis in which the mutant trypsinogens more readily autoactivate (Sahin-Tóth & Tóth, 2000).

6. SUMMARY

Introduction: The main function of pancreatic ductal epithelial cells (PDEC) is to secrete an alkaline, HCO_3^--rich isotonic fluid. HCO_3^- secretion across the apical membrane of PDEC is thought to be mediated by cystic fibrosis transmembrane conductance regulator Cl^- channel (CFTR) and solute carrier family 26 (SLC26) anion exchangers. Na^+/H^+ exchanger regulatory factor isoform-1 (NHERF-1) is a cytosolic adaptor protein, which anchors CFTR on the apical membrane of epithelial cells. Pancreatic ducts not only have prominent roles physiologically, but also pathophysiologically. There is substantial evidence that the early intra-acinar or luminal activation of trypsinogen to trypsin is a key and common event in the development of acute pancreatitis. Several studies have demonstrated that trypsin stimulates digestive enzyme secretion from acinar cells via protease-activated receptor 2 (PAR-2), whereas the effect of trypsin on PDEC is somewhat controversial. Therefore, it is crucially important to understand the effects of trypsin on PDEC.

The **aims** of this work were to evaluate the role of NHERF-1 in pancreatic ductal localization of CFTR, and in HCO_3^- and fluid secretion and to investigate the effects of trypsin on pancreatic ductal HCO_3^- secretion.

Methods: Guinea pigs, human pancreatic tissue, wild-type (WT) and NHERF-1 knock-out (KO) mice were used for experiments. Intra- and interlobular pancreatic ducts were isolated from the animals. mRNA expression was detected by real-time reverse transcription polymerase chain reaction. The expression of CFTR and PAR-2 were analysed by immunohistochemistry. Pancreatic juice was collected from anesthetized mice in basal and secretin-stimulated conditions. Fluid secretion into the closed luminal space of the ducts was analysed using a swelling technique. Intracellular Ca^{2+} concentration ($[Ca^{2+}]_i$) and intracellular pH (pH_i) were determined by microfluorometry.

Results: CFTR, down-regulated in adenoma (DRA), putative anion transporter (PAT-1), NHERF-1 and NHERF-2, but not NHERF-3 mRNA were expressed in isolated pancreatic

ducts of WT mice. Apical CFTR staining was markedly reduced in the pancreatic ducts of mice lacking NHERF-1. The volume of pancreatic juice was significantly reduced in NHERF-1 KO vs. WT mice under both basal and secretin-stimulated conditions *in vivo*. Accordingly, the HCO_3^- and fluid secretory rate was significantly lower in ducts from KO vs. WT mice in standard HCO_3^-/CO_2 solution *in vitro*. PAR-2 was localized to the apical membrane of PDEC both in the human and in the guinea pig pancreas. Trypsin and PAR-2 activating peptide (PAR-2 AP) induced dose-dependent elevation of $[Ca^{2+}]_i$ and alkalisation of pH_i, and inhibited HCO_3^- secretion via the luminal anion exchanger and the CFTR. Our functional data clearly show that the pH_i and $[Ca^{2+}]_i$ responses to luminal administration of either trypsin or PAR-2-AP were markedly diminished in PAR-2 KO PDEC. 1 μm of R122H cationic trypsin causes comparable changes in pH_i and $[Ca^{2+}]_i$ to 0.4 μM wild-type trypsin. Finally, PAR-2 expression was strongly down-regulated in the pancreatic ducts of patients suffering from chronic or acute pancreatitis, consistent with elevated intraductal trypsin activity in these diseases.

Conclusion: NHERF-1 is required for the localization of CFTR on the apical membrane of PDEC. NHERF-1 is involved in both pancreatic ductal HCO_3^- and fluid secretion. Both basal and cAMP-stimulated secretion was affected in the transgenic animals, but this effect was not caused by alterations in pancreatic blood flow.

Under pathophysiological conditions, if tryspin is present in the duct lumen, trypsin compromises pancreatic ductal bicarbonate secretion via a PAR-2 dependent inhibition of the apical anion exchanger and CFTR. This may contribute to the development of chronic pancreatitis.

7. ACKNOWLEDGEMENTS

I would like to thank all of the people who have helped and inspired me during my doctoral studies.

I am grateful to **Prof. Dr. Tibor Wittmann**, the head of the First Department of Medicine and to **Prof. Dr. András Varró**, the head of Department of Pharmacology and Pharmacotherapy, who gave me opportunity to work their Departments.

I would like express my deep and sincere gratitude to my supervisors **Dr. Zoltán Rakonczay Jr.** and **Prof. Dr. Péter Hegyi** for their support and guidance. Their wide knowledge and their logical way of thinking have been of great value for me. Their understanding and encouragement provided a good basis for this present thesis.

I would also like to thank my colleagues and friends, **Dr. József Maléth, Dr. Klaudia Farkas, Zsolt Balla, Dr. Viktória Venglovecz, Dr. Béla Ózsvári, Éva Kunstár, Andrea Geisz, Andrea Schnúr, Dr. Balázs Kui, Dr. Mátyás Czepán, Máté Katona, Dr. Anita Balázs, Dr. Eszter Végh** for all the emotional support, entertainment and care they provided.

This work would not have been possible to accomplish without the assistance of **Edit Magyarné Pálfi, Tünde Pritz, Zsoltné Árva, Miklósné Árva, Zoltánné Fuksz and Etus Enyinginé.**

I am deeply grateful to Prof. **Dr. Ursula Seidler and her research team** at the Hannover Medical School, Germany for their collaboration.

This work was supported by National Development Agency grants (TÁMOP-4.2.2.A-11/1/KONV-2012-0035, TÁMOP-4.2.2.A-11/1/KONV-2012-0073, TÁMOP-4.2.2-11/1/KONV-2012-0052), by the Hungarian Scientific Research Fund (NF105758 to Z.R., NF100677 to P.H., K101116 to T.T., and PD78087 to V.V.), by the Hungarian Academy of Sciences (BO 00334/08/5 to P.H., BO 00174/10/5 to Z.R., and DFG/192 to Z.R. and P.H.) and the Deutsche Forschungsgemeinschaft (Se460/13-4, SFB621/C9 and the Deutsch-Ungarisches Kooperationsprojekt DFG-436 UNG 113/190/01 to U.S.).

Lastly, I owe warm thanks to **my mother and my husband** for all their love, support, never-ending patience and encouragement. I dedicate this thesis to them.

8. REFERENCES

1. Alvarez C, Regan JP, Merianos D, Bass BL, 2004. Protease-activated receptor-2 regulates bicarbonate secretion by pancreatic duct cells in vitro. *Surgery* **136**, 669-76.

2. Apte MV, Pirola RC, Wilson JS, 2006. Fatty acid ethyl esters-alcohol's Henchmen in the pancreas? *Gastroenterology* **130**, 992-5.

3. Aravind L, Koonin EV, 2000. The STAS domain - a link between anion transporters and antisigma-factor antagonists. *Curr Biol* **10**, R53-5.

4. Argent BE. Cell Physiology of Pancreatic Ducts. In:Johnson LR, ed. Physiology of the Gastrointestinal Tract.Volume 2. 4 ed. San Diego:Elsevier,2006:1376-1396.

5. Argent BE, Arkle S, Cullen MJ, Green R, 1986. Morphological, biochemical and secretory studies on rat pancreatic ducts maintained in tissue culture. *Q J Exp Physiol* **71**, 633-48.

6. Behrendorff N, Floetenmeyer M, Schwiening C, Thorn P, 2010. Protons released during pancreatic acinar cell secretion acidify the lumen and contribute to pancreatitis in mice. *Gastroenterology* **139**, 1711-20, 20 e1-5.

7. Benharouga M, Sharma M, So J, *et al.*, 2003. The role of the C terminus and Na^+/H^+ exchanger regulatory factor in the functional expression of cystic fibrosis transmembrane conductance regulator in nonpolarized cells and epithelia. *J Biol Chem* **278**, 22079-89.

8. Bohm SK, Khitin LM, Grady EF, *et al.*, 1996. Mechanisms of desensitization and resensitization of proteinase-activated receptor-2. *J Biol Chem* **271**, 22003-16.

9. Bradford MM, 1976. A rapid and sensitive method for the quantitation of microgram quantities of protein utilizing the principle of protein-dye binding. *Anal Biochem* **72**, 248-54.

10. Broere N, Hillesheim J, Tuo B, *et al.*, 2007. Cystic fibrosis transmembrane conductance regulator activation is reduced in the small intestine of Na^+/H^+ exchanger 3 regulatory factor 1 (NHERF-1)-but not NHERF-2-deficient mice. *J Biol Chem* **282**, 37575-84.

11. Brone B, Eggermont J, 2005. PDZ proteins retain and regulate membrane transporters in polarized epithelial cell membranes. *Am J Physiol Cell Physiol* **288**, C20-9.

12. Burghardt B, Elkaer ML, Kwon TH, *et al.*, 2003. Distribution of aquaporin water channels AQP1 and AQP5 in the ductal system of the human pancreas. *Gut* **52**, 1008-16.

13. Cavestro GM, Zuppardo RA, Bertolini S, *et al.*, 2010. Connections between genetics and clinical data: Role of MCP-1, CFTR, and SPINK-1 in the setting of acute, acute recurrent, and chronic pancreatitis. *Am J Gastroenterol* **105**, 199-206.

14. Chernova MN, Jiang L, Shmukler BE, *et al.*, 2003. Acute regulation of the SLC26A3 congenital chloride diarrhoea anion exchanger (DRA) expressed in Xenopus oocytes. *J Physiol* **549**, 3-19.

15. Cinar A, Chen M, Riederer B, *et al.*, 2007. NHE3 inhibition by cAMP and Ca^{2+} is abolished in PDZ-domain protein PDZK1-deficient murine enterocytes. *J Physiol* **581**, 1235-46.

16. Criddle DN, Murphy J, Fistetto G, *et al.*, 2006. Fatty acid ethyl esters cause pancreatic calcium toxicity via inositol trisphosphate receptors and loss of ATP synthesis. *Gastroenterology* **130**, 781-93.

17. Criddle DN, Raraty MG, Neoptolemos JP, *et al.*, 2004. Ethanol toxicity in pancreatic acinar cells: mediation by nonoxidative fatty acid metabolites. *Proc Natl Acad Sci U S A* **101**, 10738-43.

18. Ectors N, Maillet B, Aerts R, *et al.*, 1997. Non-alcoholic duct destructive chronic pancreatitis. *Gut* **41**, 263-8.

19. Fedail SS, Harvey RF, Salmon PR, *et al.*, 1979. Trypsin and lactoferrin levels in pure pancreatic juice in patients with pancreatic disease. *Gut* **20**, 983-6.

20. Fernandez-Salazar MP, Pascua P, Calvo JJ, *et al.*, 2004. Basolateral anion transport mechanisms underlying fluid secretion by mouse, rat and guinea-pig pancreatic ducts. *J Physiol* **556**, 415-28.

21. Geokas MC, Rinderknecht H, 1974. Free proteolytic enzymes in pancreatic juice of patients with acute pancreatitis. *Am J Dig Dis* **19**, 591-8.

22. Gerasimenko JV, Lur G, Sherwood MW, *et al.*, 2009. Pancreatic protease activation by alcohol metabolite depends on Ca^{2+} release via acid store IP_3 receptors. *Proc Natl Acad Sci U S A* **106**, 10758-63.

23. Gray MA, Winpenny JP, Porteous DJ, *et al.*, 1994. CFTR and calcium-activated chloride currents in pancreatic duct cells of a transgenic CF mouse. *Am J Physiol* **266**, C213-21.

24. Greeley T, Shumaker H, Wang Z, *et al.*, 2001. Downregulated in adenoma and putative anion transporter are regulated by CFTR in cultured pancreatic duct cells. *Am J Physiol Gastrointest Liver Physiol* **281**, G1301-8.

25. Guggino WB, 2004. The cystic fibrosis transmembrane regulator forms macromolecular complexes with PDZ domain scaffold proteins. *Proc Am Thorac Soc* **1**, 28-32.

26. Guggino WB, Stanton BA, 2006. New insights into cystic fibrosis: molecular switches that regulate CFTR. *Nat Rev Mol Cell Biol* **7**, 426-36.
27. Hall RA, Premont RT, Chow CW, *et al.*, 1998. The beta2-adrenergic receptor interacts with the Na^+/H^+-exchanger regulatory factor to control Na^+/H^+ exchange. *Nature* **392**, 626-30.

28. Hegyi P, Pandol S, Venglovecz V, Rakonczay Z, Jr., 2011. The acinar-ductal tango in the pathogenesis of acute pancreatitis. *Gut* **60**, 544-52.

29. Hegyi P, Rakonczay Z, 2010. Insufficiency of electrolyte and fluid secretion by pancreatic ductal cells leads to increased patient risk for pancreatitis. *Am J Gastroenterol* **105**, 2119-20.

30. Hegyi P, Rakonczay Z, Jr., Gray MA, Argent BE, 2004. Measurement of intracellular pH in pancreatic duct cells: a new method for calibrating the fluorescence data. *Pancreas* **28**, 427-34.

31. Hegyi P, Rakonczay Z, Jr., Tiszlavicz L, *et al.*, 2005. Protein kinase C mediates the inhibitory effect of substance P on HCO_3^- secretion from guinea pig pancreatic ducts. *Am J Physiol Cell Physiol* **288**, C1030-41.

32. Hillesheim J, Riederer B, Tuo B, *et al.*, 2007. Down regulation of small intestinal ion transport in PDZK1- (CAP70/NHERF3) deficient mice. *Pflugers Arch* **454**, 575-86.

33. Hoxie JA, Ahuja M, Belmonte E, *et al.*, 1993. Internalization and recycling of activated thrombin receptors. *J Biol Chem* **268**, 13756-63.

34. Ignáth I, Hegyi P, Venglovecz V, *et al.*, 2009. CFTR expression but not Cl^- transport is involved in the stimulatory effect of bile acids on apical Cl^-/HCO_3^- exchange activity in human pancreatic duct cells. *Pancreas* **38**, 921-9.

35. Ishiguro H, Namkung W, Yamamoto A, *et al.*, 2007. Effect of Slc26a6 deletion on apical Cl^-/HCO_3^- exchanger activity and cAMP-stimulated bicarbonate secretion in pancreatic duct. *Am J Physiol Gastrointest Liver Physiol* **292**, G447-55.

36. Ishiguro H, Naruse S, Kitagawa M, *et al.*, 1999. Luminal ATP stimulates fluid and HCO3- secretion in guinea-pig pancreatic duct. *J Physiol* **519 Pt 2**, 551-8.

37. Ishiguro H, Naruse S, Steward MC, *et al.*, 1998. Fluid secretion in interlobular ducts isolated from guinea-pig pancreas. *J Physiol* **511 (Pt 2)**, 407-22.

38. Ishiguro H, Steward MC, Sohma Y, *et al.*, 2002. Membrane potential and bicarbonate secretion in isolated interlobular ducts from guinea-pig pancreas. *J Gen Physiol* **120**, 617-28.

39. Ishiguro H, Steward MC, Wilson RW, Case RM, 1996. Bicarbonate secretion in interlobular ducts from guinea-pig pancreas. *J Physiol* **495 (Pt 1)**, 179-91.

40. Ishiguro H, Yamamoto A, Nakakuki M, *et al.*, 2012. Physiology and pathophysiology of bicarbonate secretion by pancreatic duct epithelium. *Nagoya J Med Sci* **74**, 1-18.
41. Jakab RL, Collaco AM, Ameen NA, 2011. Physiological relevance of cell-specific distribution patterns of CFTR, NKCC1, NBCe1, and NHE3 along the crypt-villus axis in the intestine. *Am J Physiol Gastrointest Liver Physiol* **300**, G82-98.

42. Kawabata A, Matsunami M, Tsutsumi M, *et al.*, 2006. Suppression of pancreatitis-related allodynia/hyperalgesia by proteinase-activated receptor-2 in mice. *Br J Pharmacol* **148**, 54-60.

43. Kloppel G, Luttges J, Sipos B, *et al.*, 2005. Autoimmune pancreatitis: pathological findings. *JOP* **6**, 97-101.

44. Knauf F, Yang CL, Thomson RB, *et al.*, 2001. Identification of a chloride-formate exchanger expressed on the brush border membrane of renal proximal tubule cells. *Proc Natl Acad Sci U S A* **98**, 9425-30.

45. Ko SB, Shcheynikov N, Choi JY, *et al.*, 2002. A molecular mechanism for aberrant CFTR-dependent HCO_3^- transport in cystic fibrosis. *Embo J* **21**, 5662-72.

46. Ko SB, Zeng W, Dorwart MR, *et al.*, 2004. Gating of CFTR by the STAS domain of SLC26 transporters. *Nat Cell Biol* **6**, 343-50.

47. Kukor Z, Mayerle J, Kruger B, *et al.*, 2002. Presence of cathepsin B in the human pancreatic secretory pathway and its role in trypsinogen activation during hereditary pancreatitis. *J Biol Chem* **277**, 21389-96.

48. Lamprecht G, Heil A, Baisch S, *et al.*, 2002. The down regulated in adenoma (dra) gene product binds to the second PDZ domain of the NHE3 kinase A regulatory protein (E3KARP), potentially linking intestinal Cl^-/HCO_3^- exchange to Na^+/H^+ exchange. *Biochemistry* **41**, 12336-42.

49. Lamprecht G, Seidler U, 2006. The emerging role of PDZ adapter proteins for regulation of intestinal ion transport. *Am J Physiol Gastrointest Liver Physiol* **291**, G766-77.

50. Laukkarinen JM, Weiss ER, Van Acker GJ, *et al.*, 2008. Protease-activated receptor-2 exerts contrasting model-specific effects on acute experimental pancreatitis. *J Biol Chem* **283**, 20703-12.

51. Lee MG, Muallem S, 2008. Pancreatitis: the neglected duct. *Gut* **57**, 1037-9.

52. Lee M, Muallem S. Physiology of duct cell secretion. In: The Pancreas, edited by Beger H, Warshaw A, Büchler M, *et al.* Second ed. Massachusetts: Blackwell Publishing Ltd., 2008:78-90.

53. Lerch MM, Gorelick FS, 2000. Early trypsinogen activation in acute pancreatitis. *Med Clin North Am* **84**, 549-63.

54. Li C, Naren AP, 2005. Macromolecular complexes of cystic fibrosis transmembrane conductance regulator and its interacting partners. *Pharmacol Ther* **108**, 208-23.
55. Lohi H, Lamprecht G, Markovich D, *et al.*, 2003. Isoforms of SLC26A6 mediate anion transport and have functional PDZ interaction domains. *Am J Physiol Cell Physiol* **284**, C769-79.

56. Lukács GL, Verkman AS, 2012. CFTR: folding, misfolding and correcting the DeltaF508 conformational defect. *Trends Mol Med* **18**, 81-91.

57. Maléth J, Venglovecz V, Rázga Z, *et al.*, 2011. Non-conjugated chenodeoxycholate induces severe mitochondrial damage and inhibits bicarbonate transport in pancreatic duct cells. *Gut* **60**, 136-8.

58. Meier PJ, 1995. Molecular mechanisms of hepatic bile salt transport from sinusoidal blood into bile. *Am J Physiol* **269**, G801-12.

59. Milewski MI, Mickle JE, Forrest JK, *et al.*, 2001. A PDZ-binding motif is essential but not sufficient to localize the C terminus of CFTR to the apical membrane. *J Cell Sci* **114**, 719-26.

60. Monterisi S, Favia M, Guerra L, *et al.*, 2012. CFTR regulation in human airway epithelial cells requires integrity of the actin cytoskeleton and compartmentalized cAMP and PKA activity. *J Cell Sci* **125**, 1106-17.

61. Moyer BD, Denton J, Karlson KH, *et al.*, 1999. A PDZ-interacting domain in CFTR is an apical membrane polarization signal. *J Clin Invest* **104**, 1353-61.

62. Namkung W, Han W, Luo X, *et al.*, 2004. Protease-activated receptor 2 exerts local protection and mediates some systemic complications in acute pancreatitis. *Gastroenterology* **126**, 1844-59.

63. Namkung W, Lee JA, Ahn W, *et al.*, 2003. Ca^{2+} activates cystic fibrosis transmembrane conductance regulator- and Cl^- -dependent HCO_3 transport in pancreatic duct cells. *J Biol Chem* **278**, 200-7.

64. Nguyen TD, Moody MW, Steinhoff M, *et al.*, 1999. Trypsin activates pancreatic duct epithelial cell ion channels through proteinase-activated receptor-2. *J Clin Invest* **103**, 261-9.

65. Nousia-Arvanitakis S, 1999. Cystic fibrosis and the pancreas: recent scientific advances. *J Clin Gastroenterol* **29**, 138-42.

66. Ostedgaard LS, Randak C, Rokhlina T, *et al.*, 2003. Effects of C-terminal deletions on cystic fibrosis transmembrane conductance regulator function in cystic fibrosis airway epithelia. *Proc Natl Acad Sci U S A* **100**, 1937-42.

67. Padfield PJ, Garner A, Case RM, 1989. Patterns of pancreatic secretion in the anaesthetised guinea pig following stimulation with secretin, cholecystokinin octapeptide, or bombesin. *Pancreas* **4**, 204-9.

68. Petersen OH. Physiology of acinar cell secretion. In: The Pancreas, edited by Beger H, Warshaw A, Büchler M, *et al.* Second ed. Massachusetts: Blackwell Publishing Ltd., 2008:71-77.

69. Petersen OH, Sutton R, 2006. Ca^{2+} signalling and pancreatitis: effects of alcohol, bile and coffee. *Trends Pharmacol Sci* **27**, 113-20.

70. Preston GM, Carroll TP, Guggino WB, Agre P, 1992. Appearance of water channels in Xenopus oocytes expressing red cell CHIP28 protein. *Science* **256**, 385-7.

71. Raghuram V, Mak DO, Foskett JK, 2001. Regulation of cystic fibrosis transmembrane conductance regulator single-channel gating by bivalent PDZ-domain-mediated interaction. *Proc Natl Acad Sci U S A* **98**, 1300-5.

72. Rakonczay Z, Jr., Hegyi P, Hasegawa M, *et al.*, 2008. CFTR gene transfer to human cystic fibrosis pancreatic duct cells using a Sendai virus vector. *J Cell Physiol* **214**, 442-55.

73. Renner IG, Rinderknecht H, Douglas AP, 1978. Profiles of pure pancreatic secretions in patients with acute pancreatitis: the possible role of proteolytic enzymes in pathogenesis. *Gastroenterology* **75**, 1090-8.

74. Riordan JR, 2005. Assembly of functional CFTR chloride channels. *Annu Rev Physiol* **67**, 701-18.

75. Rossmann H, Jacob P, Baisch S, *et al.*, 2005. The CFTR associated protein CAP70 interacts with the apical Cl^-/HCO_3^- exchanger DRA in rabbit small intestinal mucosa. *Biochemistry* **44**, 4477-87.

76. Sahin-Tóth M, Tóth M, 2000. Gain-of-function mutations associated with hereditary pancreatitis enhance autoactivation of human cationic trypsinogen. *Biochem Biophys Res Commun* **278**, 286-9.

77. Schmidlin F, Amadesi S, Dabbagh K, *et al.*, 2002. Protease-activated receptor 2 mediates eosinophil infiltration and hyperreactivity in allergic inflammation of the airway. *J Immunol* **169**, 5315-21.

78. Schweinfest CW, Henderson KW, Suster S, *et al.*, 1993. Identification of a colon mucosa gene that is down-regulated in colon adenomas and adenocarcinomas. *Proc Natl Acad Sci U S A* **90**, 4166-70.

79. Shenolikar S, Voltz JW, Cunningham R, Weinman EJ, 2004. Regulation of ion transport by the NHERF family of PDZ proteins. *Physiology (Bethesda)* **19**, 362-9.

80. Shenolikar S, Voltz JW, Minkoff CM, *et al.*, 2002. Targeted disruption of the mouse NHERF-1 gene promotes internalization of proximal tubule sodium-phosphate cotransporter type IIa and renal phosphate wasting. *Proc Natl Acad Sci U S A* **99**, 11470-5.

81. Singh AK, Riederer B, Chen M, *et al.*, 2010. The switch of intestinal Slc26 exchangers from anion absorptive to HCO_3^- secretory mode is dependent on CFTR anion channel function. *Am J Physiol Cell Physiol* **298**, C1057-65.

82. Singh AK, Riederer B, Krabbenhoft A, *et al.*, 2009. Differential roles of NHERF1, NHERF2, and PDZK1 in regulating CFTR-mediated intestinal anion secretion in mice. *J Clin Invest* **119**, 540-50.

83. Singh VP, Bhagat L, Navina S, *et al.*, 2007. Protease-activated receptor-2 protects against pancreatitis by stimulating exocrine secretion. *Gut* **56**, 958-64.

84. Sohma Y, Gray MA, Imai Y, Argent BE, 2000. HCO_3^- transport in a mathematical model of the pancreatic ductal epithelium. *J Membr Biol* **176**, 77-100.

85. Steward MC, Ishiguro H, Case RM, 2005. Mechanisms of bicarbonate secretion in the pancreatic duct. *Annu Rev Physiol* **67**, 377-409.

86. Stewart AK, Yamamoto A, Nakakuki M, *et al.*, 2009. Functional coupling of apical Cl^-/HCO_3^- exchange with CFTR in stimulated HCO_3^- secretion by guinea pig interlobular pancreatic duct. *Am J Physiol Gastrointest Liver Physiol* **296**, G1307-17.

87. Swiatecka-Urban A, Duhaime M, Coutermarsh B, *et al.*, 2002. PDZ domain interaction controls the endocytic recycling of the cystic fibrosis transmembrane conductance regulator. *J Biol Chem* **277**, 40099-105.

88. Thrower EC, Gorelick FS, Husain SZ, 2010. Molecular and cellular mechanisms of pancreatic injury. *Curr Opin Gastroenterol* **26**, 484-9.

89. Tuo B, Riederer B, Wang Z, *et al.*, 2006. Involvement of the anion exchanger SLC26A6 in prostaglandin E2- but not forskolin-stimulated duodenal HCO_3^- secretion. *Gastroenterology* **130**, 349-58.

90. Tympner F, 1981. Selectively aspirated pure pancreatic secretion. Viscosity, trypsin activity, protein concentration and lactoferrin content of pancreatic juice in chronic pancreatitis. *Hepatogastroenterology* **28**, 169-72.

91. Tympner F, Rosch W, 1978. Viscosity and trypsin activity of pure pancreatic juice in chronic pancreatitis. *Acta Hepatogastroenterol (Stuttg)* **25**, 73-6.

92. Venglovecz V, Rakonczay Z, Jr., Ózsvári B, *et al.*, 2008. Effects of bile acids on pancreatic ductal bicarbonate secretion in guinea pig. *Gut* **57**, 1102-12.

93. Vergnolle N, 2000. Review article: proteinase-activated receptors - novel signals for gastrointestinal pathophysiology. *Aliment Pharmacol Ther* **14**, 257-66.

94. Verkman AS, Mitra AK, 2000. Structure and function of aquaporin water channels. *Am J Physiol Renal Physiol* **278**, F13-28.

95. Weinman EJ, Steplock D, Tate K, *et al.*, 1998. Structure-function of recombinant Na/H exchanger regulatory factor (NHE-RF). *J Clin Invest* **101**, 2199-206.
96. Weiss FU, Simon P, Bogdanova N, *et al.*, 2009. Functional characterisation of the CFTR mutations M348V and A1087P from patients with pancreatitis suggests functional interaction between CFTR monomers. *Gut* **58**, 733-4.

97. Yamamoto A, Ishiguro H, Ko SB, *et al.*, 2003. Ethanol induces fluid hypersecretion from guinea-pig pancreatic duct cells. *J Physiol* **551**, 917-26.

9. ANNEX

A NA^+/H^+ CSERÉLŐ SZABÁLYOZÓ FAKTOR 1 ÉS A TRIPSZIN SZEREPE A HASNYÁLMIRIGY VEZETÉKSEJTEK BIKARBONÁT SZEKRÉCIÓJÁBAN

Tézis kivonat

BEVEZETÉS

A pankreász vezetéksejtek fő feladata egy izotóniás, HCO_3^--ban gazdag folyadék szekréciója, mely kimossa az acinusok által termelt emésztőenzimeket a pankreász duktális rendszeréből, illetve a duodenumba jutva semlegesíti a gyomornedv savas pH-ját. A HCO_3^- a pankreász duktális epithel sejtek (PDEC) bazolaterális membránján keresztül jut be a sejtbe, majd a luminális membránon elhelyezkedő SLC26 családba tartozó anion cserélők (SLC26A3, down regulated in adenoma, DRA és SLC26A6, putative anion transporter 1, PAT-1) és a cisztás fibrózis transzmembrán konduktancia regulátor (CFTR) együttes működésével szekretálódik a pankreász vezeték lumenébe. A szekréció pontos mechanizmusa nem ismert, de a CFTR alapvető szerepe a folyamatban bizonyított, így a CFTR megfelelő lokalizációja a PDEC luminális membránján alapvető fontosságú. A Na^+/H^+ cserélő szabályozó faktor 1 (NHERF-1) egy citoszolikus adaptor fehérje, amely számos transzporter és csatorna (pl. CFTR) megfelelő lokalizációját biztosítja az epithel sejteken. Az NHERF-1 szerepét korábban már bizonyították több fiziológiai és patofiziológiai folyamatban, de a pankreász vonatkozásában még nem vizsgálták.

A pankreász vezetéksejtek az élettani folyamatokban betöltött szerepük mellett, nagy jelentőséggel bírnak a kórélettani folyamatok tekintetében is. Az elmúlt években számos tanulmány jelent meg, mely kimutatta, hogy a duktális rendszer alapvető szerepet játszhat az akut pankreátitisz kialakulásában, mint a toxikus ágensek (epesavak, etanol, tripszin) támadásának elsődleges célpontja. A pankreász duktuszok pankreátitiszben betöltött szerepének tisztázása érdekében elkerülhetetlen a tripszin hatásának vizsgálata. A tripszin a pankreász legfőbb emésztőenzime, amely inaktív formában, zimogénként termelődik, és fiziológiás körülmények között a vékonybélben, az enteropeptidáz hatására aktiválódik. Kóros körülmények között a tripszinogén a pankreászon belül aktiválódhat, mely gyulladás kialakulásához vezethet. Az eddig megjelent közlemények alapján a

tripszin hatása a PDEC-en ellentmondásos. Számos eredmény azt mutatja, hogy a tripszin aktiválja az ioncsatornák (Ca^{2+}-aktiválta Cl^- és K^+ csatorna) működését kutyában, és serkenti a HCO_3^- szekréciót CAPAN-1 sejtekben. Ezzel ellentétben kimutatták, hogy a tripszin dózis-függően gátolja a HCO_3^- szekréciót marha PDEC-n.

CÉLKITŰZÉSEK

Kísérleteink fő célja a pankreász vezetéksejtek HCO_3^- szekréciójának vizsgálata fiziológiás és patofiziológiás körülmények között. Specifikus céljaink:

1. A NHERF-1 szerepének vizsgálata a CFTR lokalizációjában a pankreász vezetéksejteken, valamint a HCO_3^- és folyadék szekrécióban.

2. A tripszin hatásának vizsgálata a hasnyálmirigy vezetéksejtek HCO_3^- szekréciójában.

ANYAGOK ÉS MÓDSZEREK

Kísérleteinkhez tengerimalacokat, illetve vad-típusú (VT) és knock-out (KO) egereket használtunk. A vizsgálatokhoz inter- és intralobuláris duktuszokat izoláltunk. Az mRNS expressziós mintázat meghatározásához valós-idejű polimeráz láncreakciót alkalmaztunk. A NHERF-1, CFTR és proteáz aktiválta receptor 2 (PAR-2) lokalizációját a pankreászban immunhisztokémia segítségével határoztuk meg. Az intracelluláris pH (pH_i) és Ca^{2+} koncentráció ($[Ca^{2+}]_i$) méréséhez mikrofluorimetriát és mikroperfúziót használtunk. A folyadékszekréció mértékét hízásos technika felhasználásával mértük *in vitro*. Uretánnal altatott állatokból pankreász nedvet gyűjtöttünk *in vivo*. A szekretin hatását a pankreász mikrokeringésére intravitál video mikroszkópiával vizsgáltuk. A statisztikai analízishez a SigmaPlot szofvert használtuk.

EREDMÉNYEK

I. A NHERF-1 szerepe a hasnyálmirigy vezetéksejtek HCO_3^- és folyadék szekréciójában

1. Kísérleteink során kimutattuk, hogy a CFTR, DRA, PAT-1, NHERF-1 és NHERF-2 mRNS expresszálódik a VT egerekből izolált pankreász duktuszokon.

2. A NHERF-1 fehérje nagyfokú expressziót mutat a VT egerek PDEC apikális membránján, míg a pankreász acinus sejteken gyengén festődik. NHERF-1 KO

egerekben nem látható NHERF-1 festődés. A CFTR mind a VT, mind a NHERF-1 KO állatok pankreász acinus és duktusz sejtjein is detektálható. NHERF-1 hiányában a CFTR festődés erősen csökken a pankreász duktuszokban a VT állatokhoz képest.

3. Mindhárom általunk használt módszerrel (inhibitor stop, regeneráció alkalózisból és luminális Cl^- elvonás) kimutattuk, hogy a pankreász duktális HCO_3^- szekréció szignifikánsan csökkent a NHERF-1 KO állatokban, a VT egerekben mért értékhez képest.

4. A folyadékszekréciós kísérletek hasonló eredményt mutattak. Mind alap, mind stimulált (szekretin/forskolin) körülmények között jelentős mértékben alacsonyabb folyadékszekréciós értéket kaptunk NHERF-1 KO egerekben *in vitro* és *in vivo* egyaránt.

5. A pankreász mikrokeringésének tekintetében sem alap, sem szekretin-stimulált állapotban nem találtunk szignifikáns különbséget a VT és NHERF-1 KO állatok között.

II. A tripszin hatásának vizsgálata pankreász vezetéksejtek HCO_3^- szekréciójában

1. Kísérleteink során megállapítottuk, hogy a pankreász acinusok közelében lévő intralobuláris (kis) duktuszok luminális membránja felől PAR-2 receptorok expresszálódnak mind a tengerimalac, mind az ember esetében.

2. A luminális membrán felől adott PAR-2 aktiváló peptid (PAR-2-AP) dózis-függő $[Ca^{2+}]_i$ emelkedést okozott, amely emelkedés Ca^{2+} kelátor BAPTA-AM adásával és PAR-2 antagonistával (PAR-2-ant) kivédhető volt. Az extracelluláris Ca^{2+} elvonása nem volt hatással a PAR-2-AP által kiváltott $[Ca^{2+}]_i$ emelkedésre.

3. A tripszin ugyancsak dózis-függő $[Ca^{2+}]_i$ emelkedést okozott a luminális oldal felől, amely teljesen blokkolható volt Ca^{2+} kelátor BAPTA-AM adásával, PAR-2-ant-val és szójabab tripszin inhibitor alkalmazásával. Az extracelluláris Ca^{2+} elvonása nem volt hatással a tripszin által kiváltott $[Ca^{2+}]_i$ emelkedésre sem.

4. A luminális membrán felől adott tripszin és PAR-2-AP alkalózist indukált, ami PAR-2-ant és tripszin inhibitor hatására kivédhető volt. A luminális Cl^- elvonás,

H_2DIDS és CFTR inhibitor pH_i emelkedést váltott ki, amely emelkedést a tripszin alkalmazása tovább fokozott. A H_2DIDS és CFTR inhibitor együttes alkalmazása jelentősen csökkentette a tripszin pH_i-ra kifejtett hatását.

5. Krónikus pankreátitiszes betegek hasnyálmirigyében a PAR-2 mRNS és a membránban lévő PAR-2 fehérje szintje nagymértékben lecsökkent. Ez a változás nem volt tapasztalható a PAR-2 fehérje citoplazmában mérhető szintjében.

6. Az R122H mutáns kationos tripszinogén hasonló változást okozott a $[Ca^{2+}]_i$ és pH_i vonatkozásában mint a tripszin, így a tripszin-mediálta HCO_3^- csökkenés szerepet játszhat az örökletes pankreátitisz patogenezisében is.

7. Végül kimutattuk, hogy mind a tripszin, mind a PAR-2-AP $[Ca^{2+}]_i$-ra és pH_i-ra kifejtett hatása szignifikánsan csökkent PAR-2 KO egerekben.

KÖVETKEZTETÉSEK

Munkánk során kimutattuk, hogy a NHERF-1 szükséges a CFTR lokalizációjához a PDEC apikális membránján. Továbbá a NHERF-1 szerepet játszik a PDEC HCO_3^- és folyadék szekréciójában. Mind az alap, mind a stimulált szekréció tekintetében különbséget mutattunk ki a VT és KO egerek között, de ezt az eltérést nem a hasnyálmirigy vérkeringésében bekövetkező változás okozta.

Pathológiás körülmények között, ha a tripszin jelen van a hasnyálmirigy vezetéksejtek lumenében, a tripszin PAR-2-függő módon csökkenti a hasnyálmirigy vezetéksejtek HCO_3^- szekrécióját a luminális anion cserélő, valamint a CFTR gátlásán keresztül. Ez a folyamat szerepet játszhat a krónikus hasnyálmirigy-gyulladás kialakulásában.

Articles closely related to the subject of the thesis

I.

Trypsin Reduces Pancreatic Ductal Bicarbonate Secretion by Inhibiting CFTR Cl^- Channels and Luminal Anion Exchangers

PETRA PALLAGI,* VIKTÓRIA VENGLOVECZ,‡ ZOLTÁN RAKONCZAY Jr,* KATALIN BORKA,§ ANNA KOROMPAY,§ BÉLA ÓZSVÁRI,* LINDA JUDÁK,* MIKLÓS SAHIN–TÓTH,‖ ANDREA GEISZ,*,‖ ANDREA SCHNÚR,*,‖ JÓZSEF MALÉTH,* TAMÁS TAKÁCS,* MIKE A. GRAY,¶ BARRY E. ARGENT,¶ JULIA MAYERLE,# MARKUS M. LERCH,# TIBOR WITTMANN,* and PÉTER HEGYI*

*First Department of Medicine and ‡Department of Pharmacology, University of Szeged, Szeged, Hungary; §2nd Department of Pathology, Semmelweis University, Budapest, Hungary; ‖Department of Molecular and Cell Biology, Henry M. Goldman School of Dental Medicine, Boston University, Boston, Massachusetts; ¶Institute for Cell & Molecular Biosciences, Newcastle University, Newcastle upon Tyne, England; and #Department of Medicine A, Greifswald University Hospital, Greifswald, Germany

BACKGROUND & AIMS: The effects of trypsin on pancreatic ductal epithelial cells (PDECs) vary among species and depend on the localization of proteinase-activated receptor 2 (PAR-2). We compared PAR-2 localization in human and guinea-pig PDECs, and used isolated guinea pig ducts to study the effects of trypsin and a PAR-2 agonist on bicarbonate secretion. **METHODS:** PAR-2 localization was analyzed by immunohistochemistry in guinea pig and human pancreatic tissue samples (from 15 patients with chronic pancreatitis and 15 without pancreatic disease). Functionally, guinea pig PDECs were studied by microperfusion of isolated ducts, measurements of intracellular pH and intracellular Ca^{2+} concentration, and patch clamp analysis. The effect of pH on trypsinogen autoactivation was assessed using recombinant human cationic trypsinogen. **RESULTS:** PAR-2 localized to the apical membrane of human and guinea pig PDECs. Trypsin increased intracellular Ca^{2+} concentration and intracellular pH and inhibited secretion of bicarbonate by the luminal anion exchanger and the cystic fibrosis transmembrane conductance regulator (CFTR) Cl^- channel. Autoactivation of human cationic trypsinogen accelerated when the pH was reduced from 8.5 to 6.0. PAR-2 expression was strongly down-regulated, at transcriptional and protein levels, in the ducts of patients with chronic pancreatitis, consistent with increased activity of intraductal trypsin. Importantly, in PAR-2 knockout mice, the effects of trypsin were markedly reduced. **CONCLUSIONS: Trypsin reduces pancreatic ductal bicarbonate secretion via PAR-2–dependent inhibition of the apical anion exchanger and the CFTR Cl^- channel. This could contribute to the development of chronic pancreatitis by decreasing luminal pH and promoting premature activation of trypsinogen in the pancreatic ducts.**

Keywords: Acinar Cells; Ductal Epithelium; Animal Model; Pancreatic Enzymes.

Trypsinogen is the most abundant digestive protease in the pancreas. Under physiologic conditions, trypsinogen is synthesized and secreted by acinar cells, transferred to the duodenum via the pancreatic ducts, and then activated by enteropeptidase in the small intestine.[1] There is substantial evidence that early intra-acinar[2,3] or luminal[4,5] activation of trypsinogen to trypsin is a key and common event in the development of acute and chronic pancreatitis. Importantly, almost all forms of acute pancreatitis are due to autodigestion of the gland by pancreatic enzymes.[6]

Several studies have shown that trypsin stimulates enzyme secretion from acinar cells via proteinase-activated receptor 2 (PAR-2),[7,8] whereas the effect of trypsin on pancreatic ductal epithelial cells (PDECs) is somewhat controversial. Trypsin activates ion channels in dog PDECs[9] and stimulates bicarbonate secretion in the CAPAN-1 human pancreatic adenocarcinoma cell line,[10] whereas it dose-dependently inhibits bicarbonate efflux from bovine PDECs.[11] The effect of trypsin differs not only among species, but also with respect to the localization of PAR-2. When PAR-2 is localized to the basolateral membrane and activated by trypsin, the result is stimulation of bicarbonate secretion.[9,10] In contrast, when the receptor is localized to the luminal membrane, the effect is inhibition.[11] Interestingly, there are no data available concerning the effects of trypsin on guinea pig PDECs which, in terms of bicarbonate secretion, are an excellent model of human PDECs.[12]

The human pancreatic ductal epithelium secretes an alkaline fluid that may contain up to 140 mmol/L $NaHCO_3$.[12,13] The first step in HCO_3^- secretion is the accumulation of HCO_3^- inside the cell, which is driven by basolateral Na^+/HCO_3^- cotransporters, Na^+/H^+ exchangers, and H^+-adenosine triphosphatases.[12,13] Only 2 transporters have been identified on the apical membrane of

Abbreviations used in this paper: BAPTA-AM, 1,2-bis(o-aminophenoxy)ethane-*N,N,N′,N′*-tetraacetic acid; CFTR, cystic fibrosis transmembrane conductance regulator Cl^- channel; CFTRinh-172, CFTR inhibitor-172; $[Ca^{2+}]_i$, intracellular Ca^{2+} concentration; H_2DIDS, dihydro-4,4′-diisothiocyanostilbene-2,2′-disulfonic acid; PAR-2, proteinase-activated receptor-2; PAR-2-AP, PAR-2 activating peptide; PAR-2-ANT, PAR-2 antagonist; PDEC, pancreatic ductal epithelial cell; pH_i, intracellular pH; pH_L, luminal pH; SBTI, soybean trypsin inhibitor; SLC26, solute carrier family 26.

0016-5085/$36.00
doi:10.1053/j.gastro.2011.08.039

cells in the proximal ducts that are the major sites of HCO_3^- secretion: cystic fibrosis transmembrane conductance regulator (CFTR) and the solute carrier family 26 (SLC26) anion exchangers.[12,13] How these transporters act in concert to produce a high HCO_3^- secretion is controversial.[14] Most likely, HCO_3^- is secreted through the anion exchanger until the luminal concentration reaches about 70 mmol/L, after which the additional HCO_3^- required to raise the luminal concentration to 140 mmol/L is transported via CFTR.[15,16]

The role of PAR-2 in experimental acute pancreatitis is also controversial and highly dependent on the model of pancreatitis studied. PAR-2 was found to be protective in secretagogue-induced pancreatitis in mice[7,17–19] and rats.[20] However, PAR-2 is clearly harmful when pancreatitis is evoked by the clinically more relevant luminal administration of bile salts in mice.[17]

In this study, we show for the first time that (1) PAR-2 is localized to the apical membrane of the human proximal PDECs, (2) the localization of PAR-2 in the guinea pig pancreas is identical to that in the human gland, (3) trypsin markedly reduces bicarbonate efflux through a dihydro-4,4′-diisothiocyanostilbene-2,2′-disulfonic acid (H_2DIDS)-sensitive apical SLC26 anion exchanger and strongly inhibits CFTR, (4) a decrease in pH within the ductal lumen will strongly accelerate the autoactivation of trypsinogen, and (5) trypsin down-regulates PAR-2 expression at both transcriptional and protein levels in PDECs of patients with chronic pancreatitis.

Materials and Methods

A brief outline of the materials and methods is given in the following text. For further details, please see Supplementary Materials and Methods.

Solutions

The compositions of the solutions used for microfluorimetry are shown in Table 1.

Isolation of Pancreatic Ducts and Individual Ductal Cells

Small intralobular proximal ducts and individual ductal cells were isolated from guinea pigs or PAR-2 wild-type (PAR-$2^{+/+}$) and knockout (PAR-$2^{-/-}$) mice with a C57BL6 background by microdissection as described previously.[21]

Table 1. Composition of Solutions for Microfluorimetry Studies

	Standard HEPES	Standard HCO_3^-	Cl^--free HCO_3^-	Ca^{2+}-free HEPES
NaCl	130	115		132
KCl	5	5		5
$MgCl_2$	1	1		1
$CaCl_2$	1	1		
Sodium HEPES	10			10
Glucose	10	10	10	10
$NaHCO_3$		25	25	
Sodium gluconate			115	
Magnesium gluconate			1	
Calcium gluconate			6	
Potassium sulfate			2.5	

NOTE. Values are concentrations in mmol/L.

Measurement of Intracellular pH and Ca^{2+} Concentration

Intracellular pH (pH_i) and calcium concentration ($[Ca^{2+}]_i$) were estimated by microfluorimetry using the pH- and Ca^{2+}-sensitive fluorescent dyes 2,7-bis-(2-carboxyethyl)-5-(and-6-)carboxyfluorescein, acetoxymethyl ester (BCECF-AM) and 2-(6-(bis(carboxymethyl)amino)-5-(2-(2-(bis(carboxymethyl)amino)-5-methylphenoxy)-ethoxy)-2-benzofuranyl)-5-oxazolecarboxylic acetoxymethyl ester (FURA 2-AM), respectively.

Microperfusion of Intact Pancreatic Ducts

The luminal perfusion of the cultured ducts was performed as described previously.[22]

Electrophysiology

CFTR Cl^- channel activity was investigated by whole cell patch clamp recordings on guinea pig single pancreatic ductal cells.

Measuring Autoactivation of Trypsinogen

Autoactivation of human cationic trypsinogen was determined in vitro at pH values ranging from 6.0 to 8.5. Experimental details are described in Supplementary Materials and Methods.

Immunohistochemistry

Five guinea pig, 2 PAR-$2^{+/+}$, 2 PAR-$2^{-/-}$, and 30 human pancreata were studied to analyze the expression pattern of PAR-2 protein. Relative optical densitometry was used to quantify the protein changes in the histologic sections. Patients' data and the full methods are described in Supplementary Supplementary Materials and Methods.

Real-Time Reverse-Transcription Polymerase Chain Reaction

RNA was isolated from 30 human pancreata. Following reverse transcription, messenger RNA (mRNA) expression of PAR-2 and β-actin was determined by real-time polymerase chain reaction analysis.

Results

Expression of PAR-2 in Guinea Pig and Human Pancreata

PAR-2 was highly expressed in the luminal membrane of small intralobular and interlobular ducts (Figure 1*A* [i]; cuboidal epithelial cells forming the proximal pancreatic ducts) but was almost undetectable in the larger interlobular ducts (Figure 1*A* [ii]; columnar epithelial cells forming the distal pancreatic ducts). The localization of PAR-2 in the human pancreas was identical to that in the guinea pig gland (Figure 1*A* [iv–vi]). Measurements of relative optical density confirmed the significant differences between the expression of PAR-2 in small intralobular and interlobular ducts and the larger interlobular ducts in both species (Figure 1*C*).

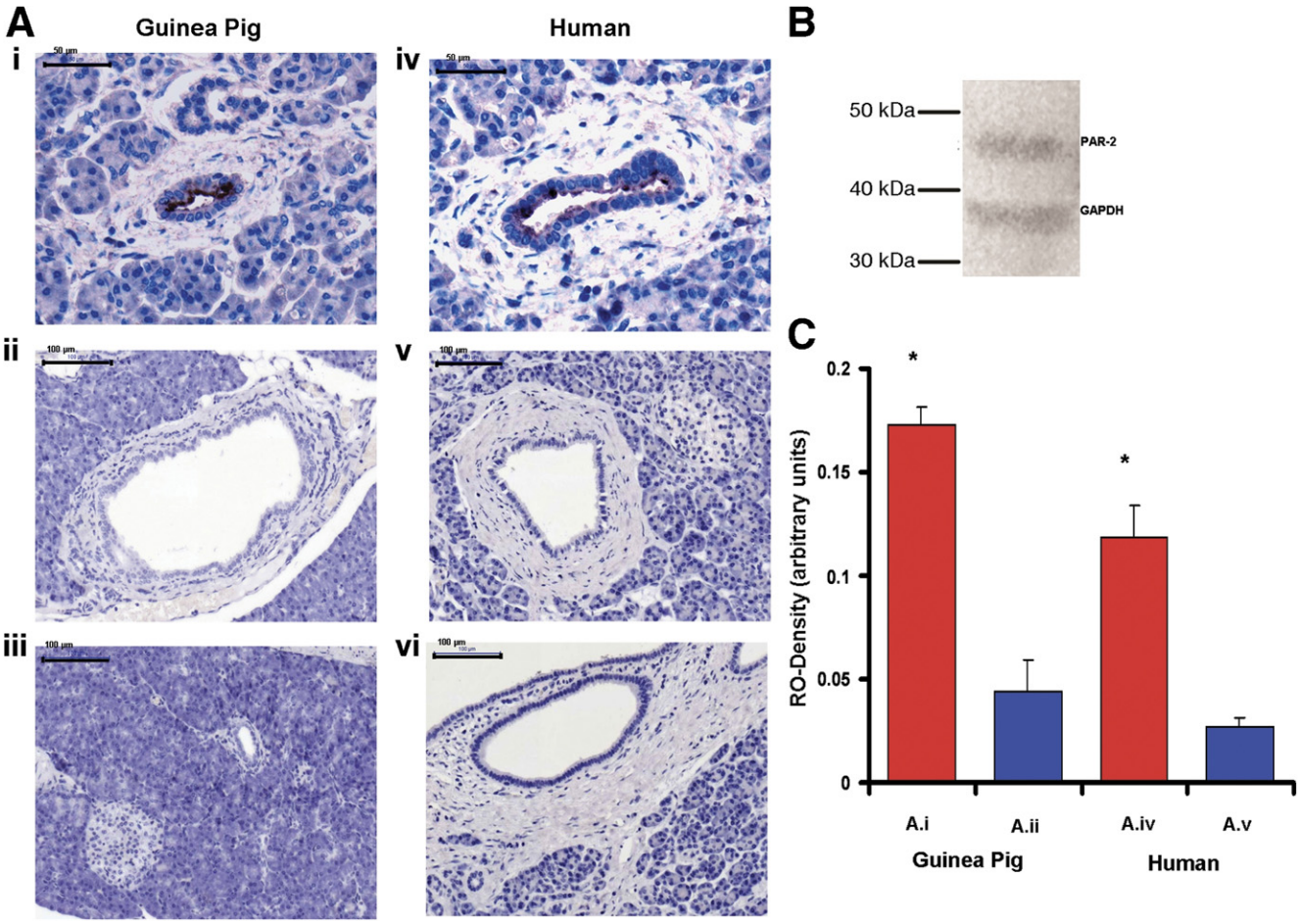

Figure 1. Localization of PAR-2 on human and guinea pig pancreatic ducts. Light micrographs of (*A* [i–iii]) guinea pig and (*A* [iv–vi]) human pancreas are shown. (i) PAR-2 is localized to the luminal membrane of PDECs in small intralobular and interlobular ducts (original magnification 400×). (ii) Large interlobular ducts do not express PAR-2 (original magnification 200×). (iii) No primary antiserum (original magnification 200×). (iv and v) Sections from human pancreas exhibit a similar localization of PAR-2 compared with the guinea pig gland (original magnification 400× and 200×). (vi) No primary antiserum (original magnification 200×). (*B*) Western blot analysis was used to determine the specificity of the PAR-2 antibody. Polyclonal anti–PAR-2 showed a single 44-kilodalton band. (*C*) Quantitative measurement of relative optical densities (RO-Density) of small intralobular and interlobular ducts (A.i,iv), and large interlobular ducts (A.ii,v) is shown. n = 12. $^*P < .05$ vs A.ii or A.v, respectively. *Scale bar* = 50 μm for *A* (i, iv) and 100 μm for *A* (ii and iii) and *A* (v and vi).

Luminal Administration of PAR-2-AP and Trypsin Induces Dose-Dependent $[Ca^{2+}]_i$ Signals

Because PAR-2 expression was detected only on the luminal membrane of intralobular duct cells, we used the microperfusion technique to see whether these receptors can be activated by PAR-2 agonists. First, the experiments were performed at pH 7.4 to understand the effects of trypsin and PAR-2 under quasi-physiologic conditions (Figure 2). The fluorescent images in Figure 2*A* clearly show that luminal administration of PAR-2 activating peptide (PAR-2-AP) increased $[Ca^{2+}]_i$ in perfused pancreatic ducts. The $[Ca^{2+}]_i$ response was dose dependent and consisted of a peak in $[Ca^{2+}]_i$ that decayed in the continued presence of the agonist, possibly reflecting PAR-2 inactivation or depletion of intracellular Ca^{2+} stores (Figure 2*B*). Pretreatment of PDECs with 10 μmol/L PAR-2 antagonist (PAR-2-ANT) for 10 minutes completely blocked the effects of 10 μmol/L PAR-2-AP on $[Ca^{2+}]_i$ (Figure 2*A* and *C*). Removal of extracellular Ca^{2+} had no effect on the increase in $[Ca^{2+}]_i$ evoked by luminal administration of 10 μmol/L PAR-2-AP; however, preloading ducts with the calcium chelator 1,2-bis(o-aminophenoxy)ethane-*N,N,N′,N′*-tetraacetic acid (BAPTA-AM) at 40 μmol/L totally blocked the response (Figure 2*A* and *C*).

Trypsin also induced a dose-dependent elevation in $[Ca^{2+}]_i$ similar to that evoked by PAR-2-AP (Figure 2*E* and *F*). Addition of 5 μmol/L soybean trypsin inhibitor (SBTI), 10 μmol/L PAR-2-ANT, and 40 μmol/L BAPTA-AM totally blocked the increase in $[Ca^{2+}]_i$ (Figure 2*D* and *F*). These data show that trypsin activates PAR-2 on the luminal membrane of the duct cell, which leads to release of Ca^{2+} from intracellular stores and an elevation of $[Ca^{2+}]_i$.

Because the pH of pancreatic juice can vary between approximately 6.8 and 8.0,[23,24] we also evaluated the effects of trypsin and PAR-2-AP on $[Ca^{2+}]_i$ at these pH values (Supplementary Figures 1 and 2, respectively). The

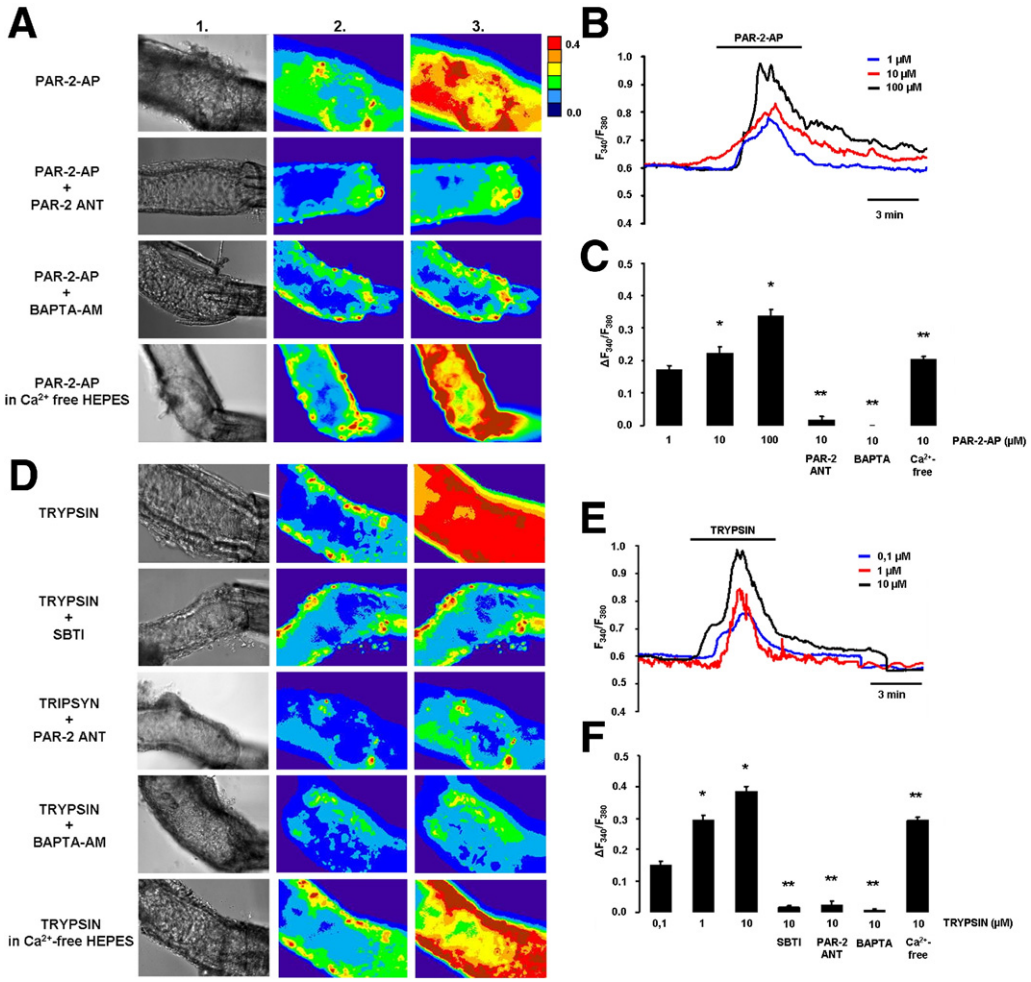

Figure 2. Effects of PAR-2-AP and trypsin on $[Ca^{2+}]_i$ in microperfused guinea pig pancreatic ducts at pH 7.4. (*A*) Light (1) and fluorescent ratio images (2 and 3) of microperfused pancreatic ducts showing the effects of luminal administration of 10 μmol/L PAR-2-AP, 10 μmol/L PAR-2-ANT, or 40 μmol/L BAPTA-AM on $[Ca^{2+}]_i$. Images were taken before (1 and 2) and after (3) exposure of the ducts to PAR-2-AP or trypsin. (*B* and *C*) Representative experimental traces and summary data of the changes in $[Ca^{2+}]_i$. (*D*) The same protocol was used to evaluate the effects of trypsin. Addition of 5 μmol/L SBTI was used to inhibit trypsin activity. (*E* and *F*) Representative experimental traces and summary data of the changes in $[Ca^{2+}]_i$. n = 5 for all groups. $^{*}P < .05$ vs 1 μmol/L PAR-2-AP or 0.1 μmol/L trypsin, respectively. $^{**}P < .001$ vs 10 μmol/L PAR-2-AP or 10 μmol/L trypsin, respectively.

elevations of $[Ca^{2+}]_i$ at pH 6.8 and 8.0 were generally very similar to the changes observed at pH 7.4. However, the increases in $[Ca^{2+}]_i$ evoked by 1 μmol/L PAR-2-AP and 0.1 μmol/L trypsin were significantly lower at pH 6.8 compared with either pH 7.4 or 8.0 (Supplementary Figure 3).

Luminal Exposure to PAR-2-AP and Trypsin Evokes Intracellular Alkalosis in PDECs

Figure 3 shows pH_i recordings from microperfused pancreatic ducts. Luminal application of the CFTR inhibitor (CFTRinh) 172 (10 μmol/L) and the anion exchanger inhibitor H_2DIDS (500 μmol/L) induced intracellular alkalization in PDECs (Figure 3*A* [i]). These data indicate that when bicarbonate efflux across the luminal membrane of PDECs (ie, bicarbonate secretion) is blocked, elevation of duct cell pH_i occurs, presumably because the basolateral transporters continue to move bicarbonate ions into the duct cell. Note also that the increase in pH_i evoked by the inhibitors is not sustained and begins to reverse before the inhibitors are withdrawn (Figure 3*A* [i]), which might be explained by the regulation of pH_i by basolateral acid/base transporters.

Both luminal PAR-2-AP and trypsin induced a dose-dependent elevation of pH_i (Figure 3*A* [ii and iii]), suggesting that activation of PAR-2 inhibits bicarbonate efflux across the apical membrane of the duct cell. Preincubation of PDECs with either 10 μmol/L PAR-2-ANT or 5 μmol/L SBTI or 40 μmol/L BAPTA-AM for 30 minutes totally blocked the effect of trypsin on pH_i (Figure 3*A* [iv]). The inhibitory effect of the calcium chelator BAPTA-AM suggests that the actions of trypsin and PAR-2-AP on pH_i are mediated by the increase in $[Ca^{2+}]_i$ that they evoke (Figure 2). Therefore, in this case, the transient nature of the pH_i response may reflect the transient effect that PAR-2 activators have on $[Ca^{2+}]_i$ (Figure 2*B* and *E*), as well as pH_i regulation by basolateral acid/base transporters.

Next we tested the effects of trypsin on pH_i in Cl^--free conditions and during pharmacologic inhibition of the

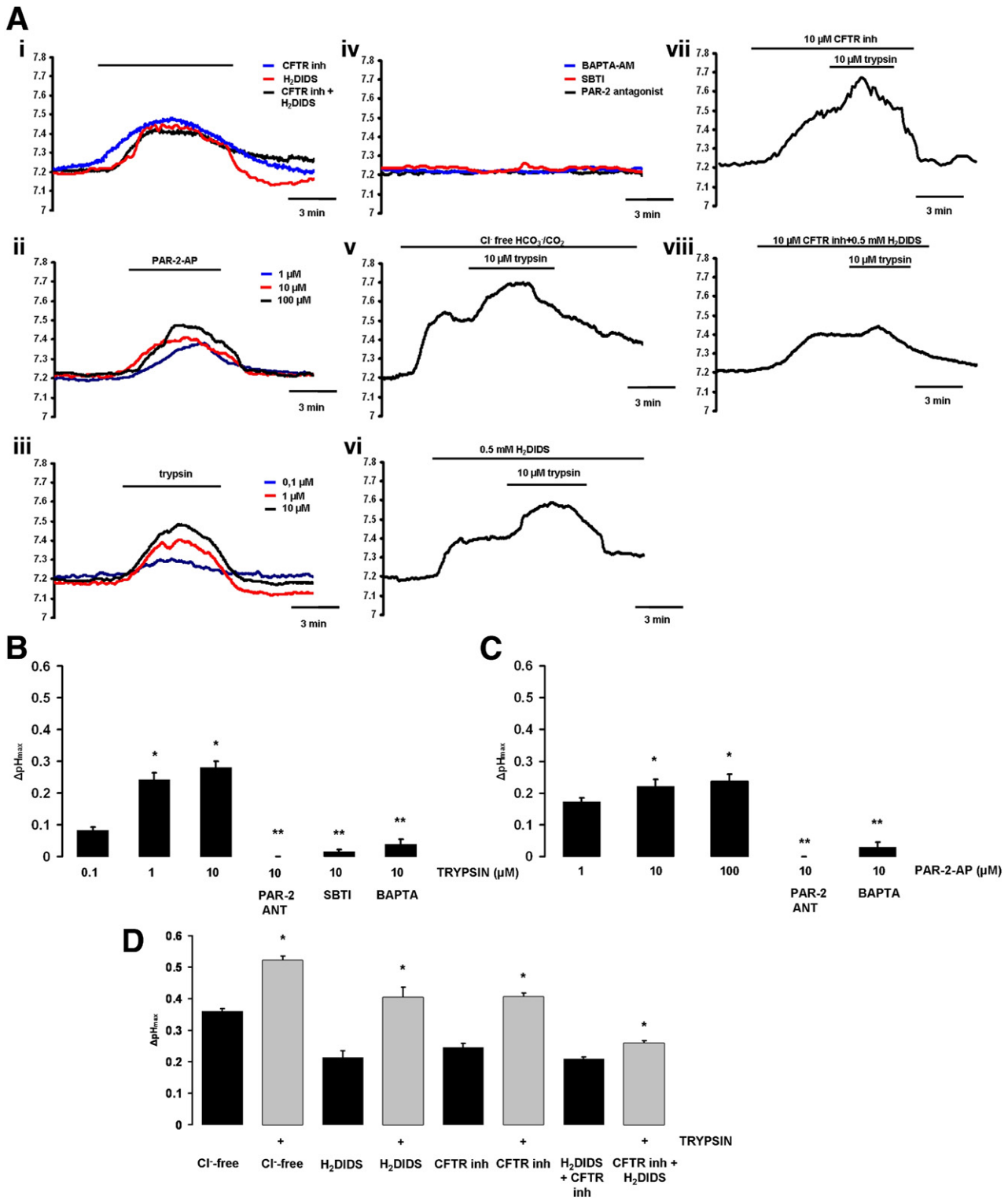

Figure 3. Effects of PAR-2-AP and trypsin on pH_i in microperfused guinea pig pancreatic ducts. (*A*) Representative pH_i traces showing the effects of luminal administration of different agents in microperfused pancreatic ducts. (i) A total of 10 µmol/L CFTRinh-172 and/or 500 µmol/L H_2DIDS caused alkalization of pH_i. (ii) PAR-2-AP and (iii) trypsin induced a dose-dependent pH_i elevation. (iv) Preincubation of ductal cells with 10 µmol/L PAR-2-ANT or 5 µmol/L SBTI or 40 µmol/L BAPTA-AM totally blocked the alkalization caused by 10 µmol/L trypsin. (v) Removal of luminal Cl^- or (vi) administration of H_2DIDS (500 µmol/L) decreased, but did not totally abolish, the effects of 10 µmol/L trypsin on pH_i. (vii) Pretreatment with 10 µmol/L CFTRinh-172 also decreased the effects of trypsin (10 µmol/L) on pH_i. (viii) Simultaneous administration of H_2DIDS and CFTRinh-172 strongly inhibited the effect of 10 µmol/L trypsin. (*B* and *C*) Summary of the effects of PAR-2-AP and trypsin on changes in pH_i. ΔpH_{max} was calculated from the experiments shown in *A*. (*D*) Effects of Cl^--free conditions. Cl^--free conditions, H_2DIDS, CFTRinh-172, and a combination of the inhibitors all induced an intracellular alkalosis. Trypsin further increased the alkalinization of pH_i, although the effect was markedly reduced when both H_2DIDS and CFTRinh-172 were present. n = 4–5 for all groups. (*B*) $^*P < .05$ vs 0.1 µmol/L trypsin; $^{**}P < .001$ vs 10 µmol/L trypsin. (*C*) $^*P < .05$ vs 0.1 µmol/L PAR-2-AP; $^{**}P < .001$ vs 10 µmol/L PAR-2-AP. (*D*) $^*P < .05$ vs the respective filled column.

luminal anion exchangers and/or CFTR (Figure 3*A* [v–viii]). Luminal Cl^--free conditions increased the pH_i of PDECs, presumably by driving HCO_3^- influx on the apical anion exchangers (Figure 3*A* [v]). Note that luminal administration of trypsin further elevated pH_i in Cl^--free conditions (Figure 3*A* [v]) and also in the presence of H_2DIDS (Figure 3*A* [vi]) and CFTRinh-172 (Figure 3*A* [vii]). However, pretreatment of ducts with a combination of H_2DIDS and CFTRinh-172 markedly reduced the effect of trypsin on pH_i (Figure 3*A* [viii]).

Figure 3*B–D* is a summary of the pH_i experiments. Trypsin (Figure 3*B*) and PAR-2-AP (Figure 3*C*) both induced statistically significant, dose-dependent increases in pH_i and these effects were blocked by PAR-2-ANT, SBTI, and BAPTA-AM. Exposure of the ducts to luminal Cl^--free conditions, H_2DIDS, CFTRinh-172, or a combination of the inhibitors also induced an intracellular alkalosis (Figure 3*D*). Also shown in Figure 3*D* is the additional, statistically significant increase in pH_i caused by trypsin in ducts exposed to Cl^--free conditions and the individual inhibitors. However, when ducts were exposed to both CFTRinh-172 and H_2DIDS simultaneously, the effect of trypsin on pH_i was markedly reduced, although it remained statistically significant (Figure 3*D*). We interpret these results as indicating that trypsin inhibits both Cl^--dependent (ie, anion exchanger mediated; revealed when CFTR is blocked by CFTRinh-172) and Cl^--independent (ie, CFTR mediated; revealed in Cl^--free conditions and when the luminal exchangers are blocked by H_2DIDS) bicarbonate secretory mechanisms in PDECs. Reduced bicarbonate secretion will lead to a decrease in intraductal pH.

Trypsin and PAR-2-AP Inhibit CFTR

Exposure of guinea pig PDECs to 5 μmol/L forskolin, which elevates intracellular adenosine 3′5′-cyclic monophosphate levels, increased basal whole cell currents (Figure 4*A–D* [i]) from 8.9 ± 2.3 to 91.2 ± 13.5 pA/pF (Figure 4*A–D* [ii]) at +60 mV in 78% of cells (38/49). The forskolin-activated currents were time- and voltage-independent, with a near linear I/V relationship and a reversal potential of −5.15 ± 1.12 mV (Figure 4*A–D* [iv]). These biophysical characteristics indicate that the currents are carried by CFTR.

Exposure of PDECs to 10 μmol/L trypsin did not affect the basal currents; however, administration of either 10 μmol/L PAR-2-AP (Figure 4*A* [iii]) or 10 μmol/L trypsin (Figure 4*B* [iii]) inhibited forskolin-stimulated CFTR currents by 51.7% ± 10.5% and 57.4% ± 4.0%, respectively. In both cases, the inhibition was voltage independent and irreversible. Pretreatment with either SBTI (10 μmol/L; Figure 4*C* [iii]) or PAR-2-ANT (10 μmol/L; Figure 4*D* [iii]) completely prevented the inhibitory effect of trypsin on the forskolin-stimulated CFTR currents. Figure 4*E* is a summary of these data, which suggest that trypsin inhibits CFTR Cl^- currents by activation of PAR-2.

Autoactivation of Trypsinogen Is pH Dependent

Trypsinogen can undergo autocatalytic activation during which trace amounts of trypsin are generated, which, in turn, can further activate trypsinogen in a self-amplifying reaction. Human trypsinogens are particularly prone to autoactivation, and mutations that facilitate autoactivation are associated with hereditary pancreatitis. To assess the effect of a decrease in intraductal pH (caused by reduced bicarbonate secretion) on trypsinogen activation, we measured autoactivation of human cationic trypsinogen in vitro at pH values ranging from 6.0 to 8.5 using a mixture of various buffers. As shown in Figure 5*A*, the rate at which cationic trypsinogen autoactivates was markedly increased as the pH was reduced from 8.5 to 7.0 when the buffer solution contained 1 mmol/L $CaCl_2$ and no NaCl. However, a further reduction in pH, from 7.0 to 6.0, had little effect (Figure 5*A* [i]).

To rule out that the differences observed in autoactivation were due to the different ionic strengths of the buffers used, we repeated the experiments in the presence of a higher concentration of sodium (100 mmol/L NaCl, Figure 5*A* [ii]) or lower concentration of calcium (0.1 mmol/L $CaCl_2$, Figure 5*A* [iii]). Although the overall autoactivation rates were much slower in the presence of NaCl, the pH profile of autoactivation was essentially identical to that observed in the absence of added salt (Figure 5*A* [ii]). Also, pH-dependent changes in the autoactivation of trypsinogen were still detectable when the experiments were performed using a low calcium buffer (Figure 5*A* [iii]).

PAR-2 Is Down-regulated in Patients With Chronic Pancreatitis

It has been documented that there is activated trypsin in the pancreatic ductal lumen in chronic pancreatitis in humans.[25–28] If trypsin activity is elevated in the duct lumen, PAR-2 down-regulation should occur, which could be due to either (1) changes in PAR-2 mRNA transcription and/or (2) receptor internalization and translocation to the cytoplasm. Our data show a marked reduction in membranous PAR-2 protein level but no significant changes in cytoplasmic PAR-2 protein in chronic pancreatitis (Figure 5*B* [i–iv] and *C*). Furthermore, PAR-2 mRNA expression was markedly reduced in chronic pancreatitis (Figure 5*D*), suggesting that reduced PAR-2 mRNA transcription may cause PAR-2 down-regulation in chronic pancreatitis.

Luminal Exposure to R122H Mutant Cationic Trypsin Induces Elevation of $[Ca^{2+}]_i$ and Evokes Alkalosis in PDECs

It has been shown that mutations in cationic trypsinogen increase the risk of chronic pancreatitis, most likely because of the enhanced autoactivation exhibited by the mutant trypsinogens.[29] Here we tested whether the commonest mutation in cationic trypsin, R122H, affected the ability of the protease to interact with PAR-2.

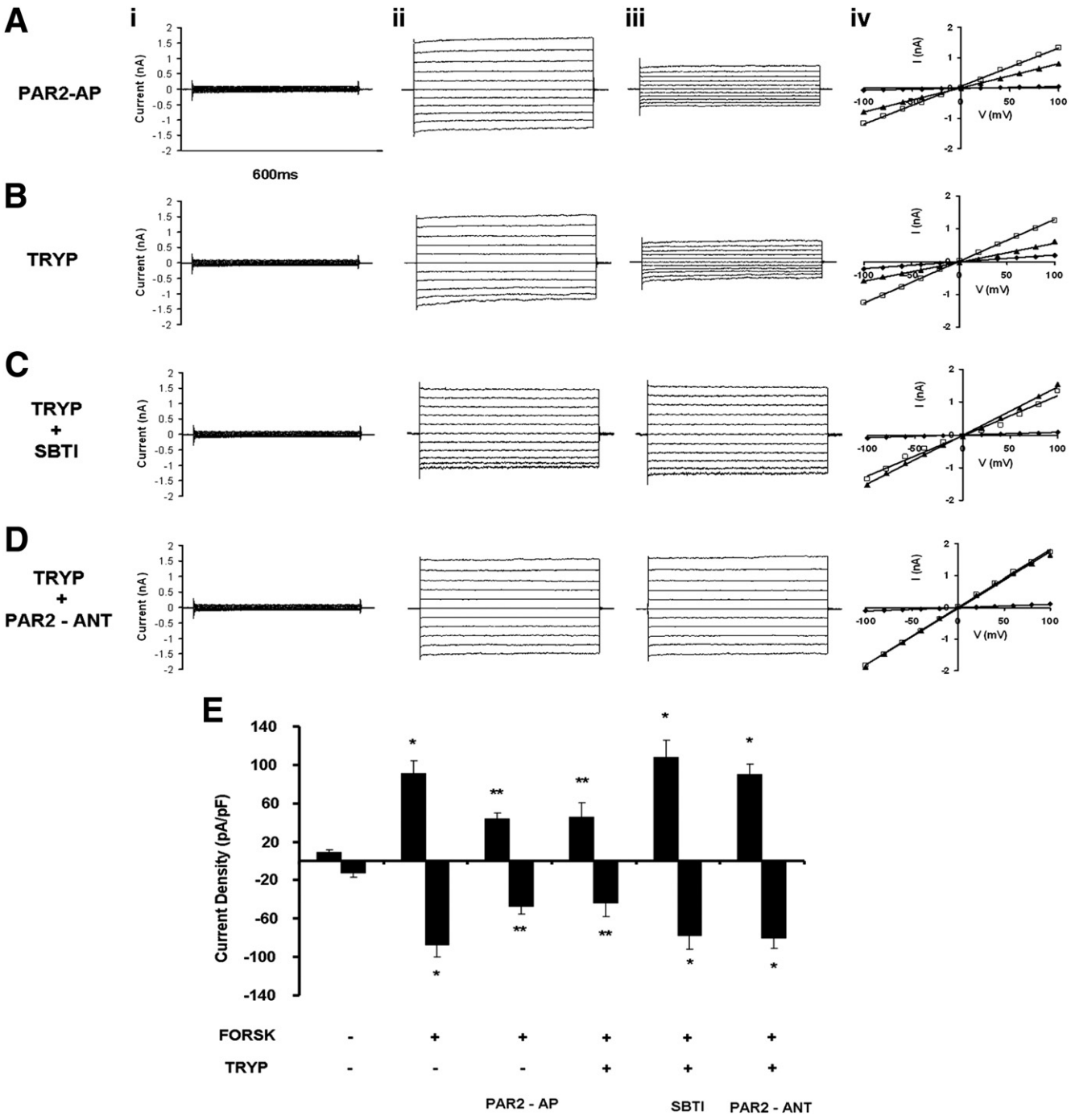

Figure 4. Effects of trypsin and PAR-2-AP on CFTR Cl^- currents of guinea pig pancreatic duct cells. Representative fast whole cell current recordings from PDECs. (*A–D*) (i) Unstimulated currents, (ii) currents after stimulation with 5 μmol/L forskolin, and (iii) currents following 3-minute exposure to (*A*) 10 μmol/L PAR-2-AP, (*B*) 10 μmol/L trypsin, (*C*) 10 μmol/L trypsin/5 μmol/L SBTI, and (*D*) 10 μmol/L trypsin/10 μmol/L PAR-2-ANT. (iv) I/V relationships. *Diamonds* represent unstimulated currents, *squares* represent forskolin-stimulated currents, and *triangles* represent forskolin-stimulated currents in the presence of the tested agents (see previous text). (*E*) Summary of the current density (pA/pF) data obtained from *A–D* measured at $E_{rev} \pm 60$ mV. Exposing PDECs to either PAR-2-AP or trypsin blocked the forskolin-stimulated CFTR Cl^- currents, while administration of SBTI or PAR-2-ANT prevented the inhibitory effect of trypsin. n = 6 for all groups. $^*P < .05$ vs the unstimulated cells, $^{**}P < .05$ vs forskolin. FORSK, forskolin; TRYP, trypsin.

Figure 6*A* and *B* shows that 1 μm of R122H human cationic trypsin causes comparable changes in pH_i and $[Ca^{2+}]_i$ to 0.4 μmol/L wild-type bovine trypsin, suggesting that a trypsin-mediated inhibition of bicarbonate secretion could play a role in the pathogenesis of hereditary as well as chronic pancreatitis.

Activation of PAR-2 Is Diminished in PAR-2$^{-/-}$ Mice

Finally, we investigated the effects of both PAR-2-AP and trypsin on PDECs isolated from PAR-$2^{+/+}$ and PAR-$2^{-/-}$ mice (Figure 6*C–E*). First we confirmed using

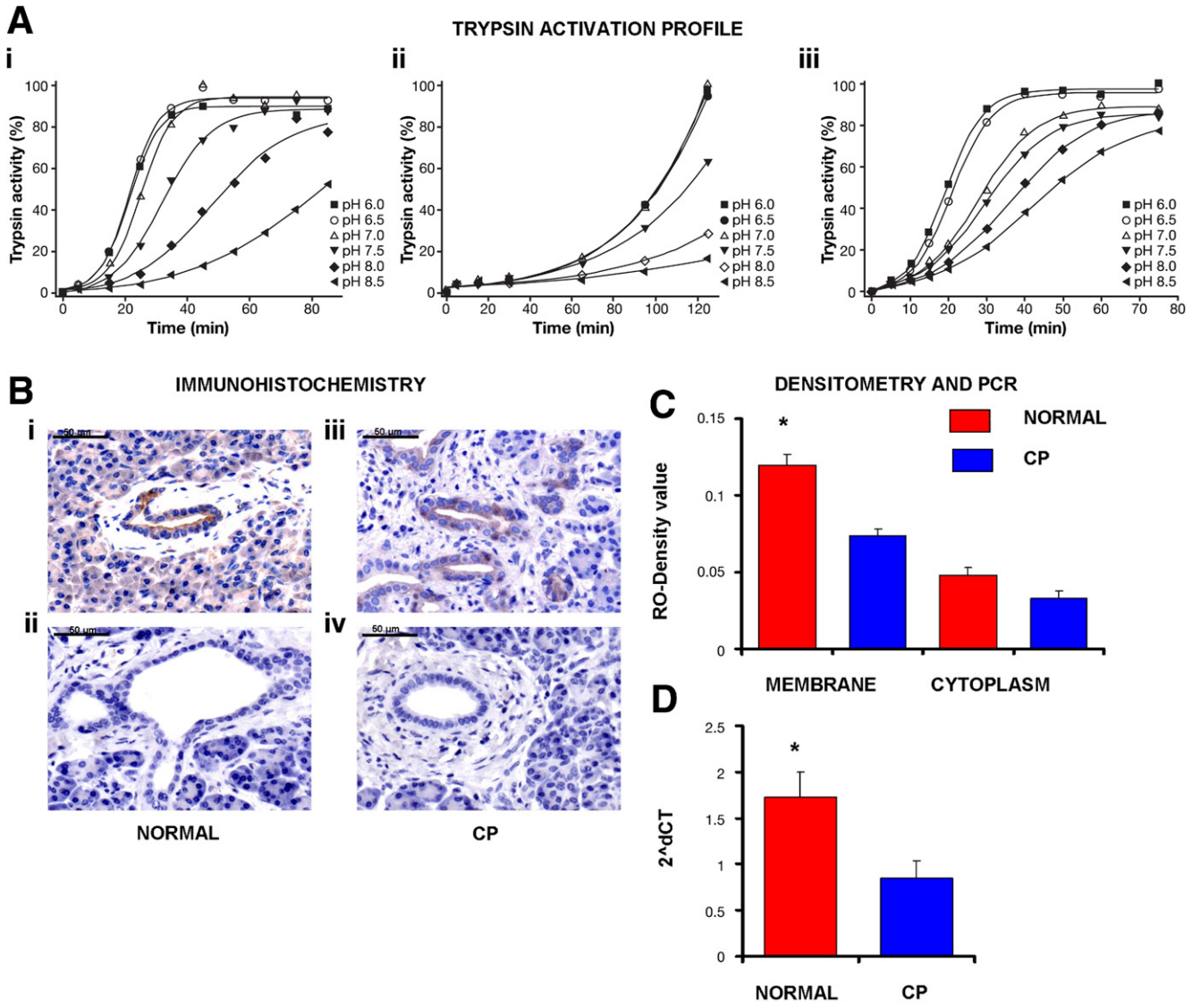

Figure 5. The effects of pH on trypsinogen activation and analyses of PAR-2 expression in human pancreatic samples. The autoactivation of human cationic trypsinogen was determined in vitro at pH values ranging from 6.0 to 8.5. (*A*) (i) Trypsinogen at 2 μmol/L concentration was incubated with 40 nmol/L trypsin at 37°C in 0.1 mol/L Tris + HEPES + 2-(*N*-morpholino)ethanesulfonic acid2-(*N*-morpholino)ethanesulfonic acid buffer mixture containing 1 mmol/L $CaCl_2$. (ii) The same protocol was used in high (100 mmol/L) NaCl buffer solution. Autoactivation of cationic trypsinogen significantly increased as the pH was reduced from 8.5 to 6.0. (iii) The same protocol was used in low (0.1 mmol/L) Ca^{2+}-buffered solution buffer solution. (*B*) (i–iv) PAR-2 expression. (i) Representative section of normal human pancreas. (ii) No primary antiserum. (iii) Representative section of human pancreas from a patient with chronic pancreatitis (CP). (iv) No primary antiserum. (*C*) Relative optical density. n = 15. $^*P < .05$ vs CP membrane. (*D*) Real-time reverse-transcription polymerase chain reaction analysis of PAR-2 mRNA expression of human pancreas. Data are given in 2^dCT. n = 15. $^*P < .05$ vs CP.

immunohistochemistry that PAR-$2^{+/+}$ mice do, whereas PAR-$2^{-/-}$ mice do not, express PAR-2 in their PDECs (Figure 6*C* [i and iii]). Accordingly, our functional data clearly show that the pH_i and $[Ca^{2+}]_i$ responses to luminal administration of either trypsin or PAR-2-AP were markedly diminished in PAR-$2^{-/-}$ PDECs (Figure 6*D* and *E*).

Discussion

The human pancreatic ductal epithelium secretes 1 to 2 L of alkaline fluid every 24 hours that may contain up to 140 mmol/L $NaHCO_3$.[12,13] The physiologic function of this alkaline secretion is to wash digestive enzymes down the ductal tree and into the duodenum and to neutralize acidic chyme entering the duodenum from the stomach. There are important lines of evidence supporting the idea that pancreatic ducts play a role in the pathogenesis of pancreatitis: (1) ductal fluid and bicarbonate secretion are compromised in acute and chronic pancreatitis,[30,31] (2) one of the main end points of chronic pancreatitis is the destruction of the ductal system,[32,33] (3) mutations in CFTR may increase the risk of pancreatitis,[30,31,34–36] and (4) etiologic factors for pancreatitis, such as bile acids or ethanol in high concentration, inhibit pancreatic ductal bicarbonate secretion.[37–39] Despite the previously men-

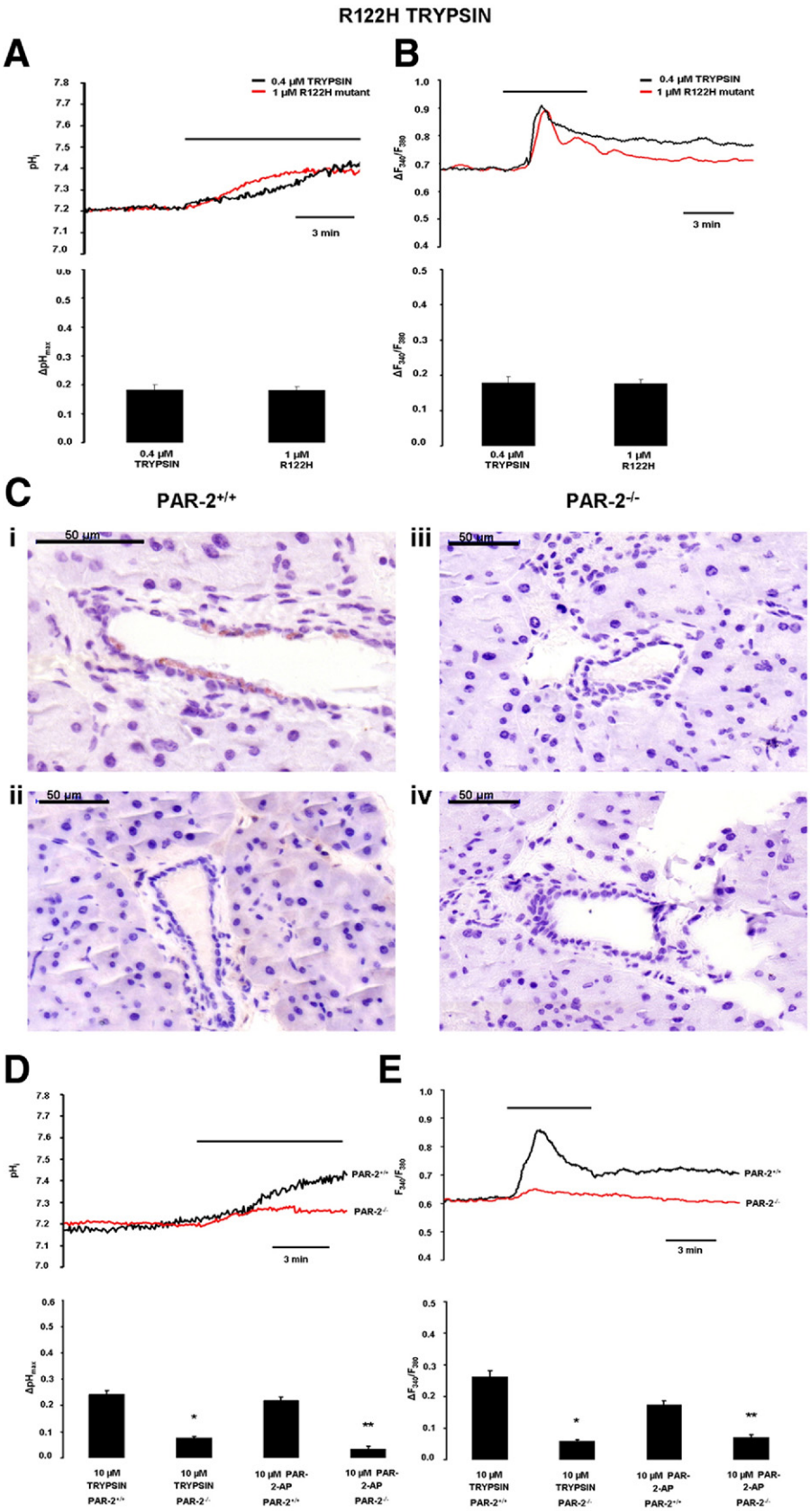

Figure 6. Experiments using R122H human mutant cationic trypsin and PAR-2$^{-/-}$ mice. Representative (*A*) pH_i and (*B*) $[Ca^{2+}]_i$ measurements using luminal administration of normal and R122H mutant cationic trypsin in microperfused guinea pig pancreatic ducts. n = 5 for all experiments. (*C*) (i–iv) PAR-2–expressing cells were visualized by immunohistochemistry as described in Figure 1. (i) Representative section of the pancreas removed from PAR-2$^{+/+}$ mice. (ii) Section without primary antiserum. (iii) Pancreas removed from PAR-2$^{-/-}$ mice. (iv) Section without primary antiserum. (*D*) pH_i and (*E*) $[Ca^{2+}]_i$ measurements using luminal administration of trypsin in microperfused pancreatic ducts isolated from PAR-2 knockout (*red curve*) and PAR-2 wild-type mice (*black curve*). n = 5 for all experiments. $^{*}P < .05$ vs 10 μmol/L trypsin PAR-2$^{+/+}$, $^{**}P < .05$ vs 10 μmol/L PAR-2-AP PAR-2$^{+/+}$.

tioned data, the role of PDECs in the development of pancreatitis has received relatively little attention.[40]

There are important species differences regarding the localization of PAR-2 in pancreatic ducts and in the effect of its activation on bicarbonate secretion. For example, CAPAN-1 cells[10] and dog PDECs[9] express PAR-2 only on the basolateral membrane, whereas bovine PDECs express PAR-2 on the luminal membrane.[11] Therefore, one of our

first aims was to determine which animal model best mimics human PAR-2 expression and thus would be the best for studying the effects of trypsin on PDEC function. Our results showed that in the human pancreas PAR-2 is localized to the luminal membrane of small proximal pancreatic ducts, which are probably the major site of bicarbonate and fluid secretion. Because CAPAN-1 cells and dog PDECs express PAR-2 only on the basolateral membrane, they do not mimic the human situation. Rats or mice are also not good models for the human gland because they secrete only 70 to 80 mmol/L bicarbonate.[41,42] However, the guinea pig pancreas secretes ~140 mmol/L bicarbonate, as does the human gland, and the regulation of bicarbonate secretion is similar in both species.[41,42] Because PAR-2 expression in the guinea pig pancreas was localized to the luminal membrane of duct cells, we performed our experiments on isolated guinea pig ducts.

First we characterized the effects of PAR-2 activation by trypsin and PAR-2-AP on PDECs. Previously, it has been shown that activation of the G protein–coupled PAR-2 by proteinases requires proteolytic cleavage of the receptor, which is followed by an elevation of $[Ca^{2+}]_i$.[43–45] As expected, luminal trypsin and PAR2-AP caused a dose-dependent elevation of $[Ca^{2+}]_i$ in guinea pig ducts. Importantly, the trypsin inhibitor SBTI, PAR-2-ANT, and the intracellular calcium chelator BAPTA-AM all completely blocked the elevation of $[Ca^{2+}]_i$, whereas removal of extracellular Ca^{2+} had no effect. Acidosis (pH 6.8) also slightly reduced the changes in $[Ca^{2+}]_i$ evoked by trypsin, most probably due to reduced cleavage activity of trypsin at an acidic pH. Next we characterized the effects of PAR-2 activation on pH_i. Luminal application of trypsin and PAR-2-AP both caused a dose-dependent intracellular alkalosis in PDECs. This alkalosis is most likely explained either by a reduction in the rate of bicarbonate efflux (ie, secretion) across the apical membrane of PDECs or by an increase in the rate of bicarbonate influx at the basolateral side of the cell. We favor the former explanation because luminal application of the anion exchange inhibitor H_2DIDS or the CFTR inhibitor CFTRinh-172 produced a similar intracellular alkalization.[22,46] Thus, PAR-2 activation inhibits bicarbonate secretion in PDECs by inhibiting SLC26 anion exchangers and CFTR Cl^- channels expressed on the apical membrane of the duct cell. In similarity with the $[Ca^{2+}]_i$ signals, the effect of PAR-2 activation on pH_i was blocked by SBTI, PAR-2-ANT, and BAPTA-AM, with the action of BAPTA-AM suggesting that the inhibition of bicarbonate secretion follows from the increase in $[Ca^{2+}]_i$. Interestingly, an elevation of $[Ca^{2+}]_i$ is crucial for both stimulatory (eg, acetylcholine,[13] low concentrations of bile acids,[39] and ethanol[38]) and inhibitory pathways (eg, basolateral adenosine triphosphate, arginine vasopressin, and high concentrations of ethanol) that control bicarbonate secretion by PDECs. Such marked differences in the outcome of $[Ca^{2+}]_i$ signals in PDECs probably reflect differences in the source of Ca^{2+} and/or in the intracellular compartmentalization of $[Ca^{2+}]_i$ signals generated by different secretory agonists and antagonists.

Remarkably, trypsin was still able to evoke an elevation of pH_i when Cl^- was removed from the duct lumen and when PDECs were pretreated with H_2DIDS, conditions that should inhibit bicarbonate efflux on the exchanger. These results suggested the involvement of CFTR, the only other known bicarbonate efflux pathway on the apical membrane, in the inhibitory effect of trypsin. This hypothesis was confirmed by patch clamp experiments in which trypsin decreased CFTR whole cell currents in isolated guinea pig PDECs by 50% to 60%. Finally, the fact that the trypsin-induced alkalinization was completely blocked by a combination of CFTRinh-172 and H_2DIDS confirms the involvement of both CFTR and SLC26 anion exchangers. Our conclusion from these pH_i and patch clamp data is that PAR-2 activation inhibits both the SLC26 anion exchanger (probably SLC26A6 [PAT-1][47] because SLC26A3 [DRA] is only weakly inhibited by disulfonic stilbenes[47,48]) and CFTR Cl^- channels expressed on the apical membrane of the duct cell.

The pH of pancreatic juice (and therefore the luminal pH [pH_L] in the duct) can vary between approximately 6.8 and 8.0. It has recently been shown that protons coreleased during exocytosis cause significant acidosis (up to 1 pH unit) in the lumen of the acini.[23] However, Ishiguro et al[49] have clearly shown that the pH_L in pancreatic ducts is dependent on the level of bicarbonate secretion. pH_L can be elevated from 7.2 to 8.5 by stimulation with secretin or forskolin, and this effect was strictly dependent on the presence of bicarbonate.[24,49,50] Also, inhibition of ductal bicarbonate secretion with H_2DIDS can decrease the pH_L to less than 8.0.[49] In view of these results, we tested whether trypsinogen autoactivation was affected by pH over the range of 6.0 to 8.5. Autoactivation of trypsinogen was relatively slow at pH 8.5, but decreasing the pH from 8.5 to 7 progressively stimulated autoactivation. These results suggest that under physiologic conditions bicarbonate secretion by PDECs is not only important for elevating the pH in the duodenum, but also for keeping pancreatic enzymes in an inactive state in the ductal system of the gland.

Receptor down-regulation is a phenomenon that occurs in the continued presence of an agonist and leads to a reduction in the sensitivity of the cell to the agonist. Potentially, there are 2 mechanisms that could underlie receptor down-regulation of PAR-2: (1) after proteolytic activation, the PAR-2 is internalized by a clathrin-mediated mechanism and then targeted to lysosomes[45] and (2) if trypsin is present for a longer time in the lumen, PAR-2 may be down-regulated at the transcriptional level. In this study, we provide evidence that the second mechanism, transcriptional down-regulation, explains the reduced expression of PAR-2 seen in chronic pancreatitis.

Conflicting data can be found in the literature concerning the role of PAR-2 in acute pancreatitis. Singh et al[7] showed that in secretagogue-induced experimental pancreatitis, PAR-2 deletion is associated with a more severe

pancreatitis. Although Laukkarinen et al[17] confirmed these results in cerulein-induced pancreatitis, they also clearly showed that in taurocholate-induced pancreatitis, PAR-2 deletion markedly reduced the severity of the disease. There is no evidence to suggest that clinical pancreatitis is evoked by supramaximal secretagogue stimulation; however, the taurocholate-induced pancreatitis model may mimic the clinical situation. Therefore, Laukkarinen et al[17] speculated that PAR-2 activation promotes the worsening of clinical pancreatitis and our data are consistent with that hypothesis.

Besides the clear pathophysiologic role of the trypsin/PAR-2 interaction in chronic pancreatitis, there is still a debate as to why PAR-2 are localized to the luminal membrane of PDEC in small ducts close to the acinar cells. What could the physiologic role of this PAR-2 be? A number of agents have been shown to have dual effects on PDECs at different concentrations. For example, bile acids in low concentrations stimulate but in high concentrations inhibit bicarbonate secretion.[39] The same applies to ethanol.[38] Under physiologic conditions, trypsin inhibitors are coreleased from acinar cells with trypsinogen and should block the activity of any trypsin that is generated spontaneously. Therefore, only very small amounts of active trypsin, if any, will be present in the duct lumen under normal conditions. However, there remains a possibility that very small amounts of active trypsin (ie, concentrations less than 0.1 μmol/L that would not cause an elevation of $[Ca^{2+}]_i$ or change in pH) could bind to PAR-2 on the luminal membrane of the ducts and augment other stimulatory mechanisms so as to enhance flushing of digestive enzymes down the ductal tree.

In conclusion, we suggest for the first time that one of the physiologic roles of bicarbonate secretion by PDECs is to curtail trypsinogen autoactivation within the pancreatic ductal system. However, if trypsin is present in the duct lumen (as may occur during the early stages of pancreatitis due to leakage from acinar cells), PAR-2 on the duct cell will be activated, leading to Ca^{2+} release from intracellular stores and an increase in cytosolic Ca^{2+} concentration. This causes inhibition of the luminal anion exchangers and CFTR Cl^- channels, reducing bicarbonate secretion by the duct cell. The decrease in bicarbonate secretion will increase the transit time of zymogens down the duct tree and decrease pH_L, both of which will promote the autoactivation of trypsinogen. The trypsin so formed will further inhibit bicarbonate transport, leading to a vicious cycle generating further decreases in pH_L and enhanced trypsinogen activation, which will favor development of the pancreatitis (Supplementary Figure 4). Finally, the R122H mutant cationic trypsin also elevated $[Ca^{2+}]_i$ and pH_i in duct cells, suggesting that this mechanism may be particularly important in hereditary pancreatitis in which the mutant trypsinogens more readily autoactivate.[29]

Supplementary Material

Note: To access the supplementary material accompanying this article, visit the online version of *Gastroenterology* at www.gastrojournal.org, and at doi: 10.1053/j.gastro.2011.08.039.

References

1. Petersen OH. Physiology of acinar cell secretion. In: Hans Beger, Andrew Warshaw, Markus Büchler, et al, eds. The pancreas. 2nd ed. Malden, MA: Blackwell Publishing, 2008:71–77.
2. Lerch MM, Gorelick FS. Early trypsinogen activation in acute pancreatitis. Med Clin North Am 2000;84:549–563.
3. Thrower EC, Gorelick FS, Husain SZ. Molecular and cellular mechanisms of pancreatic injury. Curr Opin Gastroenterol 2010;84:549–563.
4. Geokas MC, Rinderknecht H. Free proteolytic enzymes in pancreatic juice of patients with acute pancreatitis. Am J Dig Dis 1974;19:591–598.
5. Renner IG, Rinderknecht H, Douglas AP. Profiles of pure pancreatic secretions in patients with acute pancreatitis: the possible role of proteolytic enzymes in pathogenesis. Gastroenterology 1978;75:1090–1098.
6. Withcomb D, Beger H. Definitions of pancreatic diseases and their complications. In: Hans Beger, Andrew Warshaw, Markus Büchler, et al, eds. The pancreas. 2nd ed. Malden, MA: Blackwell Publishing, 2008:1–6.
7. Singh VP, Bhagat L, Navina S, et al. Protease-activated receptor-2 protects against pancreatitis by stimulating exocrine secretion. Gut 2007;56:958–964.
8. Kawabata A, Kuroda R, Nishida M, et al. Protease-activated receptor-2 (PAR-2) in the pancreas and parotid gland:Immunolocalization and involvement of nitric oxide in the evoked amylase secretion. Life Sci 2002;71:2435–2446.
9. Nguyen TD, Moody MW, Steinhoff M, et al. Trypsin activates pancreatic duct epithelial cell ion channels through proteinase activated receptor-2. J Clin Invest 1999;103:261–269.
10. Namkung W, Lee JA, Ahn W, et al. Ca^{2+} activates cystic fibrosis transmembrane conductance regulator- and Cl^--dependent HCO_3^- transport in pancreatic duct cells. J Biol Chem 2003;278:200–207.
11. Alvarez C, Regan JP, Merianos D, et al. Protease-activated receptor-2 regulates bicarbonate secretion by pancreatic duct cells in vitro. Surgery 2004;136:669–676.
12. Lee M, Muallem S. Physiology of duct cell secretion. In: Hans Beger, Andrew Warshaw, Markus Büchler, et al, eds. The pancreas. 2nd ed. Malden, MA: Blackwell Publishing, 2008:78–90.
13. Argent BE. Cell physiology of pancreatic ducts. In: Johnson LR, ed. Physiology of the gastrointestinal tract. Volume 2. 4th ed. San Diego, CA: Elsevier, 2006:1376–1396.
14. Hegyi P, Rakonczay Z Jr, Farkas K, et al. Controversies in the role of SLC26 anion exchangers in pancreatic ductal bicarbonate secretion. Pancreas 2008;37:232–234.
15. Ishiguro H, Steward MC, Sohma Y, et al. Membrane potential and bicarbonate secretion in isolated interlobular ducts from guinea-pig pancreas. J Gen Physiol 2002;120:617–628.
16. Sohma Y, Gray MA, Imai Y, et al. HCO_3^- transport in a mathematical model of the pancreatic ductal epithelium. J Membr Biol 2000;176:77–100.
17. Laukkarinen JM, Weiss ER, van Acker GJ, et al. Protease-activated receptor-2 exerts contrasting model-specific effects on acute experimental pancreatitis. J Biol Chem 2008;283:20703–20712.
18. Kawabata A, Matsunami M, Tsutsumi M, et al. Suppression of pancreatitis-related allodynia/hyperalgesia by proteinase-activated receptor-2 in mice. Br J Pharmacol 2006;148:54–60.
19. Sharma A, Tao X, Gopal A, et al. Protection against acute pancreatitis by activation of protease-activated receptor-2. Am J Physiol Gastrointest Liver Physiol 2005;288:G388–G395.

20. Namkung W, Han W, Luo X, et al. Protease-activated receptor 2 exerts local protection and mediates some systemic complications in acute pancreatitis. Gastroenterology 2004;126:1844–1859.
21. Argent BE, Arkle S, Cullen MJ, et al. Morphological, biochemical and secretory studies on rat pancreatic ducts maintained in tissue culture. Q J Exp Physiol 1986;71:633–648.
22. Hegyi P, Rakonczay Z Jr, Tiszlavicz L, et al. Protein kinase C mediates the inhibitory effect of substance P on HCO_3^- secretion from guinea pig pancreatic ducts. Am J Physiol Cell Physiol 2005; 288:C1030–C1041.
23. Behrendorff N, Floetenmeyer M, Schwiening C, et al. Protons released during pancreatic acinar cell secretion acidify the lumen and contribute to pancreatitis in mice. Gastroenterology 2010; 139:1711–1720.
24. Ishiguro H, Steward MC, Wilson RW, et al. Bicarbonate secretion in interlobular ducts from guinea-pig pancreas. J Physiol 1996;495:179–191.
25. Kukor Z, Mayerle J, Kruger B, et al. Presence of cathepsin B in the human pancreatic secretory pathway and its role in trypsinogen activation during hereditary pancreatitis. J Biol Chem 2002;277:21389–21396.
26. Tympner F, Rosch W. Viscosity and trypsin activity of pure pancreatic juice in chronic pancreatitis. Acta Hepatogastroenterol (Stuttg) 1978;25:73–76.
27. Fedail SS, Harvey RF, Salmon PR, et al. Trypsin and lactoferrin levels in pure pancreatic juice in patients with pancreatic disease. Gut 1979;20:983–986.
28. Tympner F. Selectively aspirated pure pancreatic secretion. Viscosity, trypsin activity, protein concentration and lactoferrin content of pancreatic juice in chronic pancreatitis. Hepatogastroenterology 1981;28:169–172.
29. Sahin-Tóth M, Tóth M. Gain-of-function mutations associated with hereditary pancreatitis enhance autoactivation of human cationic trypsinogen. Biochem Biophys Res Commun 2000;278:286–289.
30. Cavestro GM, Zuppardo RA, Bertolini S, et al. Connections between genetics and clinical data:Role of MCP-1, CFTR, and SPINK-1 in the setting of acute, acute recurrent, and chronic pancreatitis. Am J Gastroenterol 2010;105:199–206.
31. Hegyi P, Rakonczay Z. Insufficiency of electrolyte and fluid secretion by pancreatic ductal cells lead to increase patients risk to pancreatitis. Am J Gastroenterol 2010;105:2119–2120.
32. Kloppel G, Luttges J, Sipos B, et al. Autoimmune pancreatitis: pathological findings. Jop 2005;6:97–101.
33. Ectors N, Maillet B, Aerts R, et al. Non-alcoholic duct destructive chronic pancreatitis. Gut 1997;41:263–268.
34. Hegyi P, Pandol S, Venglovecz V, et al. The acinar-ductal tango in the pathogenesis of acute pancreatitis. Gut 2011;60:544–552.
35. Nousia-Arvanitakis S. Cystic fibrosis and the pancreas: recent scientific advances. J Clin Gastroenterol 1999;29:138–142.
36. Weiss FU, Simon P, Bogdanova N, et al. Functional characterisation of the CFTR mutations M348V and A1087P from patients with pancreatitis suggests functional interaction between CFTR monomers. Gut 2009;58:733–734.
37. Maleth J, Venglovecz V, Rázga Z, et al. The non-conjugated chenodeoxycholate induces severe mitochondrial damage and inhibits bicarbonate transport in pancreatic duct cells. Gut 2011;60:136–138.
38. Yamamoto A, Ishiguro H, Ko SB, et al. Ethanol induces fluid hypersecretion from guinea-pig pancreatic duct cells. J Physiol 2003;551:917–926.
39. Venglovecz V, Rakonczay Z Jr, Ozsvari B, et al. Effects of bile acids on pancreatic ductal bicarbonate secretion in guinea pig. Gut 2008;57:1102–1112.
40. Lee MG, Muallem S. Pancreatitis: the neglected duct. Gut 2008; 57:1037–1039.
41. Padfield PJ, Garner A, Case RM. Patterns of pancreatic secretion in the anaesthetised guinea pig following stimulation with secretin, cholecystokinin octapeptide, or bombesin. Pancreas 1989;4:204–209.
42. Steward MC, Ishiguro H, Case RM. Mechanisms of bicarbonate secretion in the pancreatic duct. Annu Rev Physiol 2005;67:377–409.
43. Vergnolle N. Review article: proteinase-activated receptors-novel signals for gastrointestinal pathophysiology. Aliment Pharmacol Ther 2000;14:257–266.
44. Bohm SK, Khitin LM, Grady EF, et al. Mechanisms of desensitization and resensitization of proteinase-activated receptor-2. J Biol Chem 1996;271:22003–22016.
45. Hoxie JA, Ahuja M, Belmonte E, et al. Internalization and recycling of activated thrombin receptors. J Biol Chem 1993;268:13756–13763.
46. Stewart AK, Yamamoto A, Nakakuki M, et al. Functional coupling of apical Cl^-/HCO_3^- exchange with CFTR in stimulated HCO_3^- secretion by guinea pig interlobular pancreatic duct. Am J Physiol Gastrointest Liver Physiol 2009;296:G1307–G1317.
47. Ko SB, Shcheynikov N, Choi JY, et al. A molecular mechanism for aberrant CFTR-dependent HCO_3^- transport in cystic fibrosis. EMBO J 2002;21:5662–5672.
48. Chernova MN, Jiang L, Shmukler BE, et al. Acute regulation of the SLC26A3 congenital chloride diarrhoea anion exchanger (DRA) expressed in Xenopus oocytes. J Physiol 2003;549:3–19.
49. Ishiguro H, Naruse S, Steward MC, et al. Fluid secretion in interlobular ducts isolated from guinea-pig pancreas. J Physiol 1998; 511:407–422.
50. Ishiguro H, Naruse S, Kitagawa M, et al. Luminal ATP stimulates fluid and HCO_3^- secretion in guinea-pig pancreatic duct. J Physiol 1999;519:551–558.

Received October 26, 2010. Accepted August 5, 2011.

Reprint requests

Address requests for reprints to: Péter Hegyi, MD, PhD, DSc, First Department of Medicine, University of Szeged, Faculty of Medicine, Korányi fasor 8-10, H-6720, Szeged, Hungary. e-mail: hegyi.peter@med.u-szeged.hu; fax: (36) 62 545-185.

Conflicts of interest

The authors disclose no conflicts.

Funding

Supported by grants from the Hungarian Scientific Research Fund to V.V., Z.R., and P.H. (PD78087, K78311, and NNF 78851), Bolyai postdoctoral fellowships to P.H. and Z.R. (00334/08/5, 00174/10/5) awarded by the Hungarian Academy of Sciences, a European Pancreatic Club travel grant, National Office for Research and Technology grants (TÁMOP-4.2.2-08/1/2008-0002 and 0013, TÁMOP 4.2.1.B-09/1/KONV), National Institutes of Health grant DK058088 (to M.S.-T.), and scholarships from the Rosztoczy Foundation (to A.G. and A.S.).

Supplementary Materials and Methods

Ethics

All experiments were conducted in compliance with the Guide for the Care and Use of Laboratory Animals (USA NIH publication No 85-23, revised 1985). Animal experiments were approved by the Regional Ethical Board at the University of Szeged, Hungary.

Solutions and Chemicals

HEPES-buffered solutions were gassed with 100% O_2, and their pH was set to 7.4 with HCl at 37°C. HCO_3^--buffered solutions were gassed with 95% O_2/5% CO_2 to set pH to 7.4 at 37°C. For patch clamp studies, the standard extracellular solution contained (in mmol/L): 145 NaCl, 4.5 KCl, 2 $CaCl_2$, 1 $MgCl_2$, 10 HEPES, and 5 glucose (pH 7.4 adjusted with NaOH). The osmolarity of the extracellular solution was 300 mOsm/L. The standard pipette solution for the patch clamp experiments contained (in mmol/L): 120 CsCl, 2 $MgCl_2$, 0.2 ethylene glycol-bis(β-aminoethyl ether)-*N,N,N′,N′*-tetraacetic acid (EGTA), 10 HEPES, and 1 Na_2ATP (pH 7.2 adjusted with NaOH). Chromatographically pure collagenase was purchased from Worthington (Lakewood, NJ). 2,7-Bis-(2-carboxyethyl)-5-(and-6-)carboxyfluorescein, acetoxymethyl ester (BCECF-AM), 2-(6-(bis(carboxymethyl)amino)-5-(2-(2-(bis(carboxymethyl)amino)-5-methylphenoxy)ethoxy)-2-benzofuranyl)-5-oxazolecarboxylic acetoxymethyl ester (FURA 2-AM), dihydro-4,4′-diisothiocyanostilbene-2,2′-disulfonic acid (H_2DIDS), and 1,2-bis(o-aminophenoxy)ethane- *N,N,N′,N′*-tetraacetic acid (BAPTA-AM) were from Invitrogen (Carlsbad, CA). PAR-2-ANT (H-Phe-Ser-Leu-Leu-Arg-Tyr-NH_2) and PAR-2-AP (H-Ser-Leu-Ile-Gly-Arg-Leu-amid trifluoroacetate salt) were from Peptides International (Louisville, KY). Forskolin were from Tocris (Ellisville, MO). Rabbit PAR-2 polyclonal antibody was purchased from Santa Cruz Biotechnology (Heidelberg, Germany). All other chemicals were obtained from Sigma-Aldrich (Budapest, Hungary).

Isolation of Pancreatic Ducts and Individual Ductal Cells

Male guinea pigs weighing between 150 and 250 g or mice (PAR-$2^{+/+}$ and PAR-$2^{-/-}$) weighing between 18 and 21 g were humanely killed by cervical dislocation, the pancreas was removed, and small intralobular proximal ducts were isolated by microdissection as described previously.[1] PAR-$2^{-/-}$ mice (B6.Cg-F2rl1$^{tm1Mslb/J}$) were previously generated by Schmidlin et al[1] and a kind gift from Ashok Saluja.[2] Isolated ducts were then cultured overnight in a 37°C incubator gassed with 5% CO_2/95% air.[3]

To obtain single pancreatic ductal cells, cultured ducts were incubated for 50 minutes at 37°C in 50 U/mL elastase dissolved in storage solution (Dulbecco's modified Eagle medium containing 3% [wt/vol] bovine serum albumin [pH 7.4 with NaOH]). Then the ducts were transferred to a Ca^{2+}/Mg^{2+}-free HEPES-buffered solution and incubated for a further 10 minutes at 37°C. After the incubation, the ducts were transferred to a coverslip and teased apart using stainless steel needles. The individual ductal cells were used for experiments within 3 to 4 hours after isolation.

Measurement of pH_i and Ca^{2+} Concentration

Ducts were bathed in standard HEPES solution and loaded with BCECF-AM (2 μmol/L) or FURA 2-AM (5 μmol/L) for 30 to 60 minutes at room temperature.

Ducts were then transferred to a perfusion chamber mounted on an IX71 inverted microscope (Olympus, Budapest, Hungary) and perfused continuously with solutions at 37°C both from the luminal and basolateral side at a rate of 10 to 30 μL/min and 4 to 5 mL/min, respectively. Four to 5 small areas (region of interests) of 5 to 10 cells in each intact duct were excited with light at a given wavelength. Excitation of BCECF was at 495 and 440 nm, with emitted light monitored at 535 nm. Excitation of FURA-2 was at 380 and 340 nm, with emitted light monitored at 510 nm. The fluorescence emissions were captured by a charge-coupled device camera and digitized by a Cell imaging system (Olympus, Budapest, Hungary). Ratio images were collected at 1-second intervals. In situ calibration of pH_i measured with BCECF was performed using the high K^+-nigericin technique.[4,5]

Electrophysiology

Guinea pig PDECs were isolated by an enzymatic microdissection procedure as described previously. Using a glass pipette, a few drops of cell suspension were placed within a perfusion chamber mounted on the stage of an inverted microscope (TMS; Nikon, Tokyo, Japan). The ductal cells were allowed to settle and attach to the bottom of the chamber for at least 30 minutes before the perfusion was started.

Patch clamp micropipettes were fabricated from borosilicate glass capillaries (Clark, Reading, England) by using a P-97 Flaming/Brown micropipette puller (Sutter Co, Novato, CA). These pipettes had resistances between 1.5 and 2.5 MΩ. Membrane currents were recorded with an Axopatch 1D amplifier (Axon Instruments, Union City, CA) using the whole cell configuration of the patch clamp technique at 37°C. After establishing a high-resistance seal (1–10 GΩ) by gentle suction, the cell membrane beneath the tip of the pipette was disrupted by suction or by application of short electrical pulses. The series resistance was typically 4 to 8 MΩ before compensation (50%–80%, depending on the voltage protocol). Current-voltage (I/V) relationships were obtained by holding V_m at 0 mV and clamping to ±100 mV in 20-mV increments. Membrane currents were digitized by using a 333-kHz analog-to-digital converter (Digidata 1200; Axon Instruments) under software control (pClamp 6;

Axon Instruments). Analyses were performed by using pClamp 6 software after low-pass filtering at 1 kHz.

Expression and Purification of Human Trypsinogens

Wild-type and R122H mutant human cationic trypsinogen was expressed in *Escherichia coli* and purified by ecotin-affinity chromatography as reported previously.[6]

Measuring Autoactivation of Trypsinogen

Autoactivation of trypsinogen was measured at 2 μmol/L concentration at 37°C in a polybuffer system (American Bioanalytical Inc, Natick, MA) containing 100 mmol/L 2-(*N*-morpholino)ethanesulfonic acid, 100 mmol/L HEPES, and 100 mmol/L Tris in 100 μL final volume. The pH of the Polybuffer was adjusted to given values with HCl (pH 6.0 and 6.5) or NaOH (pH 7.0, 7.5, 8.0, and 8.5). Reactions also contained 1 mmol/L or 0.1 mmol/L $CaCl_2$ and 100 mmol/L NaCl, as indicated. At given times, 2-μL aliquots were removed and trypsin activity was determined using the N-CBZ-Gly-Pro-Arg-p-nitroanilide substrate at 150 μmol/L final concentration.

Immunohistochemistry

Pancreatic tissue from 5 guinea pigs, 15 patient samples without pancreatic disease near neuroendocrine tumors (average age, 59.5; female/male, 7:8), and 15 patients (average age, 56.6; female/male, 4:11) who had chronic pancreatitis (13 alcohol, 2 gallstone) were investigated. The human samples were obtained with the permission of the Regional Ethical Committee of Semmelweis University (#172/2003).

The pancreatic tissues were fixed in 10% neutral buffered formalin for 24 hours, followed by paraffin embedding, and were then cut and stained with H&E to establish the diagnosis. Paraffin-embedded, 3- to 4-μm-thick sections were used for immunohistochemistry to detect PAR-2 expression. The slides were treated for 30 minutes with target retrieval solution (Dako, Glostrup, Denmark) in a microwave oven, followed by incubation with the primary rabbit polyclonal antibody (Santa Cruz Biotechnology Inc, Heidelberg, Germany) in 1:100 dilution overnight at 4°C. Signal detection was achieved by using ImPRESS reagent with secondary anti-rabbit immunoglobulin G antibody (20 minutes) (Vector Laboratories, Burlingame, CA). Diaminobenzidine was used to visualize immune complexes, and nuclear counterstaining was performed with hematoxylin. For negative controls, the appropriate antibody was omitted and either the antibody diluent alone or isotype-matched immunoglobulin G serum was used. The negative controls exhibited no signal. Normal skin epithelial cells were used as positive controls to confirm correct immunohistochemical staining for PAR-2 (results not shown).

The immunohistochemical reactions were digitalized with a Mirax MIDI slide scanner (3DHistech Ltd, Budapest, Hungary). Relative optical (RO) density was calculated using ImageJ program (National Institutes of Health, Bethesda, MD). Pixel values (PV) were normalized to erythrocyte density ($PV_{Norm} = PV_{Measured} - PV_{Erythrocyte}$) in all sections. RO-Density value was calculated from the $RO\text{-}Density = \log_{10}(255/PV_{Norm})$ equation, assuming that the brightest value in the image equals 255.

Western blot analysis was used to determine the specificity of the PAR-2 antibody. Proteins were extracted from fresh-frozen guinea pig (n = 3) and human (n = 3) pancreatic tissue stored at −80°C. Isolation was performed by using lysis buffer (20 mmol/L Tris, pH 7.5, 150 mmol/L NaCl, 2 mmol/L EDTA, 1% Triton X-100 containing protease inhibitor complex [Sigma Aldrich Co, Budapest, Hungary]). Samples (50 mg) were homogenized, followed by centrifugation at 13,200 rpm at 4°C for 5 minutes. Measurements of protein concentration were performed using Bradford analysis.[7] A total of 30 μg of protein samples were loaded in each lane, run on 10% sodium dodecyl sulfate/polyacrylamide electrophoresis at 200 V for 35 minutes, and then transferred to nitrocellulose membranes at 100 V, 4°C, for 75 minutes. For aspecific protein blocking, nonfat dry milk (5%, phosphate-buffered saline) was used for 30 minutes. Blots were incubated with polyclonal PAR-2 rabbit antibody (1:300; Santa Cruz Biotechnology Inc, Heidelberg, Germany) and anti-GAPDH antibody (1:5000; AbDSerotec, Kidlington, England) at 4°C overnight. After washing in 0.1% Tris, the secondary antibodies as anti-mouse GAPDH (1:2000; AbDSerotec, Düsseldorf, Germany) and horseradish peroxidase–conjugated anti-rabbit antibody (1:2000, Dako Cytomation, Ghostrup, Denmark) were applied at room temperature for 90 minutes. Following 3 series of washings in Tris-buffered saline with Tween 20, signals were visualized by enhanced chemiluminescent detection.

Real-Time Reverse-Transcription Polymerase Chain Reaction

RNA extraction. Fifteen formalin-fixed, paraffin-embedded normal pancreatic tissue samples and 15 samples of chronic pancreatitis tissue were selected for real-time reverse-transcription polymerase chain reaction analysis. Total RNA was isolated from five 5- to 10-μm macrodissected sections (connective tissue excluded) using RNeasy FFPE Kit (Qiagen, Hilden, Germany) in accordance with the manufacturer's instructions. RNA concentrations were obtained using a NanoDrop Spectrophotometer ND-1000 (Thermo Fisher Scientific Inc, Waltham, MA).

Reverse transcription of RNA. Complementary DNA samples were prepared from 1 μg total RNA using a High Capacity RNA-to-cDNA Kit (Applied Biosystems, Carlsbad, CA) as specified by the manufacturer.

Primer design. Gene-specific primers were designed by AlleleID 6.01 primer design software (Premier Biosoft International, Palo Alto, CA) for real-time reverse-

transcription polymerase chain reaction. Isoform specificity and primer sizes were checked by BioEdit biological sequence alignment editor software (Tom Hall Ibis Therapeutics, Carlsbad, CA). Primer specificity was checked by BiSearch software (Hungarian Academy of Sciences, Institute of Enzymology, Budapest, Hungary). Primer specific amplification degree (58°C) was optimized by gradient polymerase chain reaction. The used primer sequences are shown in Supplementary Table 1.

Reverse-transcription polymerase chain reaction. Real-time reverse-transcription polymerase chain reaction analysis was performed using SYBR Green technology on an ABI Prism 7000 Sequence Detection System (Applied Biosystems, Foster City, CA), according to the manufacturer's instructions. β-actin was used as the internal control gene. Primer-specific amplification was controlled by 2% agarose gel electrophoresis, as well as by melting temperature analysis. The final 20 μL reaction mixture contained Power SYBR Green PCR Master Mix (Applied Biosystems), 10 pmol/L of forward and reverse primers, and 100 ng complementary DNA as template. Amplification conditions were as follows: incubation at 95°C for 10 minutes, followed by 45 cycles at 95°C for 15 seconds, 60°C for 60 seconds, and 72°C for 15 seconds, with subsequent melting analysis, heating to 95°C for 20 seconds, cooling to 45°C for 10 seconds, and then reheating to 95°C.

Statistical Analysis

Data are expressed as means ± SEM. Significant difference between groups was determined by analysis of variance. Statistical analysis of the immunohistochemical data was performed using the Mann–Whitney *U* test. Probability values of $P < .05$ were accepted as being significant.

Supplementary References

1. Schmidlin F, Amadesi S, Dabbagh K, et al. Protease-activated receptor 2 mediates eosinophil infiltration and hyperreactivity in allergic inflammation of the airway. J Immunol 2002;169:5315–5321.
2. Singh VP, Bhagat L, Navina S, et al. Protease-activated receptor-2 protects against pancreatitis by stimulating exocrine secretion. Gut 2007;56:958–964.
3. Argent BE, Arkle S, Cullen MJ, et al. Morphological, biochemical and secretory studies on rat pancreatic ducts maintained in tissue culture. Q J Exp Physiol 1986;71:633–648.
4. Hegyi P, Rakonczay Z Jr, Gray MA, et al. Measurement of intracellular pH in pancreatic duct cells: a new method for calibrating the fluorescence data. Pancreas 2004;28:427–434.
5. Thomas JA, Buchsbaum RN, Zimniak A, et al. Intracellular pH measurements in Ehrlich ascites tumor cells utilizing spectroscopic probes generated in situ. Biochemistry 1979;18:2210–2218.
6. Sahin-Tóth M, Tóth M. Gain-of-function mutations associated with hereditary pancreatitis enhance autoactivation of human cationic trypsinogen. Biochem Biophys Res Commun 2000;278:286–289.
7. Bradford MM. A rapid and sensitive method for the quantitation of microgram quantities of protein utilizing the principle of protein-dye binding. Anal Biochem 1976;72:248–254.

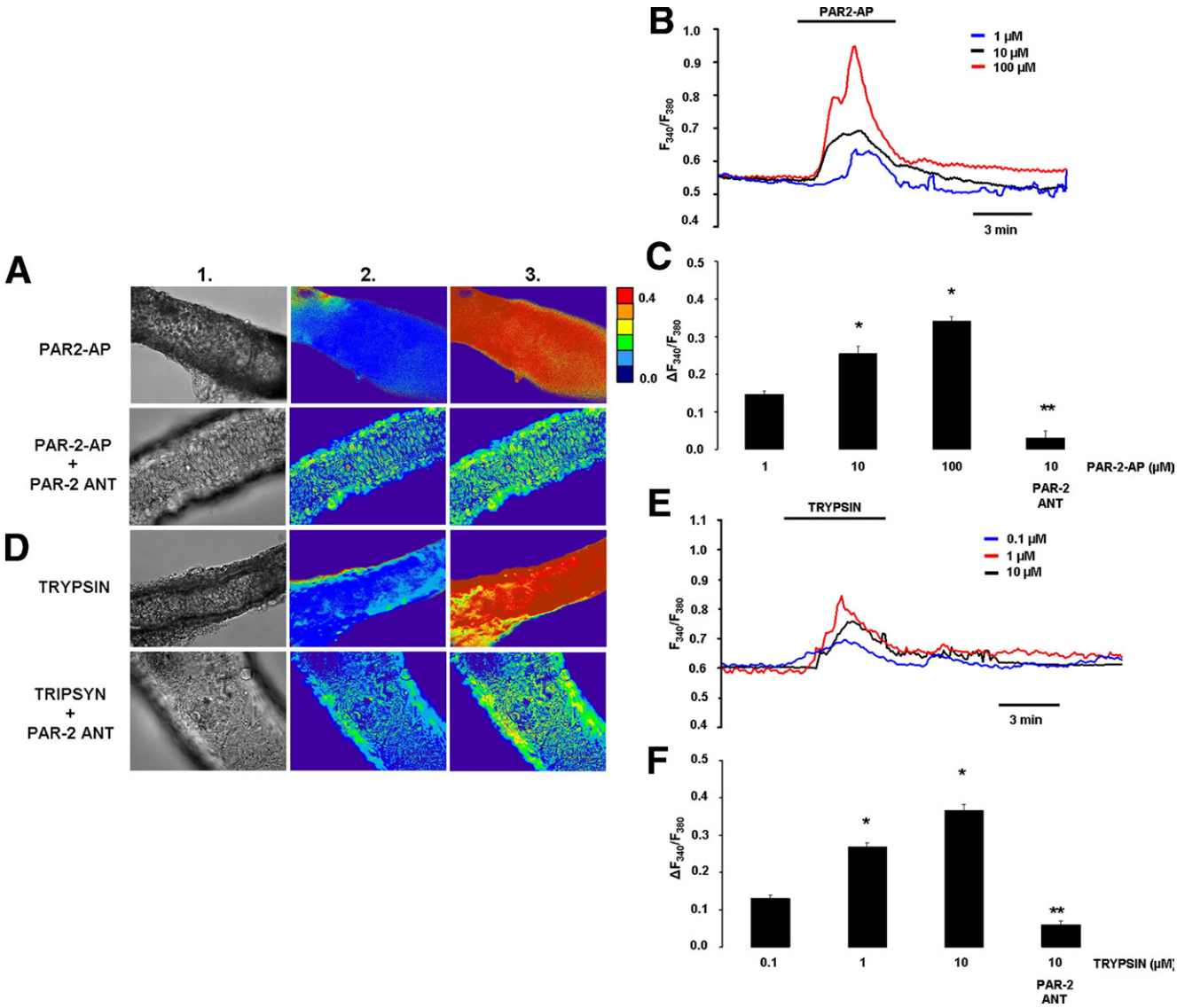

Supplementary Figure 1. Effects of PAR-2-AP and trypsin on $[Ca^{2+}]_i$ in microperfused guinea pig pancreatic ducts at pH 8.0. (*A*) Light (1) and fluorescent ratio images (2 and 3) of microperfused pancreatic ducts showing the effects of luminal administration of 10 μmol/L PAR-2-AP and 10 μmol/L PAR-2-ANT on $[Ca^{2+}]_i$ at pH 8.0. Images were taken before (1 and 2) and after (3) exposure of the ducts to PAR-2-AP or trypsin. An increase in $[Ca^{2+}]_i$ is denoted by a change from a "cold" color (*blue*) to a "warmer" color (*yellow to red*); see scale on the right. (*B* and *C*) Representative experimental traces and summary data of the changes in $[Ca^{2+}]_i$ at pH 8.0. (*D*) The same protocol was used to evaluate the effects of trypsin. (*E* and *F*) Representative experimental traces and summary data of the changes in $[Ca^{2+}]_i$. n = 3–4. $^{*}P < .05$ vs 1 μmol/L PAR-2-AP or 0.1 μmol/L trypsin, respectively. $^{**}P < .001$ vs 10 μmol/L PAR-2-AP or 10 μmol/L trypsin, respectively.

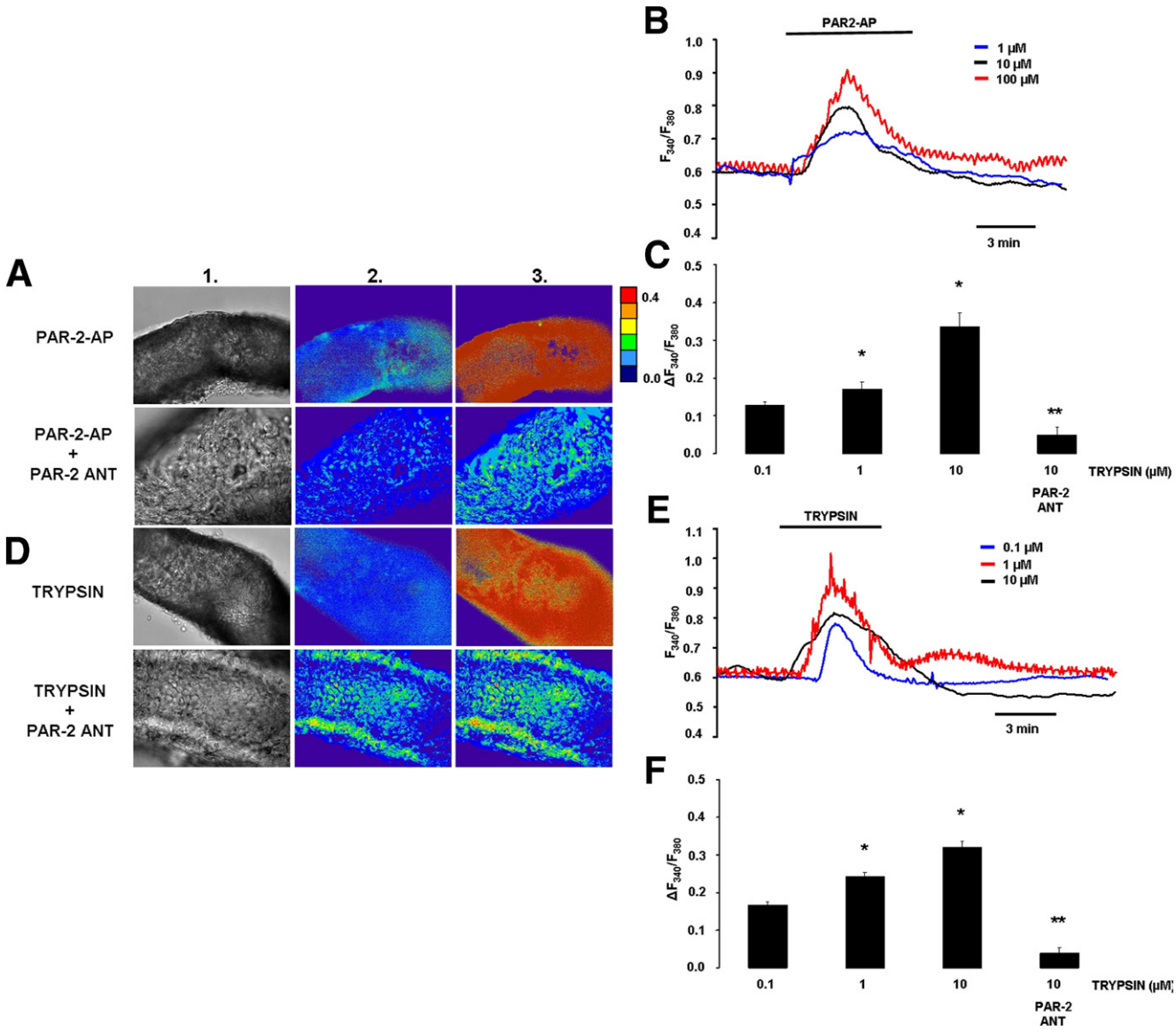

Supplementary Figure 2. Effects of PAR-2-AP and trypsin on $[Ca^{2+}]_i$ in microperfused guinea pig pancreatic ducts at pH 6.8. (*A*) Light (1) and fluorescent ratio images (2 and 3) of microperfused pancreatic ducts showing the effects of luminal administration of 10 μmol/L PAR-2-AP and 10 μmol/L PAR-2-ANT on $[Ca^{2+}]_i$ at pH 6.8. Images were taken before (1 and 2) and after (3) exposure of the ducts to either PAR-2-AP or trypsin. The colors are described in Supplementary Figure 1; see scale on the *right*. (*B* and *C*) Representative experimental traces and summary data of the changes in $[Ca^{2+}]_i$ at pH 6.8. (*D*) The same protocol was used to evaluate the effects of trypsin. (*E* and *F*) Representative experimental traces and summary data of the changes in $[Ca^{2+}]_i$ at pH 6.8. n = 3–4. $^{*}P < .05$ vs 1 μmol/L PAR-2-AP or 0.1 μmol/L trypsin, respectively. $^{**}P < .001$ vs 10 μmol/L PAR-2-AP or 10 μmol/L trypsin, respectively.

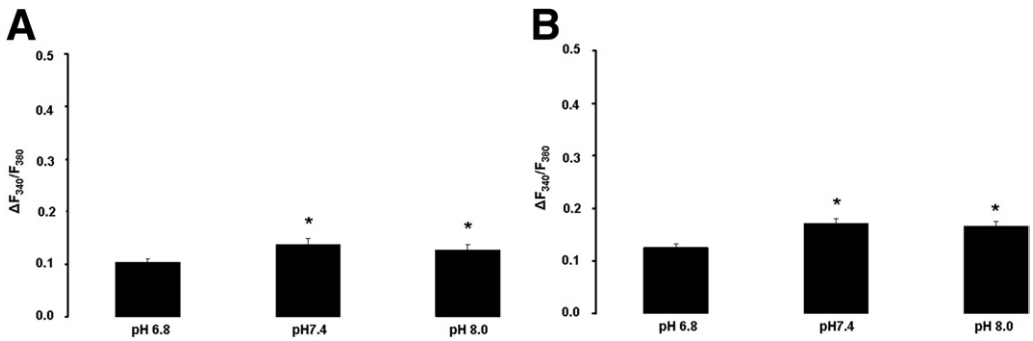

Supplementary Figure 3. Summary of the effects of PAR-2-AP and trypsin on $[Ca^{2+}]_i$ in microperfused guinea pig pancreatic ducts at different extracellular pH values. (*A*) The elevation in $[Ca^{2+}]_i$ evoked by 1 μmol/L PAR-2-AP and (*B*) 0.1 μmol/L trypsin at different extracellular pH values (6.8; 7.4; 8.0). n = 3–4. $^*P < .05$ vs at pH 6.8.

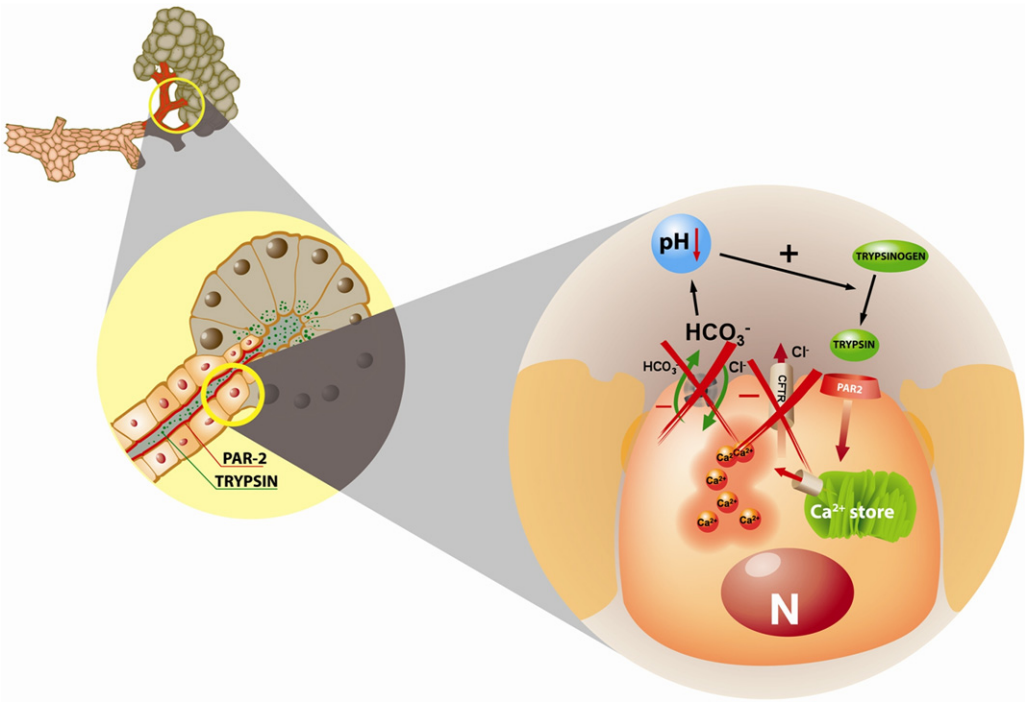

Supplementary Figure 4. The vicious trypsin cycle. If trypsin is present in the duct lumen, PAR-2 receptors on the duct cell are activated, leading to Ca^{2+} release from intracellular stores and an increase in cytosolic Ca^{2+} concentration. This causes inhibition of the luminal anion exchangers and CFTR Cl^- channels reducing bicarbonate secretion by the duct cell. The decrease in bicarbonate secretion will decrease luminal pH in the duct, which strongly accelerates the autoactivation of trypsinogen to trypsin. The activated trypsin will further inhibit bicarbonate transport by the duct cells, leading to a vicious cycle generating further decreases in luminal pH and enhanced trypsinogen activation with the potential for damaging the gland. The cycle may eventually be broken by the down-regulation of duct cell PAR-2 expression once pancreatitis is established. N, nucleus.

Supplementary Table 1. Nucleotid Sequences of the Primers Used in the Study.

Gene name	Primer sequence (5′ to 3′)	Product length (*base pairs*)	Annealing temperature (°C)
β-actin	GTACGCCAACACAGTGCTG (sense) CTTCATTGTGCTGGGTGCC (antisense)	100	55
PAR-2	GGCACCATCCAAGGAACCAATAG(sense) GCAGAAAACTCATCCACAGAAAAGAC (antisense)	128	58

II.

From: **Critical Care Medicine** <journals@sccm.org>
Date: 2013/9/15
Subject: CCMED Decision
To: Zoltan Rakonczay <rakonczay.zoltan@med.u-szeged.hu>

Sep 15 2013 04:43:19:918AM

RE: CCMED-D-13-01025R1, entitled "The role of pancreatic ductal secretion in protection against acute pancreatitis in mice"

Petra Pallagi, MSc1*; Zsolt Balla, MSc1*; Anurag K. Singh, PhD2*; Sándor Dósa, MD3; Béla Iványi, MD, PhD, DSc3; Zoltán Kukor, MD, PhD4; Adél Tóth, MSc5; Brigitte Riederer, PhD2; Yongjian Liu, MSc2; Regina Engelhardt2; Katalin Jármay, MD, PhD1; Andrea Szabó, MD, PhD6; Ágnes Janovszky, MD6; George Perides, PhD7; Viktória Venglovecz, PhD8; József Maléth, MD1; Tibor Wittmann, MD, PhD1; Tamás Takács, MD, PhD, DSc1; Mike A. Gray, PhD9; Attila Gácser, PhD5; Péter Hegyi, MD, PhD, DSc1; Ursula Seidler, MD, PhD2; Zoltán Rakonczay Jr., MD, PhD, DSc1

Dear Dr. Rakonczay,

We are pleased to inform you that your manuscript **has now been accepted for publication** in Critical Care Medicine. All manuscript materials will be forwarded immediately to the production staff for placement in the next available issue.

The manuscript is now being edited to conform to the journal format and style. When your manuscript is assigned to an issue of Critical Care Medicine it is important that we have your current contact information so that the page proofs reach you promptly. If your address, email, or telephone or fax numbers change, please notify us immediately at journals@sccm.org or by telephone at 847-827-6869.

Thank you for submitting your interesting and important work to the journal.

http://ccmed.edmgr.com/

Your username is: ZRakonczay-388
Your password is: xxxxxxxxxxx

With Kind Regards,

Edwin A. Deitch MD
Associate Editor

Joseph E. Parrillo, MD, MCCM
Editor-in-Chief
Critical Care Medicine

The role of pancreatic ductal secretion in protection against acute pancreatitis in mice

Petra Pallagi, MSc[1]*; Zsolt Balla, MSc[1]*; Anurag K. Singh, PhD[2]*; Sándor Dósa, MD[3]; Béla Iványi, MD, PhD, DSc[3]; Zoltán Kukor, MD, PhD[4]; Adél Tóth, MSc[5]; Brigitte Riederer, PhD[2]; Yongjian Liu, MSc[2]; Regina Engelhardt[2]; Katalin Jármay, MD, PhD[1]; Andrea Szabó, MD, PhD[6]; Ágnes Janovszky, MD[6]; George Perides, PhD[7]; Viktória Venglovecz, PhD[8]; József Maléth, MD[1]; Tibor Wittmann, MD, PhD[1]; Tamás Takács, MD, PhD, DSc[1]; Mike A. Gray, PhD[9]; Attila Gácser, PhD[5]; Péter Hegyi, MD, PhD, DSc[1]; Ursula Seidler, MD, PhD[2]; Zoltán Rakonczay Jr., MD, PhD, DSc[1]

*The first three authors contributed equally.

University of Szeged, [1]First Department of Medicine, [3]Department of Pathology, [5]Department of Microbiology, [6]Institute of Surgical Research, [8]Department of Pharmacology and Pharmacotherapy, Szeged, Hungary

[2]Department of Gastroenterology, Hepatology and Endocrinology, Hannover Medical School, Hannover, Germany

[4]Semmelweis University, Department of Medical Chemistry, Molecular Biology and Pathobiochemistry, Budapest, Hungary

[7]Department of Surgery, Tufts Medical Center, Boston, MA, USA

[9]Institute for Cell & Molecular Biosciences, Newcastle University, Newcastle upon Tyne, UK

Corresponding author, address reprint requests and proofs to:

Dr. Zoltán Rakonczay, First Department of Medicine, University of Szeged

P.O. Box: 427, H-6701 Szeged, Hungary, Tel.: +36-62-545-200, Fax: +36-62-545-185

E-mail: rakonczay.zoltan@med.u-szeged.hu

Key words: NHERF-1; CFTR; pancreatic ducts; secretion; acute pancreatitis

Source of funding: This study was supported by National Development Agency grants (TÁMOP-4.2.2.A-11/1/KONV-2012-0035, TÁMOP-4.2.2-A-11/1/KONV-2012-0052 TÁMOP-4.2.2.A-11/1/KONV-2012-0073), the Hungarian Scientific Research Fund (NF105758 to Z.R., NF100677 to P.H., K101116 to T.T., and PD78087 to V.V.), the Hungarian Academy of Sciences (BO 00174/10/5 to Z.R., and DFG/192 to Z.R. and P.H.), the Deutsche Forschungsgemeinschaft (Se460/13-4, SFB621/C9 and the Deutsch-Ungarisches Kooperationsprojekt DFG-436 UNG 113/190/01 to U.S.) and the National Institue of Health (DK 091327).

Abbreviations used in the paper: AP, acute pancreatitis; BCECF-AM, 2'7'-bis(carboxyethyl)-5(6)-carboxyfluorescein acetoxymethyl ester; $[Ca^{2+}]_i$, intracellular Ca^{2+} concentration; cAMP, cyclic AMP; CFTR, cystic fibrosis transmembrane conductance regulator Cl^- channel; DAPI, 4',6-diamidino-2-phenylindole; DRA, down-regulated in adenoma; ELISA, enzyme-linked immunosorbent assay; FURA-2-AM, 5-Oxazolecarboxylic acid, 2-(6-(bis(carboxymethyl)amino)-5-(2-(2-(bis(carboxymethyl)amino)-5-methylphenoxy)ethoxy)-2-benzofuranyl)-5-oxazolecarboxylic acetoxymethyl ester; H_2DIDS, dihydro-4,4'-diisothiocyanostilbene-2,2'-disulfonic acid; HSP72, heat shock protein 72; IκB, inhibitor kappa B; IL-1β, interleukin-1β; $J(B^-)$, transmembrane base flux; KO, knock-out; LDH, lactate dehydrogenase; MPO, myeloperoxidase; NHE3, Na^+/H^+ exchanger-3; NHERF-1, Na^+/H^+ exchanger regulatory factor-1; NF-κB, nuclear factor kappa B; PAT-1, Putative anion transporter 1; PBS, phosphate buffered saline; pH_i, intracellular pH; PS, physiological saline; PDZ,

postsynaptic density-95/disc-large/zonula occludens-1; SLC26, solute carrier family 26; TUNEL, terminal deoxynucleotidyl transferase dUTP nick end labeling; WT, wild type.

ABSTRACT

OBJECTIVE: A common potentially fatal disease of the pancreas is acute pancreatitis, for which there is no treatment. Most studies of this disorder focus on the damage to acinar cells since they are assumed to be the primary target of multiple stressors affecting the pancreas. However, increasing evidence suggest that the ducts may also have a crucial role in induction of the disease. To test this hypothesis, we sought to determine the specific role of the duct in the induction of acute pancreatitis using well established disease models and mice with deletion of the Na^+/H^+ exchanger regulatory factor-1 (NHERF-1) that have selectively impaired ductal function.

DESIGN: Randomized animal study.

SETTING: Animal research laboratory.

SUBJECTS: Wild-type and NHERF-1 knock-out mice.

INTERVENTIONS: Acute necrotizing pancreatitis was induced by i.p. administration of cerulein or by intraductal administration of sodium-taurocholate. The pancreatic expression of NHERF-1 and cystic fibrosis transmembrane conductance regulator (CFTR, a key player in the control of ductal secretion) was analysed by immunohistochemistry. *In vivo* pancreatic ductal secretion was studied in anesthetized mice. Functions of pancreatic acinar and ductal cells, as well as inflammatory cells were analyzed *in vitro*.

MEASUREMENTS AND MAIN RESULTS: Deletion of NHERF-1 resulted in gross mislocalization of CFTR, causing marked reduction in pancreatic ductal fluid and bicarbonate secretion. Importantly, deletion of NHERF-1 had no deleterious effect on functions of acinar and inflammatory cells. Deletion of NHERF-1 that specifically impaired ductal function increased the severity of acute pancreatitis in the two models tested.

CONCLUSIONS: Our findings provide the first direct evidence for the crucial role of ductal secretion in protecting the pancreas from acute pancreatitis, and strongly suggest that improved ductal function should be an important modality in prevention and treatment of the disease.

INTRODUCTION

A major disease of the exocrine pancreas is acute pancreatitis (AP) that is caused by multiple stressors and for which there is no specific treatment. The disorder usually develops either as a result of gallstone disease or moderate to heavy ethanol consumption [1]. It can present as mild edematous (85%) or as severe necrotizing (15%) forms, the latter of which can lead to a very high mortality rate of up to 50% in the case of multi-organ failure [1]. Most studies of AP focus on the function and damage to acinar cells since they are assumed to be the key target of stressors. However, increasing evidence point to the duct as the primary target of the stressors, which may have crucial role in induction of the disease.

The main function of the pancreatic duct is fluid and HCO_3^- secretion that is mediated by basolateral HCO_3^- influx due to Na^+-HCO_3^- contransport by NBCe1-B and luminal HCO_3^- exit mediated by the concerted action of cystic fibrosis transmembrane conductance regulator (CFTR), DRA (down-regulated in adenoma or slc26a3) and PAT-1 (putative anion transporter 1 or slc26a6) [2]. The interrelated function of CFTR and PAT-1 requires their assembly into complexes through postsynaptic density-95/disc-large/zonula occludens (PDZ) domains by an unknown scaffolding protein [3].

Na^+/H^+ exchanger regulatory factor-1 (NHERF-1) is a scaffolding protein involved in the apical targeting and trafficking of several membrane proteins and anchors them to the cytoskeleton via ezrin [4]. NHERF-1 also facilitates the association of multiprotein complexes via PDZ and ezrin-radixin-moesin binding domains, a process that is essential for the adequate function of transporters, channels, and signaling complexes [5]. The adapter protein has been shown to bind to the PDZ-binding motifs of CFTR, Na^+/H^+ exchanger-3 (NHE3), as well as a number of other proteins that functionally interact with

CFTR or NHE3, such as the β_2-adrenoreceptor [6, 7], or the Slc26 anion exchanger DRA [8].

The role of NHERF-1 in the pancreas has not yet been investigated, despite the fact that CFTR, a key regulator of epithelial function, is controlled by this scaffolding protein [4]. CFTR has very important roles in pancreatic ductal physiology [9] and in the pathogenesis of diseases like cystic fibrosis [5] and AP [10, 11]. We reasoned that the central role of NHERF-1 in CFTR function offered a unique opportunity to directly evaluate, for the first time, the role of pancreatic ducts in AP by analyzing ductal function in mice with deletion of NHERF-1 and their response to induction of AP.

MATERIALS AND METHODS

Brief outline of the methods is given below. For further details, please see the supplemental material.

Ethics

All experiments were conducted in compliance with the *Guide for the Care and Use of Laboratory Animals* (National Academies Press, Eight Edition, 2011), and were approved by Committees on investigations involving animals at the University of Szeged and at the Hannover Medical School and also by independent committees assembled by local authorities.

Animals

NHERF-1-deficient mice were originally generated and described at Duke University Medical Center [12]. NHERF-1 mutation was congenic for the FVB/N background for at least 15 generations. Genotyping was performed by PCR.

Isolation and culture of pancreatic ducts and acini

Intra-/interlobular pancreatic ducts were isolated and cultured overnight at 37°C in a humidified atmosphere containing 5% CO_2 as described previously [13]. Acinar cells were isolated by collagenase digestion and were used for experiments immediately thereafter [14].

mRNA expression of CFTR, PAT-1, DRA and NHERFs

Pancreatic ducts were homogenized by sonication in lysis-buffer and RNA was isolated with a NucleoSpin RNA XS Total RNA Isolation Kit. Reverse transcription was

performed using Superscript III RT. The primer sequences and PCR protocol used for the determination of the mRNA expression of transporters and NHERF-1-3 are described in the supplementary methods.

Localization of NHERF-1 and CFTR proteins by immunohistochemistry

Immunohistochemistry of the mouse pancreas was performed as described by Cinar et al [15] using rabbit polyclonal antibodies against NHERF-1 and CFTR.

Microperfusion and measurement of intracellular pH, Ca^{2+} concentration

The luminal and basolateral perfusions of the cultured ducts were performed as described previously [16]. Intracellular pH (pH_i) and Ca^{2+} concentration ($[Ca^{2+}]_i$) were assessed using the fluorescent dye BCECF-AM[17] and FURA 2-AM, respectively.

Determination of HCO_3^- efflux

To determine the HCO_3^- efflux across the apical membrane of the pancreatic ductal epithelia, we used three methods: inhibitory stop, alkali load and luminal Cl^- withdrawal. The measured rates of pH_i change (dpH/dt) were converted to transmembrane base flux [$J(B^-)$] which reflects the rate of HCO_3^- efflux (i.e. secretion) on luminal Cl^-/HCO_3^- exchangers [18].

Measurement of fluid secretion

Fluid secretion into the closed luminal space of *in vitro* cultured pancreatic ducts was analysed using a swelling method [19]. Basal and secretin-stimulated pancreatic fluid secretion *in vivo* was determined in anesthetized mice.

Induction of acute pancreatitis

Cerulein-induced pancreatitis

Mice were administered 1, 7 or 10 hourly i.p. injections of cerulein (50μg/kg per injection). Control mice were given physiological saline (PS: 0.9% NaCl) solution i.p. instead of cerulein.

Sodium-taurocholate-induced pancreatitis

Na-taurocholate was administered intraductally as described previously by Perides et al [20].

Assays

Amylase and lactate dehydrogenase (LDH) activities were measured with commercial kits. Acinar cell viability was determined using the trypan-blue exclusion test. Interleukin-1β (IL-1β) levels were measured by ELISA. Expression of heat shock protein72 (HSP72), IκB-α and IκB-β were determined by Western blot analysis [21]. Myeloperoxidase (MPO) activity, as a marker of tissue leukocyte infiltration, was assessed by the method of Kuebler et al [22].

Histologic examination

Pancreatic injury was evaluated by semiquantitative grading of interstitial edema, haemorrhage and leukocyte infiltration [21]. The extent (%) of cell damage was confirmed by analysis with ImageJ software (NIH, Bethesda, MD, USA). Apoptotic cells were quantified in $1mm^2$ of pancreatic tissue by TUNEL assay using an *In Situ* Cell Death Detection Kit according to the manufacturer's instructions.

Statistical analysis

Statistical analysis was performed by SigmaPlot (Systat Software Inc., Chicago, IL, USA). Data are presented as means±SEM. Both parametric (one– or two-way analysis of variance) and non-parametric (Kruskal-Wallis) tests were used based on the normality of data distribution (analyzed by the Shapiro-Wilk test). Post-hoc analysis (either Dunn's or Bonferroni's test) was performed according to the recommendations made by SigmaPlot. χ^2-test was used to determine differences between groups in the proportion of mice who died. A $P<0.05$ was accepted as statistically significant.

RESULTS

mRNA expression of CFTR, DRA, PAT-1 and NHERFs in mouse pancreatic ducts

CFTR, DRA, PAT-1, NHERF-1 and NHERF-2, but not NHERF-3 mRNA were expressed in isolated pancreatic ducts of WT mice (Fig.1). Notably, quantitative RT-PCR indicated that NHERF-1 was expressed more abundantly than the other two CFTR-binding NHERFs (NHERF-2 and NHERF-3).

Apical NHERF-1 and CFTR localization in pancreatic ducts is reduced in NHERF-1-knock-out mice

NHERF-1 was highly expressed in the apical membrane of pancreatic duct cells, but only weakly expressed in some acinar cells of WT mice (Fig.2A,B). No or weak staining was detected in NHERF-1-KO mice (Fig.2G,H). The weak staining is non-specific and was not localized to the luminal membrane.

Next, we determined whether NHERF-1 affects the localization of CFTR which was expressed in both pancreatic acinar and ductal cells. Compared to WT animals (Fig.2C), apical CFTR staining in pancreatic ducts was markedly reduced and overall CFTR staining in the pancreas appeared more diffuse in the absence of NHERF-1 (Fig.2I). Suppl.Fig. 1 shows that although the CFTR antibody gave a small amount of nonspecific staining, this was not localized to the luminal membrane. The strong cytoplasmic staining by the CFTR antibody correlates with the high CFTR mRNA expression levels in murine pancreas as compared to other gastrointestinal tissues (i.e. some cytoplasmic and basolateral staining in the duodenum [7], but not the ileum or colon of this mouse strain - unpublished observations). Expression of pancreatic ductal CFTR mRNA was not significantly different in WT and NHERF-1-KO mice (results not shown).

Pancreatic ductal HCO_3^- secretion is decreased in NHERF-1-knock-out mice

To determine if mislocalization of CFTR affects pancreatic ductal function, we investigated HCO_3^- secretion in isolated ducts using three different, but complementary methods that measure the rate at which HCO_3^- is secreted across the luminal membrane via Cl^-/HCO_3^- exchangers and/or CFTR [18].

(1) Inhibitor stop. The administration of dihydro-4,4'-diisothiocyanostilbene-2,2'-disulfonic acid (H_2DIDS, 0.2mM) and amiloride (0.2mM) resulted in a rate of $J(B^-)$ which was more than 4-fold lower in NHERF-1-KO compared to WT mice (Figs.3A,D).

(2) Alkali load. Here the recovery of pH_i from an alkali load induced by exposure to 20mM NH_4Cl in a HCO_3^-/CO_2-containing solution reflects the rate of HCO_3^- secretion [16]. Figs.3B and 3E show that the recovery from alkali load was about 2-fold lower in NHERF-1-KO vs. WT animals.

(3) Chloride removal. Figs.3C and 3F show that pH_i alkalinisation induced by removal of luminal Cl^- was significantly reduced in NHERF-1-KO compared to WT mice.

These data show that pancreatic ductal HCO_3^- secretion was significantly reduced in NHERF-1-KO compared to WT mice.

Fluid secretion is decreased in NHERF-1-knock-out mice

To investigate if fluid secretion was also compromised in KO mice, the rate of fluid secretion was measured using sealed ducts. In the absence of secretagogue, we could not detect any significant changes in the volume of WT and NHERF-1-KO ducts (Fig.4A). Stimulation of WT ducts with 5μM forskolin caused dynamic swelling of the ducts as a result of fluid secretion into the closed luminal space. In contrast, ducts from NHERF-1-KO mice had a blunted response to forskolin (Fig.4B).

We also examined the rate of pancreatic juice secretion *in vivo* in anesthetized mice. Under basal conditions, WT animals secreted pancreatic juice at a rate of 0.12±0.02 µl/h/g body weight (Fig.4C). In contrast, we could not detect any basal secretion in NHERF-1-KO animals. In response to secretin stimulation, we observed about 4-fold higher rates of pancreatic juice secretion in WT vs. NHERF-1-KO mice. These results demonstrate that pancreatic fluid secretion was significantly reduced in NHERF-1-KO compared to WT animals under both basal and secretin-stimulated conditions.

To rule out secondary alterations in pancreatic fluid secretion by changes in microcirculation due to loss of NHERF-1, we measured baseline microcirculatory plasma velocities in the capillaries of the pancreas, which were similar in WT and NHERF-1-KO animals (Suppl.Fig.2).

Cerulein-induced pancreatitis is more severe in NHERF-1-knock-out mice

To determine if the observed changes in pancreatic secretion could influence the development of AP, mice were given 10 hourly i.p. injections of either PS (control) or supramaximal doses of cerulein to induce AP (Fig.5A). The control animals had normal pancreatic histology (Fig.5A.a,d). I.p. injections of cerulein caused extensive cell damage (Fig.5A.b,c,e,f), the rates of necrosis (Fig.5B) and apoptosis (Fig.5C) were markedly higher in the NHERF-1-KO vs. WT mice. However, no significant differences were observed in the extent of interstitial edema (2.0±0.11 for WT vs. 2.2±0.2 for KO) or leukocyte infiltration (1.72±0.08 for WT vs. 1.95±0.13 for KO, p=0.08) in cerulein-treated groups.

There were also no significant differences between WT and NHERF-1-KO control groups in all laboratory parameters, except for the level of IκB-β.

Serum amylase activities were greatly elevated in cerulein-treated WT and NHERF-1-KO vs. the control groups (Fig.6A). Importantly, amylase activity was significantly higher in the cerulein-treated NHERF-1-KO vs. WT mice. Pancreatic MPO activity was significantly increased in cerulein-treated vs. control groups, but not different in WT compared to KO mice exposed to cerulein (Fig.6B). Pancreatic HSP72 expression (a sensitive marker of tissue injury) was significantly increased in cerulein-treated vs. control groups (Fig.6C), and significant differences were also observed between cerulein–treated WT and NHERF-1-KO groups.

Key events in the pathogenesis of AP include premature activation of trypsinogen [23, 24] and the activation of the proinflammatory transcription factor nuclear factor-κB (NF-κB) [25]. To exclude any potential effects of NHERF-1 deletion on early trypsinogen and NF-κB activation (regulated by IκBs), we measured pancreatic trypsin activity (Fig.6D) and expression of IκBs (Suppl.Figs.3A-B) in mice injected i.p. with 1x50μg/kg cerulein. Trypsin activity was increased by about 4-fold 0.5h after the injection of cerulein compared to the control group (Fig.6D), however, there were no significant differences between WT and NHERF-1-KO mice. Also, with respect to IκB-α expression, there was no significant differences between WT and NHERF-1-KO animals in cerulein-treated groups (Suppl.Fig.3A). The basal level of IκB-β was significantly higher in NHERF-1-KO vs. WT control mice, and no differences were observed in cerulein-treated WT and NHERF-1-KO groups (Suppl.Fig.3B). These data demonstrate that the difference in AP severity between WT and NHERF-1-KO mice is independent of pancreatic trypsinogen and NF-κB activation.

The expression of the proinflammatory cytokine IL-1β was significantly elevated in the pancreas of cerulein-treated WT and NHERF-1-KO mice vs. the control groups

(Suppl.Fig.3C), but there was no difference between the cerulein-treated WT vs. NHERF-1-KO mice.

Of note, i.p. administration of 7x50µg/kg cerulein in WT and NHERF-1-KO mice caused similar effects in the investigated histological and laboratory parameters as shown for the higher cerulein dose. A summary of these results can be found in Suppl.Figs.4-5. Overall, our results clearly demonstrate that the severity of cerulein-induced AP is lower in mice expressing NHERF-1.

To exclude any possible deleterious effects of NHERF-1 deletion on cholecystokinin receptor function, we tested the sensitivity of acinar cells to cerulein. Amylase secretion of acinar cells from WT and NHERF-1-KO animals showed no significant differences in response to cerulein stimulation (Suppl.Fig.6).

Intraductal administration of 4% sodium-taurocholate causes more extensive acinar cell necrosis in NHERF-1-knock-out compared to wild-type mice

We also investigated if NHERF-1-KO mice responded differently than WT mice when AP was induced by intraductal infusion of 4% Na-taurocholate. Postoperative mortality after administration of Na-taurocholate in KO mice (2/14 animals) was not significantly different vs. WT animals (0/10).

Intraductal infusion of PS caused no postoperative mortality, but mild pancreatic edema and inflammation was seen on histology without any significant necrosis (Fig.7A,B). The rate of leukocyte infiltration was significantly higher in the NHERF-1-KO vs. WT mice (Table1). The infusion of 4% Na-taurocholate into the pancreatic duct induced necrotizing AP in the head (Fig.7C,D), but not in the tail of the pancreas (not shown). The latter finding is in accord with that of others [20]. Therefore, only the pancreatic heads were used for analysis. Approximately 24% of acinar cells were necrotic

in WT (Fig.7C,E) and about 47% in NHERF-1-KO mice (Figs.7D,E). Table1 summarizes the histopathological changes in the various groups. Significantly higher rates of leukocyte infiltration were detected in Na-taurocholate-treated vs. PS-treated WT groups. In contrast, there were no differences in leukocyte infiltration between the Na-taurocholate-treated vs. PS-treated NHERF-1-KO groups, and Na-taurocholate-treated NHERF-1-KO vs. WT groups.

Serum amylase activities were significantly higher in Na-taurocholate-treated vs. control WT and NHERF-1-KO groups (Suppl.Fig.7A), but there were no differences between Na-taurocholate-treated NHERF-1-KO and WT mice. We did not observe any significant differences in MPO activity between WT and NHERF-1-KO mice after intraductal PS infusion (Suppl.Fig.7B). However, MPO activity was increased in Na-taurocholate-treated vs. control NHERF-1-KO mice, and even higher in the KO compared to the WT Na-taurocholate-treated mice. Pancreatic IL-1β expression was elevated in Na-taurocholate-treated WT and NHERF-1-KO mice vs. the control groups (Suppl.Fig.7C). However, there were no significant differences in the levels of IL-1β of Na-taurocholate-treated WT and NHERF-1-KO animals.

These data indicate that NHERF-1 expression reduces Na-taurocholate-induced pancreatic injury, but does not necessarily influence other laboratory parameters of the disease.

Functions of inflammatory cells are unaltered by deletion of NHERF-1

Since inflammatory cells are implicated in the pathogenesis of AP and NHERF-1 expression has been shown in neutrophils [26], we checked the bacterial killing efficiency of polymorphonuclear cells and the phagocytic activity of peritoneal macrophages. The

results in Suppl.Fig.8 demonstrate that knocking out NHERF-1 did not alter these functions.

NHERF-1 expression does not influence intracellular calcium signaling and the degree of cell damage caused by high concentrations of cerulein or sodium-taurocholate in isolated acini

To further investigate whether acinar cells are affected by the deletion of NHERF-1, we tested the effects of cerulein and Na-taurocholate on the critical intracellular Ca^{2+} signaling pathway in induction of AP, and on cell damage of isolated acini prepared from WT and NHERF-1-KO mice. Suppl.Fig.9. shows no significant differences in elevation of $[Ca^{2+}]_i$ induced by cerulein or Na-taurocholate on isolated acinar cell from WT and NHERF-1-KO mice (n=5-8). Next, we looked at the extent of *in vitro* cell damage induced by the administration of high concentrations (based on literature data) of cerulein (10^{-8}M) [27] and Na-taurocholate (1mM) [28]. Acinar viability of WT and NHERF-1-KO mice was 99.5±0.5% and 97.6±1.0% immediately after isolation, respectively (n=7); LDH release was 9.2±1.2% and 7.6±1.0%, respectively (n=7). Acinar viability significantly decreased with time and in response to cerulein or Na-taurocholate administration (Fig.8). However, we did not find any significant differences in cell viability parameters of treated WT and NHERF-1-KO acini.

DISCUSSION

We have demonstrated that NHERF-1 mRNA is highly expressed in mouse pancreatic ducts, but not acini. Furthermore, the genetic deletion of NHERF-1 greatly reduced the localisation of CFTR in the luminal ductal cell membrane and also decreased both *in vitro* and *in vivo* pancreatic bicarbonate and fluid secretion. Both basal and cAMP-stimulated secretion was reduced in the transgenic animals, but this effect was not caused by alterations in pancreatic blood flow. The diminished ductal secretion in NHERF-1-KO mice was associated with increased severity of necrotizing AP in two independent models of the disease. Importantly, early acinar events associated with AP, such as intracellular Ca^{2+} signaling, trypsinogen and NF-κB activation were unaltered by deletion of NHERF-1, but late events such as apoptosis and necrosis were increased in the KO animals. Notably, deletion of NHERF-1 had no deleterious effect on functions of acinar and inflammatory cells independent of AP, indicating that increased severity of the disease is specifically due to impaired ductal secretion.

NHERF-1 has been identified as a CFTR-interacting PDZ domain protein, which is involved in the apical targeting of CFTR, signal complex formation with a variety of receptors, and possibly the interaction with other membrane transport proteins, in a cell- and signal-specific manner [26, 29-34]. In our study, the absence of NHERF-1 greatly reduced CFTR abundance in the apical membrane of pancreatic ducts, whereas CFTR mRNA expression was unaltered. The gross mislocalization of CFTR resulted in decreased ductal fluid and HCO_3^- secretion. Consistent with our findings, mutations in CFTR that cause cystic fibrosis, impair the stability of the Cl^- channel in the plasma membrane and also result in markedly reduced bicarbonate and fluid secretion [35]. Our study does not differentiate between a loss of HCO_3^- and fluid secretion via CFTR or via a disruption between CFTR and other transporters involved in pancreatic bicarbonate and fluid

secretion, such as SLC26 anion exchangers. Of note, both DRA and PAT-1 are known to have PDZ domain binding motifs [4], and to bind to NHERF-1 [8, 36, 37]. In addition, activation of CFTR by SLC26 transporters was shown to be facilitated by PDZ ligands [3]. The reduced expression of CFTR in the apical membrane in NHERF-1-KO pancreatic ducts thus will likely decrease the activities of PAT-1 and DRA [38, 39].

Several groups have shown that binding of CFTR to NHERF may regulate CFTR activity. Two studies [7, 40] have demonstrated that NHERF-1 is required for full activation of transepithelial Cl^- and HCO_3^- secretion by cAMP- and cGMP-linked agonists in the duodenum and jejunum. This reduced activation of anion currents in NHERF-1-KO mice was independent of the total amount of CFTR expression in epithelial cells, and appeared to be due to a defect in apical targeting and/or retention of CFTR [40]. In addition, the NHERF-1 assisted formation of receptor-transporter signaling complexes in the apical membrane were disrupted [7]. A recent study has shown that CFTR activity is also dependent on NHERF-1 regulated cAMP compartmentalization and local protein kinase A activity in human airway epithelial cells [41]. The particularly high expression of NHERF-1 and CFTR in pancreatic ducts is quite different from that found in the small intestine [42, 43]. These findings suggest to us that CFTR-NHERF-1 interaction may be crucial to pancreatic ductal secretion.

Accumulating evidence suggests that pancreatic ducts not only have prominent roles physiologically, but also pathophysiologically. It is well known that insufficient electrolyte and fluid secretion by ductal cells in cystic fibrosis (caused by mutations in the CFTR gene) leads to destruction of acini [9]. Numerous CFTR mutations predispose to chronic pancreatitis [44]. Pancreatic biopsies from patients with autoimmune pancreatitis showed mislocalization of CFTR in the ducts and secretin-stimulated fluid and HCO_3^- secretion was reduced in these patients [45]. Until quite recently, the pathophysiological

relevance of pancreatic ducts in AP has been neglected. It is commonly assumed that the primary target of all stressors is the acinar cells since they are damaged in all forms of AP. However, both clinical and experimental data suggest that pancreatic ductal cells may also have fundamental roles in the development of AP [11]. Cavesto et al [10] have found statistically significant association of CFTR gene mutations in patients with recurrent AP. Pancreatic fluid secretion is greatly increased at the initiation of AP [46]. Also, *in vitro* administration of agents inducing AP such as bile acids, viruses or ethanol to pancreatic duct cells stimulate bicarbonate secretion [11, 16]. Our hypothesis is that ductal secretion serves to defend the pancreas by washing out toxic agents such as activated digestive enzymes. If this ductal defence mechanism is insufficient, ductal secretion will be inhibited and the harmful enzymes cannot leave the pancreas. The beneficial effect of ductal fluid hypersecretion is indicated by the fact that secretin, a major mediator of pancreatic ductal secretion, has been shown to protect against cerulein-induced AP [47, 48]. Furthermore, the severity of AP in galanin (a neuropeptide which has a potent inhibitory effect on pancreatic HCO_3^- secretion) KO mice was significantly reduced compared to WT littermates [49].

A striking finding of this study was that the severity of cerulein-induced acute necrotizing pancreatitis was significantly greater in animals lacking NHERF-1 (and thus reduced pancreatic ductal secretion), which suggests that normal ductal secretion in WT mice protects acinar cells against necrosis and apoptosis. This effect was independent of a change in cerulein sensitivity of acinar cells, and shows that NHERF-1 expression is not necessary for cholecystokinin receptor function. Furthermore, we did not find any significant differences in intracellular Ca^{2+} signaling and pancreatic activation of trypsinogen and NF-κB in mice lacking NHERF-1. Taken together, the latter findings show that early acinar events leading to AP are unaltered by NHERF-1 expression. Similar

to our findings, another group has shown that transgenic mice with reduced CFTR expression were more susceptible to cerulein-induced AP [50, 51]. As CFTR-KO mice exhibited constitutive overexpression of pancreatic proinflammatory mediators, this is not that surprising. However, we did not find any differences in basal pancreatic proinflammatory parameters between WT and NHERF-1-KO mice. Furthermore, in the studies by DiMagno et al, only the cerulein-induced AP model was tested and the acinar- vs. ductal-specific effects were not investigated. To confirm that the effect of diminished secretion on AP severity was not specific to the cerulein-induced model, we also determined disease severity in the clinically more relevant Na-taurocholate model [52]. Similar to the results observed in the cerulein-induced pancreatitis model, the degree of acinar cell damage in Na-taurocholate-induced AP was significantly greater in NHERF-1-KO vs. WT mice. Notably, the lower degree of necrosis was not necessarily accompanied by markedly reduced levels of inflammatory infiltration. Interestingly, leukocyte infiltration was higher in NHERF-1-KO vs. WT mice injected intraductally with PS. The latter data indicate that KO animals may even be more sensitive to increased ductal pressure.

Importantly, NHERF-1 expression did not influence the degree of cell damage caused by high concentrations of cerulein or sodium-taurocholate in isolated acini. These data indicate that the general deletion of NHERF-1 does not affect acinar cell damage caused by the latter agents. Therefore, it is likely that factors other than variations in the direct effects of cerulein or sodium-taurocholate on acinar cells are responsible for the differences in AP severities of WT and NHERF-1-KO mice.

CONCLUSIONS

Our results show for the first time that NHERF-1 plays a critical role in regulating the apical localization of CFTR in mouse pancreatic duct cells and ductal secretion which significantly influences the severity of acute necrotizing pancreatitis. Importantly, we provide *in vivo* data that strongly suggests the involvement of pancreatic ductal secretion in the pathogenesis of AP. The results obtained from this study may eventually open up new therapeutic possibilities (targeting ductal secretion) in the treatment of pancreatic inflammation which have to date mainly focused on acinar cells.

ACKNOWLEDGEMENTS

We are greatly indebted to Dr. José San Román (Salamanca, Spain) and Prof. Fred Gorelick et al (New Haven, CT, USA) for their valuable advice in setting up the *in vitro* fluid secretory measurement and acinar cell isolation techniques, respectively. The authors thank Dr. Gizella Karácsony (Szeged, Hungary) for her help with the TUNEL assay, Dr. Colin R. Muirhead (Newcastle upon Tyne, UK) for statistical review of the paper, Prof. Shmuel Muallem for thoughtful comments regarding the manuscript preparation and Brigitte Rausch, Natascha Cirpka and Silke Thiele (Hannover, Germany) for mouse breeding and genotyping. The rabbit anti-HSP72 antibody was a generous gift from Dr. István Kurucz (Budapest, Hungary).

REFERENCES

1. Pandol SJ, Saluja AK, Imrie CW, Banks PA: Acute pancreatitis: bench to the bedside. *Gastroenterology* 2007, 132(3):1127-1151.
2. Lee MG, Ohana E, Park HW, Yang D, Muallem S: Molecular mechanism of pancreatic and salivary gland fluid and HCO3 secretion. *Physiological reviews* 2012, 92(1):39-74.
3. Ko SB, Zeng W, Dorwart MR, Luo X, Kim KH, Millen L, Goto H, Naruse S, Soyombo A, Thomas PJ *et al*: Gating of CFTR by the STAS domain of SLC26 transporters. *Nat Cell Biol* 2004, 6(4):343-350.
4. Lamprecht G, Seidler U: The emerging role of PDZ adapter proteins for regulation of intestinal ion transport. *Am J Physiol Gastrointest Liver Physiol* 2006, 291(5):G766-777.
5. Guggino WB, Stanton BA: New insights into cystic fibrosis: molecular switches that regulate CFTR. *Nature reviews Molecular cell biology* 2006, 7(6):426-436.
6. Hall RA, Premont RT, Chow CW, Blitzer JT, Pitcher JA, Claing A, Stoffel RH, Barak LS, Shenolikar S, Weinman EJ *et al*: The beta2-adrenergic receptor interacts with the Na^+/H^+-exchanger regulatory factor to control Na^+/H^+ exchange. *Nature* 1998, 392(6676):626-630.
7. Singh AK, Riederer B, Krabbenhoft A, Rausch B, Bonhagen J, Lehmann U, de Jonge HR, Donowitz M, Yun C, Weinman EJ *et al*: Differential roles of NHERF1, NHERF2, and PDZK1 in regulating CFTR-mediated intestinal anion secretion in mice. *J Clin Invest* 2009, 119(3):540-550.
8. Rossmann H, Jacob P, Baisch S, Hassoun R, Meier J, Natour D, Yahya K, Yun C, Biber J, Lackner KJ *et al*: The CFTR associated protein CAP70 interacts with the apical Cl^-/HCO_3^- exchanger DRA in rabbit small intestinal mucosa. *Biochemistry* 2005, 44(11):4477-4487.
9. Steward MC, Ishiguro H: Molecular and cellular regulation of pancreatic duct cell function. *Curr Opin Gastroenterol* 2009, 25(5):447-453.
10. Cavestro GM, Zuppardo RA, Bertolini S, Sereni G, Frulloni L, Okolicsanyi S, Calzolari C, Singh SK, Sianesi M, Del Rio P *et al*: Connections between genetics and clinical data: Role of MCP-1, CFTR, and SPINK-1 in the setting of acute, acute recurrent, and chronic pancreatitis. *Am J Gastroenterol* 2010, 105(1):199-206.
11. Hegyi P, Pandol S, Venglovecz V, Rakonczay Z, Jr.: The acinar-ductal tango in the pathogenesis of acute pancreatitis. *Gut* 2011, 60(4):544-552.
12. Shenolikar S, Voltz JW, Minkoff CM, Wade JB, Weinman EJ: Targeted disruption of the mouse NHERF-1 gene promotes internalization of proximal tubule sodium-phosphate cotransporter type IIa and renal phosphate wasting. *Proc Natl Acad Sci U S A* 2002, 99(17):11470-11475.
13. Gray MA, Winpenny JP, Porteous DJ, Dorin JR, Argent BE: CFTR and calcium-activated chloride currents in pancreatic duct cells of a transgenic CF mouse. *Am J Physiol* 1994, 266(1 Pt 1):C213-221.
14. Pandol SJ, Jensen RT, Gardner JD: Mechanism of [Tyr4]bombesin-induced desensitization in dispersed acini from guinea pig pancreas. *J Biol Chem* 1982, 257(20):12024-12029.

15. Cinar A, Chen M, Riederer B, Bachmann O, Wiemann M, Manns M, Kocher O, Seidler U: NHE3 inhibition by cAMP and Ca^{2+} is abolished in PDZ-domain protein PDZK1-deficient murine enterocytes. *J Physiol* 2007, 581(Pt 3):1235-1246.
16. Venglovecz V, Rakonczay Z, Jr., Ózsvári B, Takács T, Lonovics J, Varró A, Gray MA, Argent BE, Hegyi P: Effects of bile acids on pancreatic ductal bicarbonate secretion in guinea pig. *Gut* 2008, 57(8):1102-1112.
17. Hegyi P, Rakonczay Z, Jr., Gray MA, Argent BE: Measurement of intracellular pH in pancreatic duct cells: a new method for calibrating the fluorescence data. *Pancreas* 2004, 28(4):427-434.
18. Hegyi P, Rakonczay Z, Jr., Tiszlavicz L, Varró A, Tóth A, Rácz G, Varga G, Gray MA, Argent BE: Protein kinase C mediates the inhibitory effect of substance P on HCO3- secretion from guinea pig pancreatic ducts. *Am J Physiol Cell Physiol* 2005, 288(5):C1030-1041.
19. Fernandez-Salazar MP, Pascua P, Calvo JJ, Lopez MA, Case RM, Steward MC, San Roman JI: Basolateral anion transport mechanisms underlying fluid secretion by mouse, rat and guinea-pig pancreatic ducts. *J Physiol* 2004, 556(Pt 2):415-428.
20. Perides G, van Acker GJ, Laukkarinen JM, Steer ML: Experimental acute biliary pancreatitis induced by retrograde infusion of bile acids into the mouse pancreatic duct. *Nat Protoc* 2010, 5(2):335-341.
21. Rakonczay Z, Jr., Hegyi P, Dosa S, Ivanyi B, Jarmay K, Biczo G, Hracsko Z, Varga IS, Karg E, Kaszaki J *et al*: A new severe acute necrotizing pancreatitis model induced by L-ornithine in rats. *Crit Care Med* 2008, 36(7):2117-2127.
22. Kuebler WM, Abels C, Schuerer L, Goetz AE: Measurement of neutrophil content in brain and lung tissue by a modified myeloperoxidase assay. *Int J Microcirc Clin Exp* 1996, 16(2):89-97.
23. Hofbauer B, Saluja AK, Lerch MM, Bhagat L, Bhatia M, Lee HS, Frossard JL, Adler G, Steer ML: Intra-acinar cell activation of trypsinogen during caerulein-induced pancreatitis in rats. *Am J Physiol* 1998, 275(2 Pt 1):G352-362.
24. Saluja AK, Donovan EA, Yamanaka K, Yamaguchi Y, Hofbauer B, Steer ML: Cerulein-induced in vitro activation of trypsinogen in rat pancreatic acini is mediated by cathepsin B. *Gastroenterology* 1997, 113(1):304-310.
25. Rakonczay Z, Jr., Hegyi P, Takács T, McCarroll J, Saluja AK: The role of NF-kappaB activation in the pathogenesis of acute pancreatitis. *Gut* 2008, 57(2):259-267.
26. Wu Y, Wang S, Farooq SM, Castelvetere MP, Hou Y, Gao JL, Navarro JV, Oupicky D, Sun F, Li C: A chemokine receptor CXCR2 macromolecular complex regulates neutrophil functions in inflammatory diseases. *J Biol Chem* 2012, 287(8):5744-5755.
27. Thrower EC, Wang J, Cheriyan S, Lugea A, Kolodecik TR, Yuan J, Reeve JR, Jr., Gorelick FS, Pandol SJ: Protein kinase C delta-mediated processes in cholecystokinin-8-stimulated pancreatic acini. *Pancreas* 2009, 38(8):930-935.
28. Barrow SL, Voronina SG, Xavier GD, Chvanov MA, Longbottom RE, Gerasimenko OV, Petersen OH, Rutter GA, Tepikin AV: ATP depletion inhibits Ca^{2+} release, influx and extrusion in pancreatic acinar cells but not pathological Ca^{2+} responses induced by bile. *Pflug Arch Eur J Phy* 2008, 455(6):1025-1039.
29. Raghuram V, Mak DO, Foskett JK: Regulation of cystic fibrosis transmembrane conductance regulator single-channel gating by bivalent PDZ-domain-mediated interaction. *Proc Natl Acad Sci U S A* 2001, 98(3):1300-1305.

30. Moyer BD, Denton J, Karlson KH, Reynolds D, Wang S, Mickle JE, Milewski M, Cutting GR, Guggino WB, Li M *et al*: A PDZ-interacting domain in CFTR is an apical membrane polarization signal. *J Clin Invest* 1999, 104(10):1353-1361.
31. Milewski MI, Mickle JE, Forrest JK, Stafford DM, Moyer BD, Cheng J, Guggino WB, Stanton BA, Cutting GR: A PDZ-binding motif is essential but not sufficient to localize the C terminus of CFTR to the apical membrane. *J Cell Sci* 2001, 114(Pt 4):719-726.
32. Swiatecka-Urban A, Duhaime M, Coutermarsh B, Karlson KH, Collawn J, Milewski M, Cutting GR, Guggino WB, Langford G, Stanton BA: PDZ domain interaction controls the endocytic recycling of the cystic fibrosis transmembrane conductance regulator. *J Biol Chem* 2002, 277(42):40099-40105.
33. Benharouga M, Sharma M, So J, Haardt M, Drzymala L, Popov M, Schwapach B, Grinstein S, Du K, Lukacs GL: The role of the C terminus and Na^+/H^+ exchanger regulatory factor in the functional expression of cystic fibrosis transmembrane conductance regulator in nonpolarized cells and epithelia. *J Biol Chem* 2003, 278(24):22079-22089.
34. Ostedgaard LS, Randak C, Rokhlina T, Karp P, Vermeer D, Ashbourne Excoffon KJ, Welsh MJ: Effects of C-terminal deletions on cystic fibrosis transmembrane conductance regulator function in cystic fibrosis airway epithelia. *Proc Natl Acad Sci U S A* 2003, 100(4):1937-1942.
35. Lukács GL, Verkman AS: CFTR: folding, misfolding and correcting the DeltaF508 conformational defect. *Trends Mol Med* 2012, 18(2):81-91.
36. Lamprecht G, Heil A, Baisch S, Lin-Wu E, Yun CC, Kalbacher H, Gregor M, Seidler U: The down regulated in adenoma (dra) gene product binds to the second PDZ domain of the NHE3 kinase A regulatory protein (E3KARP), potentially linking intestinal Cl^-/HCO_3^- exchange to Na^+/H^+ exchange. *Biochemistry* 2002, 41(41):12336-12342.
37. Lohi H, Lamprecht G, Markovich D, Heil A, Kujala M, Seidler U, Kere J: Isoforms of SLC26A6 mediate anion transport and have functional PDZ interaction domains. *Am J Physiol Cell Physiol* 2003, 284(3):C769-779.
38. Rakonczay Z, Jr., Hegyi P, Hasegawa M, Inoue M, You J, Iida A, Ignáth I, Alton EW, Griesenbach U, Ovari G *et al*: CFTR gene transfer to human cystic fibrosis pancreatic duct cells using a Sendai virus vector. *J Cell Physiol* 2008, 214(2):442-455.
39. Chernova MN, Jiang L, Shmukler BE, Schweinfest CW, Blanco P, Freedman SD, Stewart AK, Alper SL: Acute regulation of the SLC26A3 congenital chloride diarrhoea anion exchanger (DRA) expressed in Xenopus oocytes. *J Physiol* 2003, 549(Pt 1):3-19.
40. Broere N, Hillesheim J, Tuo B, Jorna H, Houtsmuller AB, Shenolikar S, Weinman EJ, Donowitz M, Seidler U, de Jonge HR *et al*: Cystic fibrosis transmembrane conductance regulator activation is reduced in the small intestine of Na^+/H^+ exchanger 3 regulatory factor 1 (NHERF-1)- but Not NHERF-2-deficient mice. *J Biol Chem* 2007, 282(52):37575-37584.
41. Monterisi S, Favia M, Guerra L, Cardone RA, Marzulli D, Reshkin SJ, Casavola V, Zaccolo M: CFTR regulation in human airway epithelial cells requires integrity of the actin cytoskeleton and compartmentalized cAMP and PKA activity. *J Cell Sci* 2012, 125(Pt 5):1106-1117.
42. Hillesheim J, Riederer B, Tuo B, Chen M, Manns M, Biber J, Yun C, Kocher O, Seidler U: Down regulation of small intestinal ion transport in PDZK1-(CAP70/NHERF3) deficient mice. *Pflugers Arch* 2007, 454(4):575-586.

43. Singh AK, Riederer B, Chen M, Xiao F, Krabbenhoft A, Engelhardt R, Nylander O, Soleimani M, Seidler U: The switch of intestinal Slc26 exchangers from anion absorptive to HCO3- secretory mode is dependent on CFTR anion channel function. *Am J Physiol Cell Physiol* 2010, 298(5):C1057-1065.
44. Chen JM, Ferec C: Chronic pancreatitis: genetics and pathogenesis. *Annu Rev Genomics Hum Genet* 2009, 10:63-87.
45. Ko SB, Mizuno N, Yatabe Y, Yoshikawa T, Ishiguro H, Yamamoto A, Azuma S, Naruse S, Yamao K, Muallem S *et al*: Corticosteroids correct aberrant CFTR localization in the duct and regenerate acinar cells in autoimmune pancreatitis. *Gastroenterology* 2010, 138(5):1988-1996.
46. Czako L, Yamamoto M, Otsuki M: Exocrine pancreatic function in rats after acute pancreatitis. *Pancreas* 1997, 15(1):83-90.
47. Renner IG, Wisner JR, Jr., Rinderknecht H: Protective effects of exogenous secretin on ceruletide-induced acute pancreatitis in the rat. *J Clin Invest* 1983, 72(3):1081-1092.
48. Niederau C, Ferrell LD, Grendell JH: Caerulein-induced acute necrotizing pancreatitis in mice: protective effects of proglumide, benzotript, and secretin. *Gastroenterology* 1985, 88(5 Pt 1):1192-1204.
49. Bhandari M, Thomas AC, Hussey DJ, Li X, Jaya SP, Woods CM, Schloithe AC, Mayne GC, Carati CJ, Toouli J *et al*: Galanin mediates the pathogenesis of cerulein-induced acute pancreatitis in the mouse. *Pancreas* 2010, 39(2):182-187.
50. DiMagno MJ, Lee SH, Owyang C, Zhou SY: Inhibition of acinar apoptosis occurs during acute pancreatitis in the human homologue DeltaF508 cystic fibrosis mouse. *Am J Physiol Gastrointest Liver Physiol* 2010, 299(2):G400-412.
51. Dimagno MJ, Lee SH, Hao Y, Zhou SY, McKenna BJ, Owyang C: A proinflammatory, antiapoptotic phenotype underlies the susceptibility to acute pancreatitis in cystic fibrosis transmembrane regulator (-/-) mice. *Gastroenterology* 2005, 129(2):665-681.
52. Hegyi P, Perides G, Steer ML, et al: Commonly employed rodent models of experimental acute pancreatitis: Their strengths and weaknesses, relevance to human disease, selection, and appropriate use. *The Pancreapedia: Exocrine Pancreas Knowledge Base* 2013; DOI: 10.3998/panc.2013.4.

FIGURES

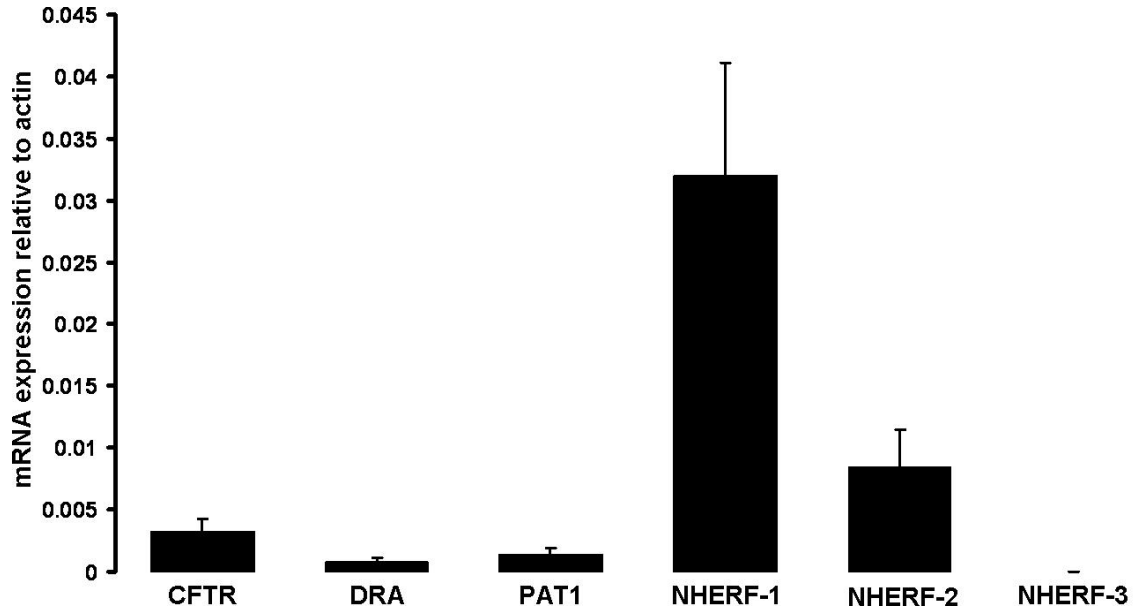

Fig. 1. mRNA expression of CFTR, DRA, PAT1, NHERF-1, NHERF-2 and NHERF-3 in isolated mouse pancreatic ducts. Total RNA was prepared from isolated interlobular pancreatic ducts of wild-type (WT) mice (n=6) after overnight culture and mRNA expression of transporters/NHERF1-3 was measured by real-time RT-PCR. Data are shown as means ± SEM.

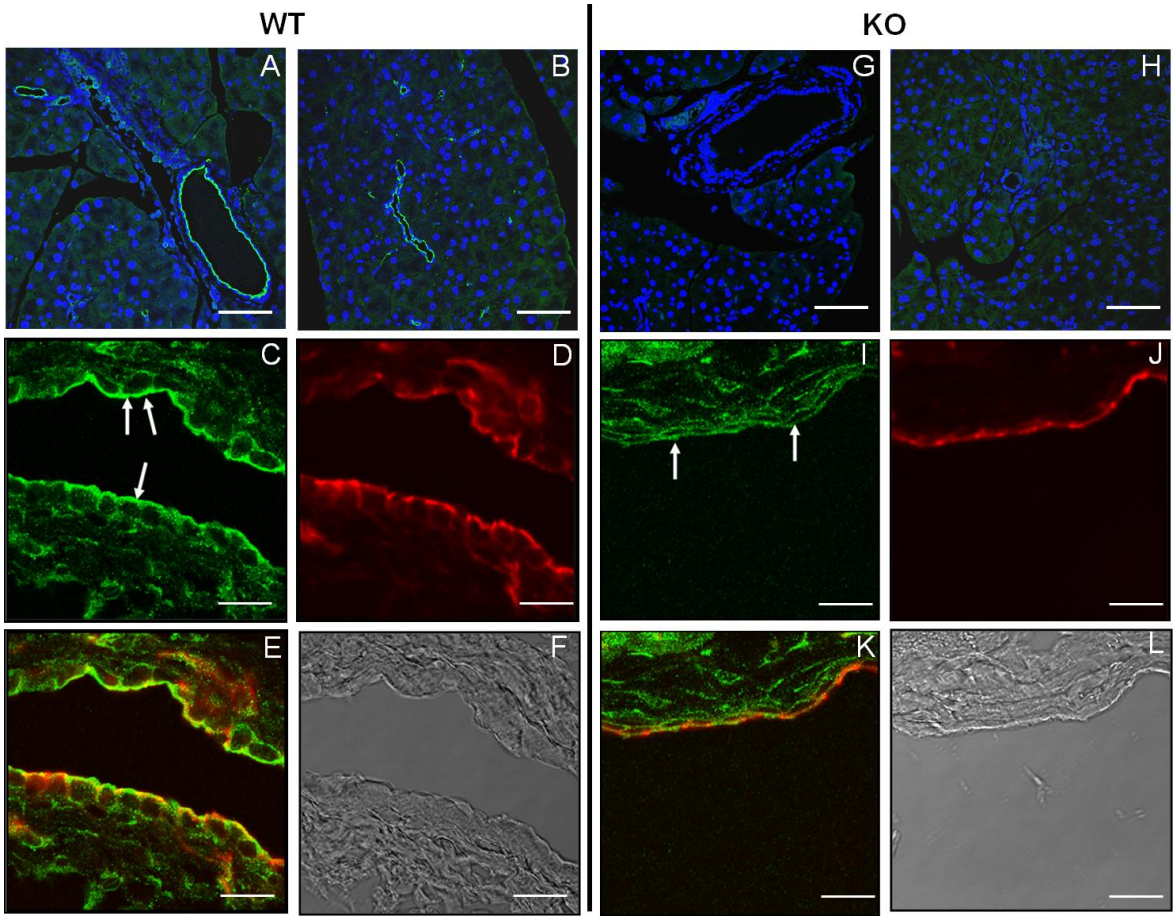

Fig. 2. NHERF-1 and CFTR staining in wild-type and NHERF-1-knock-out pancreata.

Representative immunohistochemical staining of NHERF1 (**A, B, G, H**) and CFTR (**C, I**) in the pancreas of WT and NHERF-1-knock-out (KO) mice. NHERF-1 was localized in the apical membrane of intra- and interlobular duct cells; only weak staining was noted in some acinar cells of WT mice (**A, B**). No or weak staining was detected in NHERF-1-KO mice (**G, H**). CFTR staining in the pancreas of WT and NHERF-1-KO mice showed that apical (white arrow) CFTR localization (green) was reduced in NHERF-1-KO (**I**) vs. WT (**C**) ducts. Red staining shows F-actin expression (**D, J**). **E, K** show merged images of CFTR and F-actin (yellow color indicates co-localization). **F, L** are phase contrast pictures. Scale bar = 50 μm.

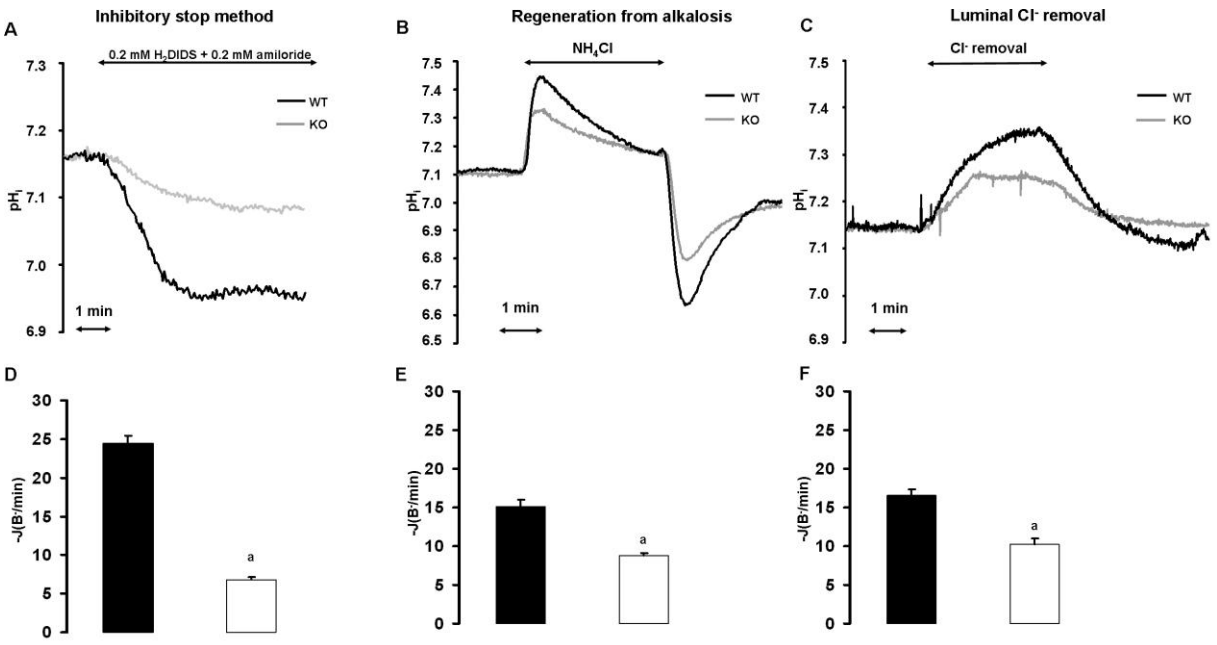

Fig. 3. Pancreatic ductal HCO_3^- secretion is decreased in NHERF-1-knock-out mice. Panels **A-C** show representative intracellular pH traces of isolated pancreatic ducts bathed in standard HCO_3^-/CO_2 solution demonstrating the effects of 0.2mM amiloride and 0.2mM H_2DIDS administered from the basolateral membrane (**A**), the recovery from alkalosis via administration of 20mM NH_4Cl (**B**), or after luminal Cl^- removal (**C**). Bar charts show summary data for the base fluxes [-J(B^-/min)] after exposure of the transport inhibitors (**D**), 20mM NH_4Cl (**E**) or luminal Cl^- removal (**F**) in WT (closed columns) and NHERF-1-KO (open columns) mice. Means ± SEM are from 30-50 regions of interest from 5-8 ducts.
a: $P<0.05$ vs. the respective WT group.

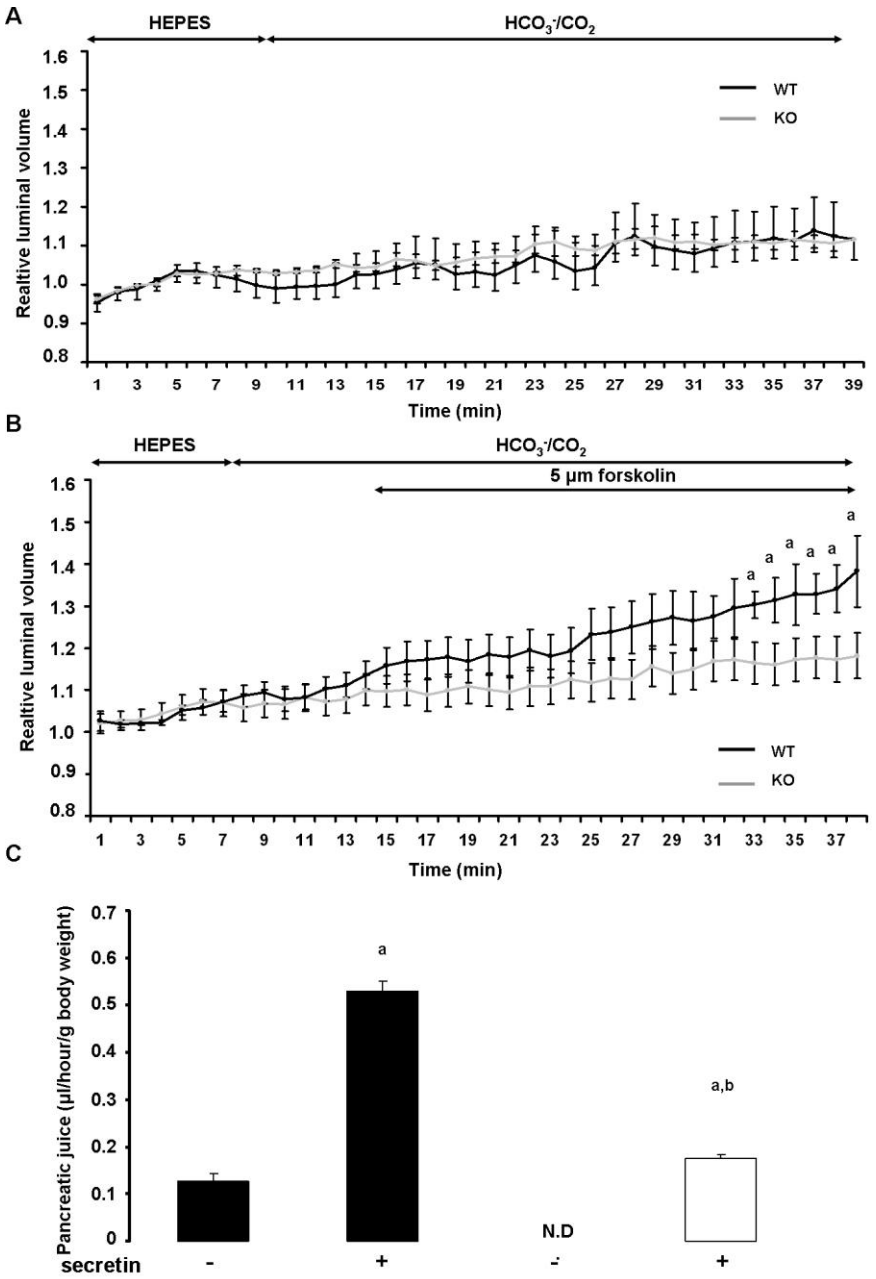

Fig. 4. Fluid secretion is decreased in NHERF-1-knock-out vs. wild-type mice. A and **B** show changes in the relative luminal volume of pancreatic ducts from WT (black line, n=8 from 3 animals) and NHERF-1-KO (gray line, n=8 from 3 animals) mice. Initially, ducts were perfused with HEPES-buffered solution, then perfusion was switched to standard HCO_3^-/CO_2-buffered solution (**A**). In some cases the ductal secretion was stimulated with 5 µM forskolin (**B**). Panel **C** shows the volume of pancreatic juice collected *in vivo* under basal (secretin -) and secretin-stimulated (secretin +, 0.75 CU/kg i.v.) conditions from WT (closed columns) and NHERF-1-KO (open column) mice anesthetized with urethane. Means ± SEM are from 5-6 animals. $P<0.05$ vs. a: the

respective secretin– group or b: vs. the WT secretin+ group. N.D.: not detected in case of NHERF-1-KO mice.

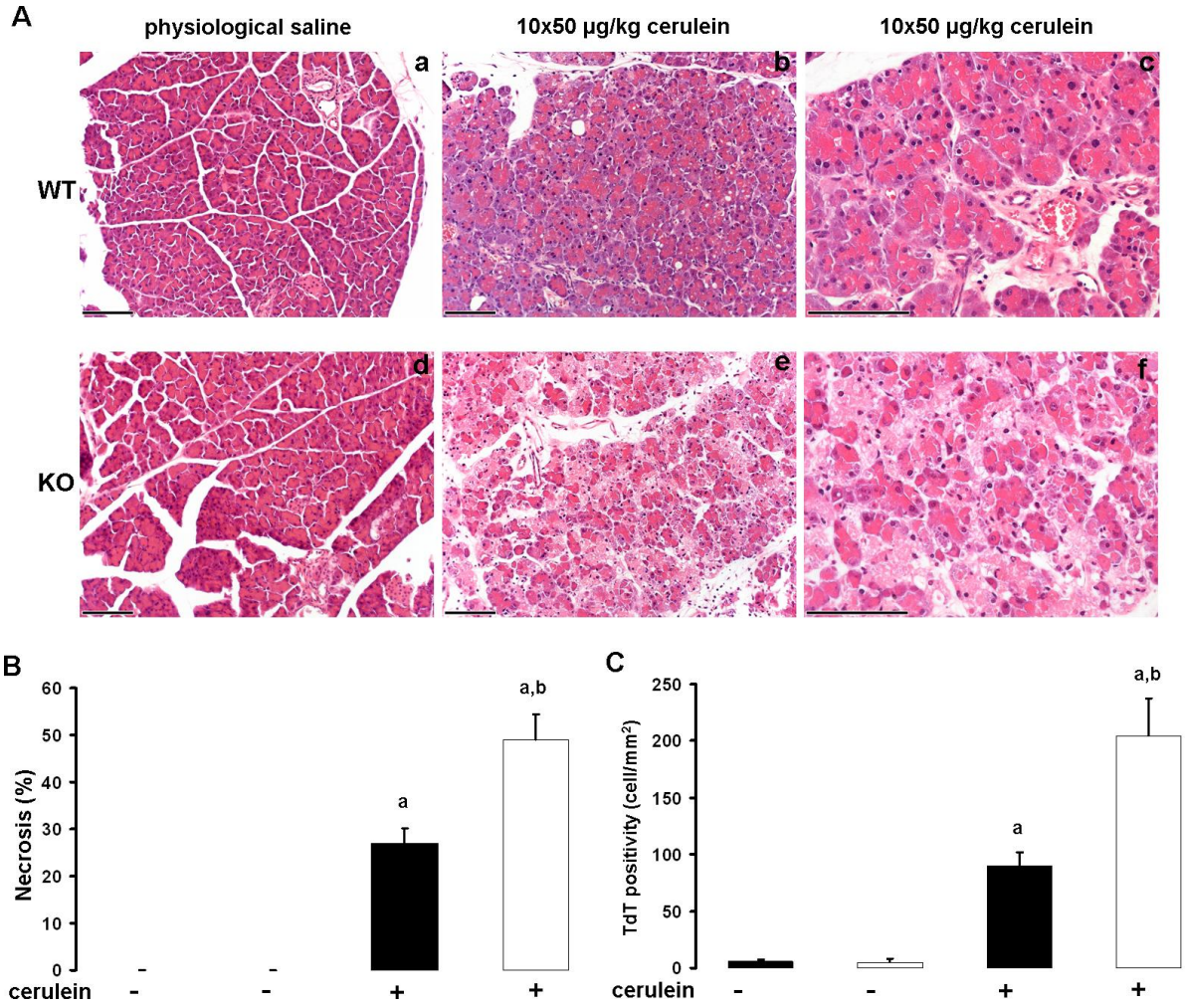

Fig. 5. Histopathologic changes of the pancreas in response to intraperitoneal administration of cerulein in wild-type and NHERF-1-knock-out mice. Acute pancreatitis was induced by administering 10 hourly i.p. injections of cerulein (50 µg/kg per injection, cerulein+). Control mice were given PS (cerulein-) instead of cerulein. Mice were exsanguinated through the inferior vena cava 12 h after the first i.p. injection. (**A**)The pictures show representative light micrographs (H&E staining) of the pancreata of WT control (**a**) and cerulein-treated (**b-c**) and NHERF-1-KO control (**d**) and cerulein-treated (**e-f**) mice. Scale bar=100µm. The bar diagrams show the rates of pancreatic necrosis (**B**) (n=9-10) and apoptosis (**C**) (n=4-6). Data are shown as means±SEM. P<0.05 vs. a: the respective control group or b: vs. the WT cerulein+ group. WT (closed columns), NHERF-1-KO (open columns).

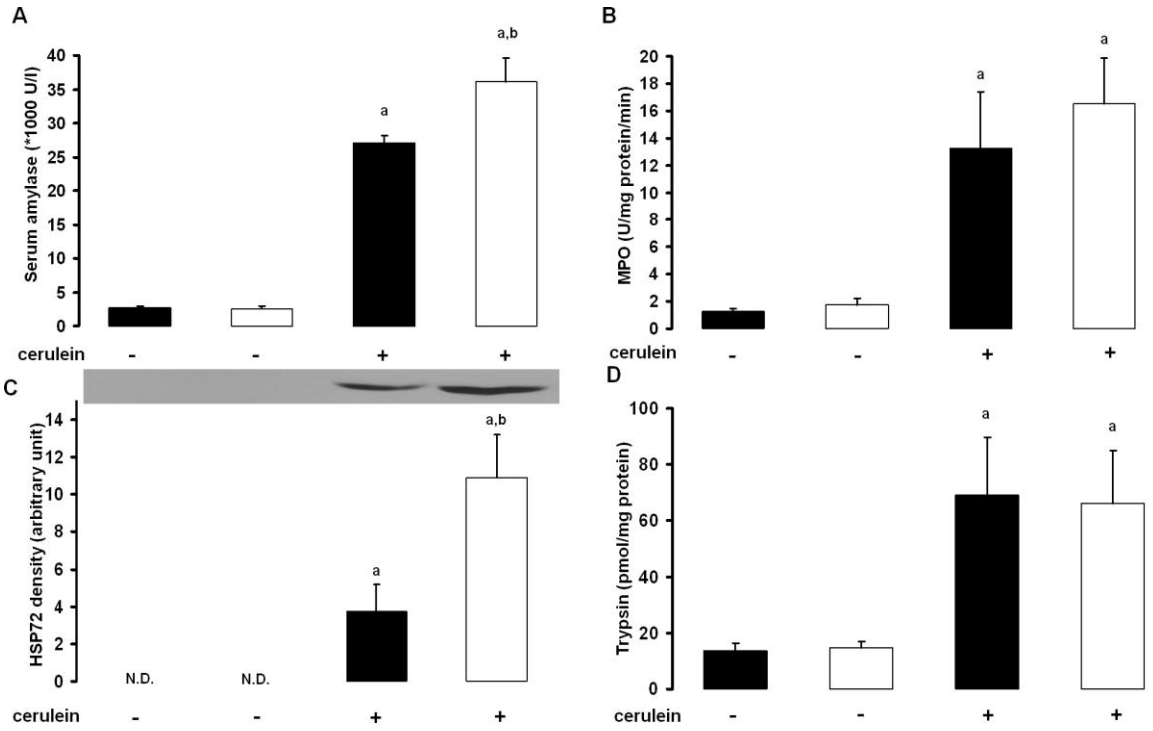

Fig. 6. Severity of cerulein-induced acute pancreatitis and pancreatic trypsinogen activation in wild-type and NHERF-1-knock-out mice. Acute pancreatitis was induced in WT (closed columns) and NHERF-1-KO (open columns) mice by administering 1x50μg/kg (for measurement of trypsin activity) or 10 hourly i.p. injections of 50 μg/kg cerulein (cerulein+). Control mice were given PS (cerulein-) instead of cerulein. Mice were exsanguinated through the inferior vena cava 0.5h (in case of measurement of trypsin activity) or 12h after the first i.p. injection. The bar diagrams show serum amylase activity (**A**), the pancreatic myeloperoxidase (MPO) activity (**B**), heat shock protein-72 (HSP72) expression (**C**) and trypsin (**D**) activities. Data are shown as means ± SEM, n=4-6. $P<0.05$ vs. a: the respective control group or b: vs. the WT cerulein+ group. N.D.: not detected.

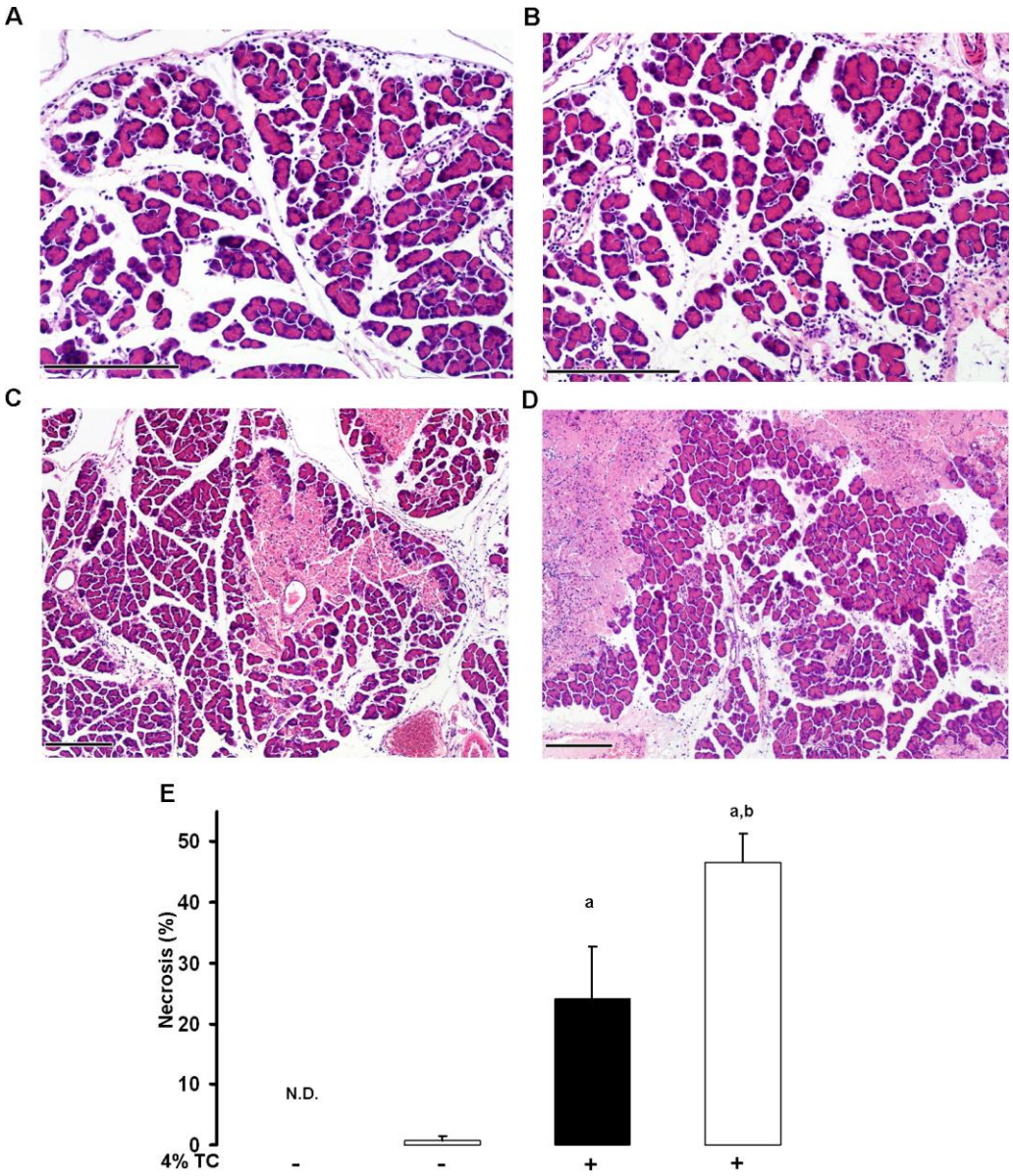

Fig. 7. Histopathologic changes of the pancreatic head in response to intraductal administration of physiological saline and 4% sodium-taurocholate in wild-type and NHERF-1-knock-out mice. The diagrams show representative light micrographs (H&E staining) of pancreata of WT (**A, C**) and NHERF-1-KO (**B, D**) mice 24 h after intraductal treatment with 50µl (10µl/min) PS (4%TC-) (**A, B**) or 4% Na-taurocholate (4%TC+) (**C, D**). Inflammatory infiltration was significantly higher in NHERF-1-KO (**A**) vs. WT (**B**) PS-treated mice. Intraductal infusion with 4% Na-taurocholate caused the development of severe acute necrotizing pancreatitis in WT (**C**) and NHERF-1-KO (**D**) mice. The bar diagram shows the rates of pancreatic necrosis (**E**) in the various groups. Data are shown as means ± SEM, n=5-7. $P<0.05$ vs. a: the respective control group or b: vs. the WT 4%TC+ group. N.D.: not detected in the WT group. Scale bar = 200 µm. WT (closed columns), NHERF-1-KO (open columns).

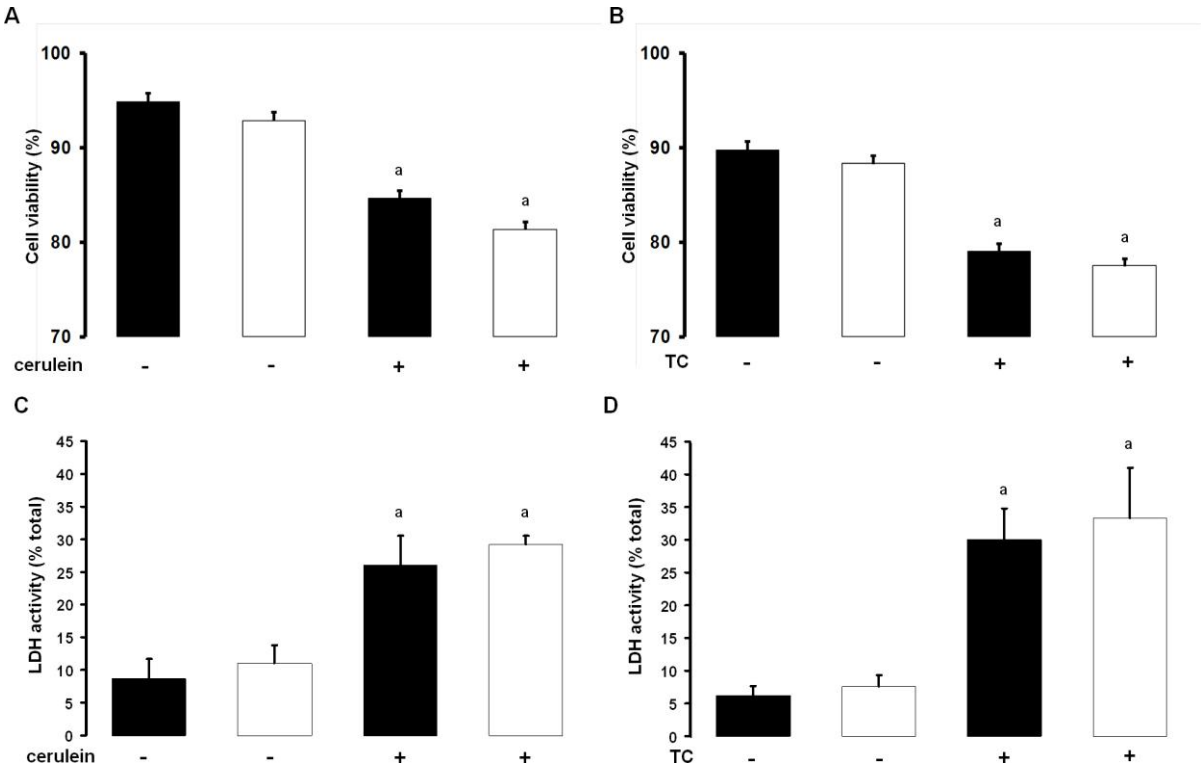

Fig. 8. NHERF-1 expression does not influence the degree of cell damage caused by high concentrations of cerulein or sodium-taurocholate in isolated acinar cells. Acinar cells were isolated from WT and NHERF-1-KO mice by collagenase digestion. *In vitro* cell damage was induced by the administration of high concentrations of 10^{-8} M cerulein (cerulein+) for 2h or 1 mM Na-taurocholate (TC+) for 3h. Alternatively, cells were treated with the vehicle for cerulein (cerulein-) or Na-taurocholate (TC-) for the same time-periods. Cell viability was determined by trypan blue staining (**A, B**) and measurement of lactate dehydrogenase (LDH) release (**C, D**) from acini. Data are shown as means ± SEM, n=7. P<0.05 vs. a: the respective control group. WT (closed columns), NHERF-1-KO (open columns).

TABLE

	WT physiological saline	WT 4% Na-taurocholate	KO physiological saline	KO 4% Na-taurocholate
Interstitial edema (0-3)	1.75 ± 0.47	2 ± 0.06	1.8 ± 0.2	2.35 ± 0.14
Hemorrhage (0-3)	0	0.42 ± 0.2 a	0	0.71 ± 0.28 a
Leukocyte infiltration (0-3)	0.8 ± 0.3	1.9 ± 0.38 a	1.6 ± 0.36 b	1.9 ± 0.45

Table 1. Histopathological changes in response to intraductal infusion of 4% sodium-taurocholate and physiological saline in wild-type and NHERF-1-knock-out mice. WT and NHERF-1-KO mice were infused intraductally with 4% Na-taurocholate or physiological saline (PS, control) and were sacrificed after 24h. Histological scores are shown as means ± SEM for 5-7 animals. $P<0.05$ vs. a: the respective PS-treated group or b: vs. the WT PS-treated group.

SUPPLEMENTARY MATERIALS AND METHODS

Materials

All laboratory chemicals were obtained from Sigma-Aldrich (Munich, Germany) unless indicated otherwise. Forskolin was from Tocris Bioscience (Bristol, UK), purified CLSPA collagenase was from Worthington Biochemical Corporation (Lakewood, NJ, USA) and cerulein was from American Peptide Company (Sunnyvale, CA, USA). H_2DIDS, Superscript III RT, TrypLE™ Express solution, Alexa Fluor 488-labelled goat anti-rabbit IgG, phalloidin-633 and SlowFade Gold antifade reagent were purchased from Invitrogen Corporation (Carlsbad, CA, USA). CP-Ketamine (10%) and CP-Xylazine (2%) were obtained from CP-Pharma-Handelsgesellschaft MBH (Burgdorf, Germany). Urethane was from Reanal (Budapest, Hungary) and pentobarbital was from Bimeda MTC (Cambridge, Canada). DirectPCR (Tail) reagent was obtained from Viagen Biotech Inc. (Los Angeles, CA, USA). NucleoSpin RNA XS Total RNA Isolation Kit was from Machery & Nagel (Düren, Germany). MesaGreen was from Eurogentec (Seraing, Liège, Belgium). CellTak was purchased from Becton Dickinson Labware (Bedford, Massachusetts, USA). Background reducing buffer was from DAKO (Glostrup, Denmark). Mr Pink rabbit polyclonal antibody against human CFTR provided by W.E. Balch, Scripps Research Institute (La Jolla, CA, USA). An IL-1β ELISA kit was purchased from R&D Systems (Minneapolis, MN, USA). Laboratory chow was from Biofarm (Zagyvaszántó, Hungary). Dulbecco's Modified Eagle Medium (DMEM) and heat-inactivated fetal bovine serum were purchased from Lonza (Basel, Switzerland). Amylase and lactate dehydrogenase activities were determined using commercial kits (DIALAB GmbH, Neudorf, Austria and Diagnosticum ZRt., Budapest, Hungary, respectively). Isolation of polymorphonuclear cells was performed by Polymorphprep (Axis-Shield, Oslo, Norway).

Apoptotic cells were quantitated by using an *In Situ* Cell Death Detection Kit from Roche Diagnostics (Mannheim, Germany). Concentrated stock solutions of forskolin (100mM), cerulein (4mM) and amiloride (50mM) were prepared in dimethylsulfoxide. 2% stock solution of dextran was dissolved in physiological saline (PS).

Maintenance and genotyping of mice

The mice were housed in a standard animal care facility with a 12-h light/12-h dark cycle and were allowed free access to water and standard laboratory chow. Genotyping of mice was performed after DNA extraction from tail samples using the DirectPCR (Tail) reagent supplemented with proteinase K. The primer sequences for genotyping NHERF-1 mice were as follows: wild-type forward, 5'-TCGGGGTTGTTGGCTGGAGAC-3'; common reverse, 5'-AGCCCAACCCGCACTTACCA-3'; KO forward, 5'-AGGGCTGGCACTCTGTCG-3'. Amplicons generated by PCR were 294 bp for the WT gene and 242 bp for the KO gene.

mRNA expression of CFTR, PAT-1, DRA, NHERF-1, NHERF-2 and NHERF-3 in mouse pancreatic ducts

The primer sequences for CFTR Homolog NM_021050 are forward: 5′-TTCTTCACGCCCCTATGTCGA-3′ reverse: 5′-GCTCCAATCACAATGAACACCA-3′ (PCR product length: 145 bp), for slc26a3 (DRA) NM_021353 are forward: 5′-TTCCCCTCAACATCACCATCC-3′, reverse: 5′-GTAAAATCGTTCTGAGGCCCC-3′ (PCR-product length: 110 bp), for NHERF-2 NM_023449:2 are forward: 5′-TAGTCGATCCTGAGACTGATG-3′, reverse: 5′-ATTGTCCTTCTCTGAGCCTG-3′ (PCR-product length: 173 bp), and for NHERF-3 NM_021517:1 are forward: 5′-TGACGGTGTGGTGGAAATG-3′, reverse: 5′-TGGCAGTAAAGAAGTGGAGAC-3′

(PCR-product length: 117 bp) were designed with “Primer Express” (Applied Biosystems, Foster City, CA, USA). The primers sequences for slc26a6 (putative anion transporter-1, PAT-1) and NHERF-1 were published before [1, 2]. Real-time polymerase chain reactions (qRT-PCR) were carried out using MesaGreen in the Applied Biosystems 7300 Real-time PCR System. PCR extension was performed at 60 °C with 40 repeats. Data were analyzed using Sequence Detection Software 1.2.3 (Applied Biosystems) and exported to Microsoft Excel. Relative quantification was carried out using β-actin as a reference gene [3].

Immunohistochemistry

Briefly, for NHERF-1 staining, paraformaldehyde-fixed, paraffin-embedded tissue sections (5 μm) from mice of different genotypes were prepared on the same slide. After deparaffinization with xylene, sections were treated with 0.01 M sodium citrate solution at 100 °C for 10 min. For CFTR staining, pancreata were fixed in 2% paraformaldehyde (in PBS). Fixed tissue was rinsed with PBS and transferred to 30% sucrose in PBS overnight. The tissue was embedded in tissue-freezing medium (TissueTec O.C.T., Sakura). Cryosectioning was done with a microtome cryostat at −20 °C and 10 μm thick sections were collected on microscope slides (SuperFrost Plus, Menzel-Gläser, Germany).

Pancreatic sections were incubated sequentially with PBS for 5 min, washing buffer of PBS with 50 mM NH_4Cl twice for 10 min each, background reducing buffer for 20 min and 5-10% goat serum for 30 min for blocking and incubated with rabbit anti-NHERF-1 (1:500) [4] antibody or Mr. Pink rabbit polyclonal antibody against human CFTR (1:100) in background reducing buffer overnight at 4 °C. Washing 4 times for 5 min in the washing buffer was followed by secondary antibody (Alexa Fluor 488-labelled goat anti-rabbit IgG) incubation for 1 h at room temperature at a dilution of 1:300-1:500 in background reducing buffer. After 2-4 washes for 5 min each, in case of NHERF-1 staining, the sections were

treated with 5U/ml phalloidin-633 in PBS with 1% bovine serum albumin, 0.2% Triton X-100 for 30 min which was followed by washes with washing buffer (six times). After washing, each cover slide was mounted with SlowFade Gold antifade reagent with DAPI, and slides were imaged on a confocal microscope (TCS SP2; Leica, Wetzlar, Germany). Excitation wavelengths used were 405, 488, and 633 nm, and emission was taken at 415–450, 490–540, and 560–700nm for detection of DAPI, Alexa Fluor 488, and phalloidin 633, respectively.

Solutions used for the determination of pancreatic ductal HCO_3^- and fluid secretion *in vivo*

The HEPES-buffered solution contained (in mM): 130 NaCl, 5 KCl, 1 $CaCl_2$, 1 $MgCl_2$, 10 glucose and 10 Na-HEPES and its pH was set to 7.4 with HCl at 37 °C. The standard HCO_3^--buffered solution contained (in mM): 115 NaCl, 25 $NaHCO_3$, 5 KCl, 1 $CaCl_2$, 1 $MgCl_2$, 10 Glucose. In the NH_4^+ pulse experiments in HCO_3^--buffered soultion, 20 mM NaCl was repleaced with NH_4Cl. The Cl^--free HCO_3^- solution contained (in mM): 25 $NaHCO_3$, 115 Na-gluconate, 1 Mg-gluconate, 6 Ca-gluconate, 2.5 KH_2-sulfate and 10 glucose. The HCO_3^--containing solutions were equilibrated with 95% O_2 and 5% CO_2 to maintain pH at 7.4 at 37 °C.

Determination of HCO_3^- efflux

To determine the HCO_3^- efflux across the apical membrane of the pancreatic ductal epithelia, we used three methods: inhibitory stop, alkali load and luminal Cl^- withdrawal. The measured rates of pH_i change (dpH/dt) were converted to $J(B^-)$ using the equation: $J(B^-)=(dpH/dt)x\beta_{total}$ where β_{total} is the total buffering capacity of the cells. $J(B^-)$ reflects the rate of HCO_3^- efflux (i.e. secretion) on luminal Cl^-/HCO_3^- exchangers [5].

Measurement of fluid secretion

In vitro

Fluid secretion into the closed luminal space of the cultured pancreatic ducts was analysed using a swelling method developed by Fernandez-Salazar et al [6]. Briefly, the ducts were transferred to a perfusion chamber (0.45 ml) and were attached to a coverslip precoated with CellTak in the base of the chamber. Bright-field images were acquired at 1 min intervals using a CCD camera (CFW 1308C, Scion Corporation, Frederick, MD, USA). The integrity of the duct wall was checked at the end of each experiment by perfusing the chamber with a hypotonic solution (standard HEPES-buffered solution diluted 1:1 with distilled water). Digital images of the ducts were analysed using Scion Image software (Scion Corporation, Frederick, MD, USA) to obtain values for the area corresponding to the luminal space in each image.

In vivo

Mice were anesthetized with 1.5 g/kg urethane by i.p. injection. The body temperature of mice was maintained by placing the animals on a warm pad (37°C) during the experiments. The abdomen was opened, and the lumen of the common biliopancreatic duct was cannulated with a blunt-end 31-gauge needle. Then the proximal end of the common duct was occluded with a microvessel clip to prevent contamination with bile, and the pancreatic juice was collected in PE-10 tube for 30 min. Using an operating microscope, the jugular vein was cannulated for i.v. administration of secretin (0.75 CU/kg) and the pancreatic juice was collected for an additional 120 min.

Isolation of pancreatic acini

Mouse pancreatic acinar cells were isolated according to the method of Pandol et al [7]. Briefly, mice were anaesthetized with 85 mg/kg pentobarbital by i.p. injection. The pancreas was quickly removed, and was cleaned from fat and lymph nodes. The extracellular solution for cell isolation contained (in mM) 120 NaCl, 5 KCl, 25 HEPES, 2 NaH_2PO_4, 2 $CaCl_2$, 1 $MgCl_2$, 5 pyruvate, 4 Na-fumarate, 4 Na-glutamate, 12 mM D-glucose, as well as 0.02% (wt/vol) soybean trypsin inhibitor, 0.2% (wt/vol) bovine serum albumin, 0.025% (vol/vol) minimal essential amino acids and 0.01% (vol/vol) vitamins eagle. The pancreas was inflated with 5ml of extracellular solution containing collagenase (105 U/ml) then subjected to three successive 20-min incubations in this solution with vigorous shaking at 37 °C. For each 20-min incubation, the extracellular solution containing collagenase was replaced with a fresh oxygenated aliquot. Acinar cells were then washed three times with extracellular solution, followed by resuspension in Medium 199 and incubated for 30 min. Acinar cells were used for experiments thereafter. Cells were incubated with cerulein (10^{-8}-10^{-12} M), 1 mM Na^+-taurocholate or physiological saline. Amylase secretion was determined in response to cerulein and is given as the percentage of total amylase content. The extent of cytotoxicity (in response to 10^{-8} M cerulein and 1 mM Na^+-taurocholate) as quantified by trypan-blue staining and by measuring the amount of lactate dehydrogenase (LDH) released into the incubation medium of acinar cells. LDH activity was measured spectrophotometrically as the production of NAD from pyruvic acid and NADH. Values for LDH release are presented as the percentage of total LDH activity (medium/medium+cells).

Isolation of polymorphonuclear cells and bacterial killing assay

Mouse polymorphonuclear cells (PMNs) were isolated from freshly drawn, heparinized blood using Polymorphprep (Axis-Shield) according to the manufacturer's

instructions. Isolated PMNs were immadiately plated in round-bottom 96-well plastic cell culture plates (10^5 PMNs/well) in DMEM supplemented with 10% autologous serum. *E. coli* bacteria were added to the cultures at an effector/target ratio of 1:5. As a control, the same number of bacterial cells were incubated in the appropriate cell culture medium without PMNs. After a 1 h incubation period, PMNs were treated with distilled water and the lysates were plated on LB agar plates and incubated overnight at 37 °C. Then, the number of colony forming units was determined and the efficiency of killing was calculated as follows: (number of live *E. coli* cells in control wells – number of live *E. coli* cells in co-cultures) / number of live *E. coli* cells in control wells x 100.

Culturing and FITC labeling of *E. coli* bacteria

E. coli (ATCC 25922) bacteria were grown overnight in LB medium (1% NaCl, 1% tryptone, 0.5% yeast extract). Cells were harvested by centrifugation, washed twice with PBS, counted in a Bürker-chamber and adjusted to the proper concentration used in subsequent experiments. For phagocytosis assay, *E. coli* were heat-killed (15 min, 100 °C), and incubated in hydrogen carbonate buffer (50 mM $NaHCO_3$, 100 mM NaCl) containing 200 μg/ml fluorescein isothiocyanate (FITC). After 1 h incubation, cells were washed extensively with PBS and adjusted to the proper concentration used in subsequent experiments.

Isolation of peritoneal macrophages and phagocytosis assay

Mouse peritoneal macrophages were obtained by lavage [8] and plated in 24-well ($8x10^5$ cells/well) flat-bottomed plates in DMEM supplemented with 10% heat-inactivated fetal bovine serum and 1% 100x penicillin-streptomycin solution. Macrophages were allowed to attach for 2 h, and their medium was replaced therafter.

Macrophages were co-cultured with the FITC-labeled *E. coli* at a ratio of 1:5 for 1 h to allow phagocytosis. After the incubation period, the cell culture medium was removed, and macrophages were washed gently with PBS. Subsequently, 500 µl TrypLE™ Express solution was added to the cultures and incubated for 45 min at 37 °C in order to detach cells from the bottom of cell culture plates. Macrophages were then gently resuspended to a single cell suspension by pipetting, harvested by centrifugation, resuspended in 400 µl PBS and measured on a FACSCalibur instrument (BD Biosciences, San Jose, CA, USA). Experiments were performed in triplicate. Data were analysed using the FlowJo software.

Intravital video microscopy and data analysis

A separate experimental series was performed to assess the possible consequences of secretin treatment on the microcirculation of the pancreas in mice anaesthetized with 1.5 g/kg urethane i.p. (n=3-4 in each group). Using an operating microscope, the right jugular vein was cannulated (with polyethylene tubing ID: 0.28 mm, OD: 0.61 mm, Smiths Medical International Ltd, Kent, UK) for i.v. administration of secretin and the fluorescence marker used for the intravital microscopic examination. The animals were placed in a supine position on a heating pad to maintain the body temperature between 36 and 37 ^{o}C, and a midline laparotomy performed. The majority of the intestines were exteriorized to gain good assess to the pancreas which was carefully placed on a specially designed stage and covered with a microscopic cover slip. The rest of the exteriorized abdominal organs were also covered with Saran wrap to minimize the fluid and heat loss.

The microcirculation of the pancreas was visualized by intravital fluorescence microscopy (Zeiss Axiotech Vario 100HD microscope, 100 W HBO mercury lamp, Acroplan 20x water immersion objective) using a single i.v. bolus of fluorescein isothiocyanate-labeled dextran (150 kDa; 75 µl/animal for plasma labeling). The

microscopic images were recorded with a charge-coupled device video camera (AVT HORN-BC 12; Aalen, Germany) attached to an S-VHS video recorder (Panasonic AG-MD 830, Budapest, Hungary) and a personal computer. Video images of the microcirculatory network of the pancreatic tail were recorded at baseline and 20 min after the i.v. application of secretin.

Plasma velocity in the pancreatic capillaries was assessed off-line by frame-to-frame analysis of the videotaped images, using image analysis software (IVM, Pictron Ltd., Budapest, Hungary). Average velocity values were measured in 3-5 separate capillaries per 3-5 microscopic fields in each animal.

Sodium-taurocholate-induced pancreatitis

Na-taurocholate was administered intraductally as described previously by Perides et al [9]. Briefly, anesthesia was achieved with a 125 mg/kg ketamine and 12.5 mg/kg xylazine cocktail. After median laparotomy, the duodenum was punctured with a 0.4mm diameter needle connected to polyethylene tubing. Leakage of Na-taurocholate was prevented by temporary ligature of the biliopancreatic duct, while the proximal bile duct was temporarily occluded with a microvessel clip. 4% Na-taurocholate or PS solution was infused with an infusion pump (10 µl/min) (TSE System GmbH, Bad Homburg, Germany) for 5 min. After the infusion, the microvessel clip, the injection needle, as well as the distal ligature were removed, and the abdominal wall and the skin were closed separately. Mice were sacrificed 24h later.

Sacrifice of animals, sample processing

Mice were anesthetized with pentobarbital (85 mg/kg i.p.). The animals were exsanguinated through the inferior vena cava and the pancreas was quickly removed,

cleaned from fat and lymph nodes and frozen in liquid nitrogen and stored at -80 °C until use for assays or put into 6% neutral formaldehyde solution for histologic examinations. In case of taurocholate-induced pancreatitis, the pancreas was removed with attached duodenum and spleen for histologic examinations. Only the pancreatic head was used for laboratory measurements. The pancreatic head (defined as the portion of the pancreas located within 5 mm of the lesser duodenal curvature) was separated from the pancreatic body/tail regions.

The pancreas fixed in 6% neutral formaldehyde solution was subsequently embedded in paraffin. Sections were cut at 4μm thickness and stained with hematoxylin and eosin. The slides were coded and read by two independent observers who were blind to the experimental protocol. In case of taurocholate-induced pancreatitis only the pancreatic head (defined as the portion of the pancreas located within ~5 mm of the lesser duodenal curvature) was investigated. The observers investigated 4-6 low-power fields in the head of the pancreas.

SUPPLEMENTARY FIGURES

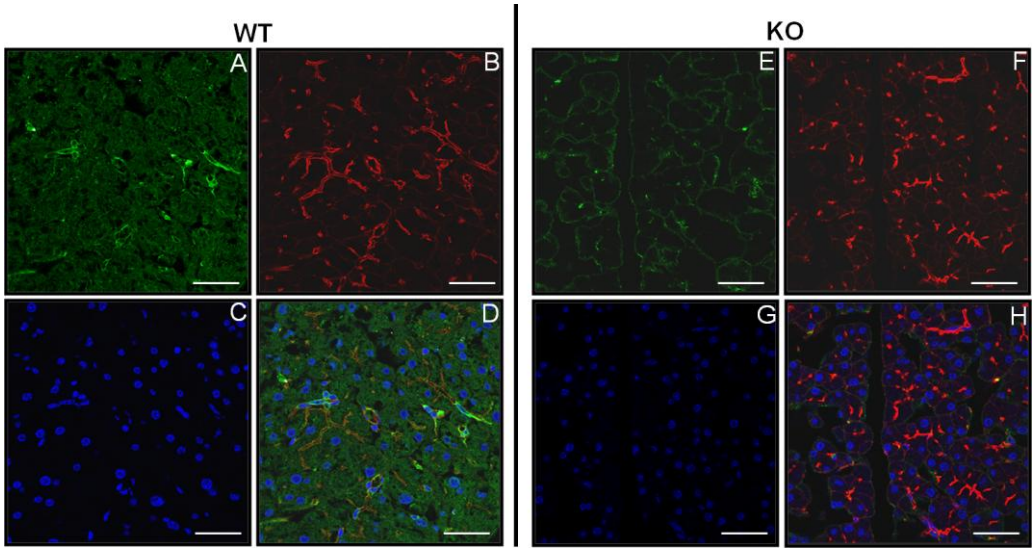

Supplementary figure 1. Specificity of Mr Pink rabbit polyclonal CFTR antibody tested in the pancreas of CFTR-knock-out mouse. Representative immunohistochemical stainings in the pancreas of WT (**A-D**) and CFTR-KO (**E-H**) mice. KO mice showed no apical-specific staining of CFTR (green) in the KO (**E**) vs. the WT (**A**) tissue. Red color indicates the staining of F-actin (**B, F**). The nuclei are stained with DAPI (blue) (**C, G**). **D** and **H** show merged images of CFTR, F-actin and nucleus. Scale bar=50 μm.

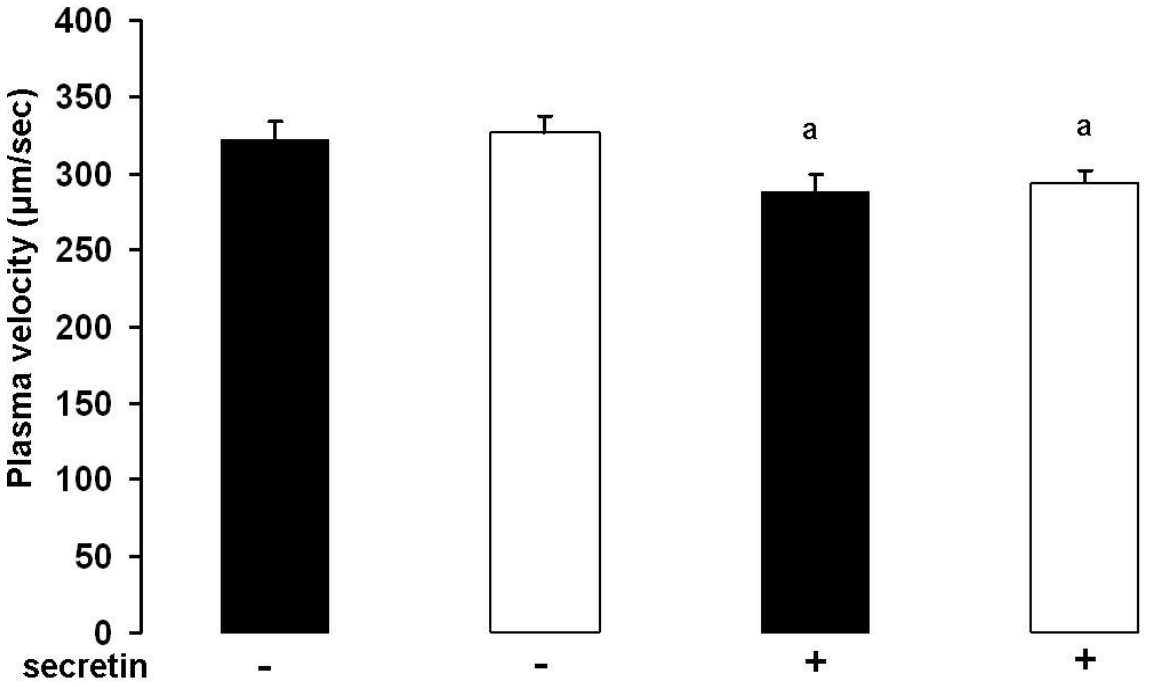

Supplementary figure 2. Pancreatic microcirculation shows similar changes in wild-type and NHERF-1-knock-out mice. The microcirculation of the pancreatic tail was visualized by intravital fluorescence microscopy (see supplementary methods) using a single i.v. bolus of fluorescein isothiocyanate-labelled dextran for plasma labeling in wild-type (closed columns) or NHERF-1-KO (open columns) mice anesthetized with urethane (1.5 g/kg i.p.). Video images were recorded at baseline (secretin -) and 20 min after the i.v. administration of secretin (0.75 CU/kg, secretin +). 20min after the i.v. injection of secretin, significantly lower plasma velocity values were observed in both experimental groups. These reduced microcirculatory velocities, however, were not due to the effect of secretin, but most likely resulted from the 20-min exteriorization period of the pancreas, since a similar degree of reduction (by about 10%) in plasma velocities was also observed in time-matched pilot studies where mice were treated with PS vehicle (data not shown). a: $P<0.05$ vs. the respective secretin – group.

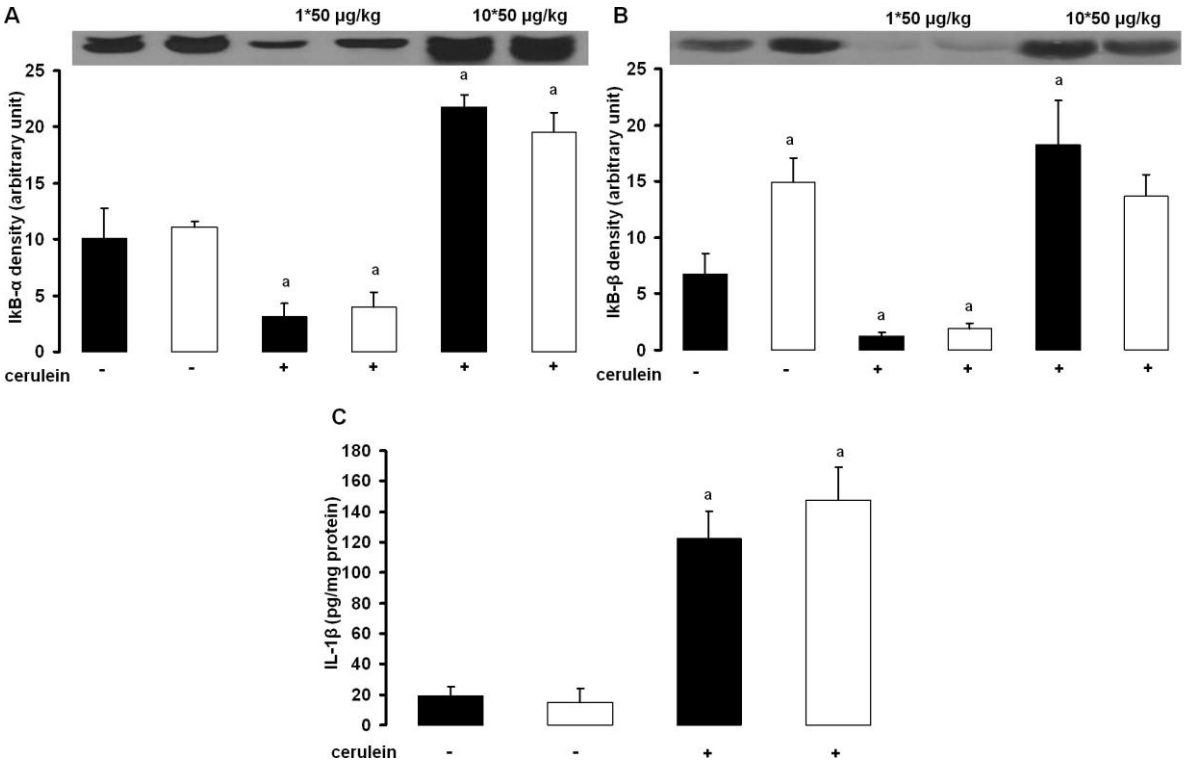

Supplementary figure 3. Effects of cerulein administration on pancreatic IκB-α, IκB-β, interleukin-1β in wild-type and NHERF-1-knock-out mice. Acute pancreatitis was induced by administering 1x50 µg/kg (for measurements of pancreatic IκB-α, IκB-β levels) or 10 hourly (**A-C**) i.p. injection of 50 µg/kg cerulein (cerulein+) in WT (closed columns) and NHERF-1-KO (open columns) mice. Control animals were given PS (cerulein-) instead of cerulein. Mice were sacrificed by exsanguination through the inferior vena cava 0.5h (in case of administration of 1x50 µg/kg cerulein) or 12 h after the first i.p. injection. The bar diagrams and the representative Western immunoblot analysis (**A, B**) of protein lysates (40 µg/lane) from the pancreas of mice, showing the expression of IκB-α (**A**) and IκB-β (**B**). Equal loading/transfer of proteins was checked by Ponceau S staining of the nitrocellulose membrane. IL-1β expression (**C**) was determined from the pancreatic homogenates by ELISA. Means ± SEM for 4-6 animals are shown. $P<0.05$ vs. a: the respective control group or b: vs. the WT cerulein+ group. N.D.: not detected.

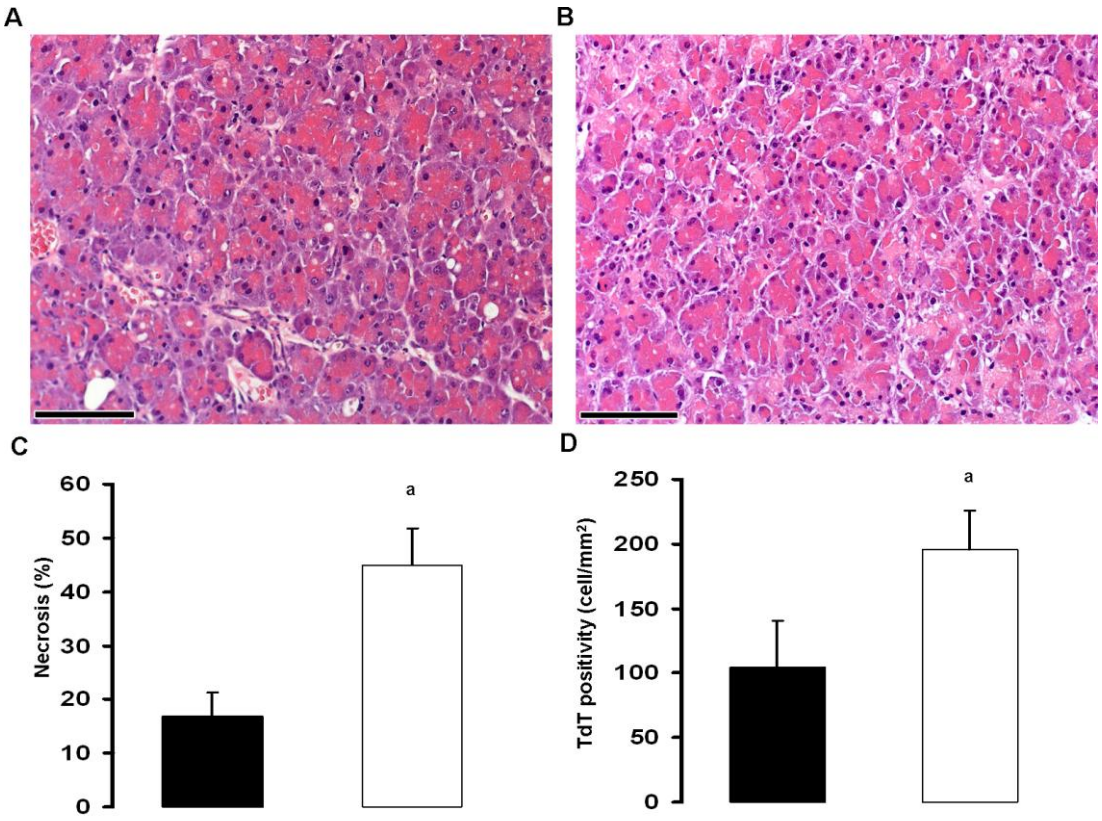

Supplementary figure 4. Histopathologic changes of the pancreas in response to intraperitoneal administration of cerulein in wild-type and NHERF-1-knock-out mice. Acute pancreatitis was induced in WT (closed columns) and NHERF-1-KO (open columns) mice by administering 7 hourly i.p. injections of cerulein (50 μg/kg per injection). The mice were sacrificed by exsanguination through the inferior vena cava 12 h after the first i.p. injection. The diagrams show representative light micrographs (hematoxylin and eosin staining) of the pancreata of cerulein-treated WT (**A**) and NHERF-1-KO (**B**) mice. The bar diagrams show the rates of pancreatic necrosis (**C**) (n=8) and apoptosis (**D**) (n=4). Data are shown as means ± SEM. a: $P<0.05$ vs. the WT group. Scale bar=100 μm.

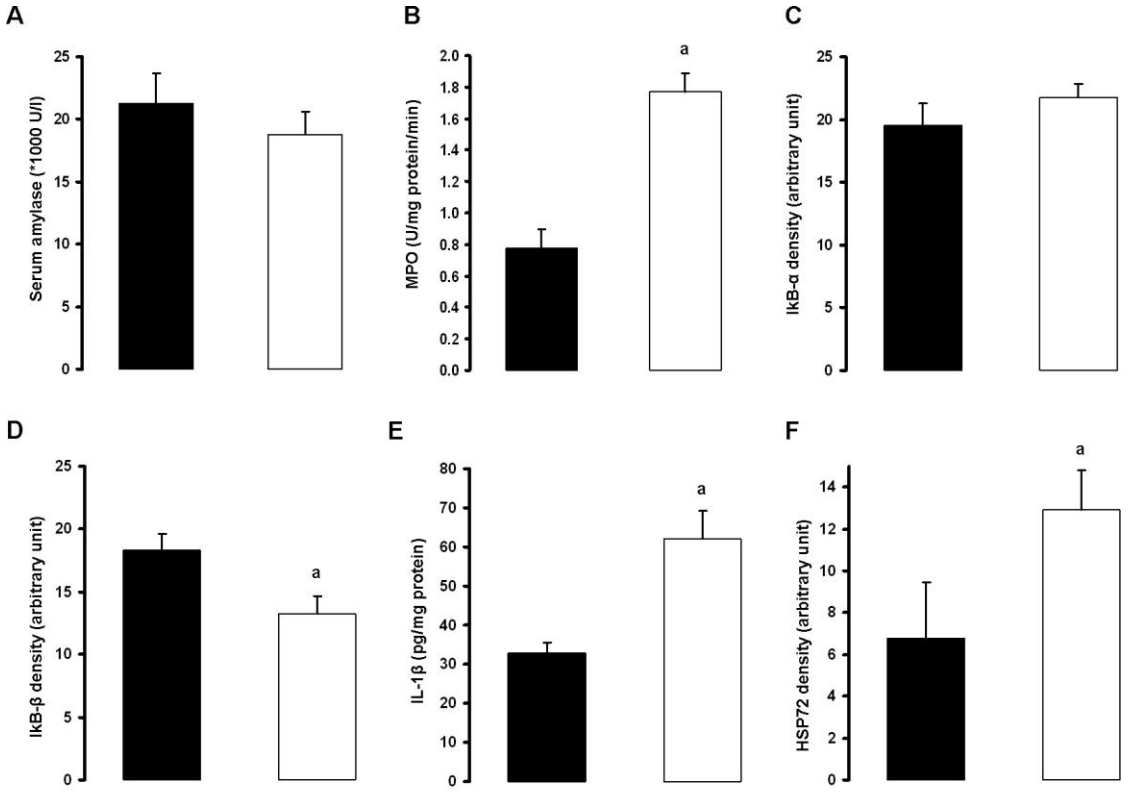

Supplementary figure 5. Severity of cerulein-induced acute pancreatitis in wild-type and NHERF-1-knock-out mice. Acute pancreatitis was induced in WT (closed columns) and NHERF-1-KO (open columns) mice by administering 7 hourly i.p. injections of 50 μg/kg cerulein. The mice were sacrificed by exsanguination through the inferior vena cava 12 h after the first i.p. injection. There was no significant difference in serum amylase activity of WT and NHERF-1-KO mice (**A**). Pancreatic MPO activity was significantly increased in NHERF-1-KO vs. WT mice (**B**). No significant difference was detected between WT and NHERF-1-KO mice in expression of pancreatic IκB-α (**C**). The expression of pancreatic IκB-β was significantly lower in NHERF-1-KO vs. WT mice (**D**). The expression of pancreatic IL-1β (**E**) and HSP72 (**F**) were significantly higher in NHERF-1-KO vs. WT animals. Data are shown as means ± SEM, n=4-6. a: $P<0.05$ vs. the respective control group.

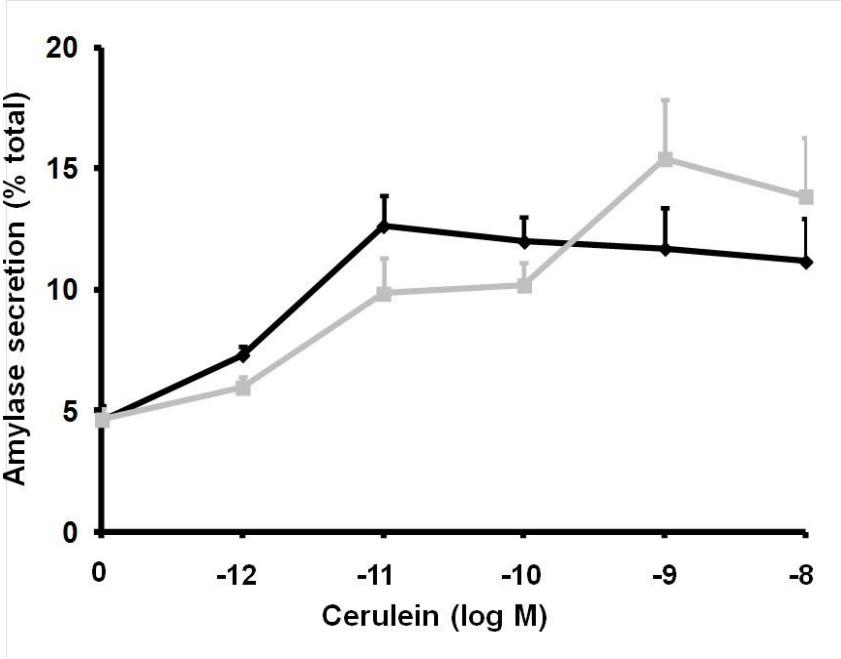

Supplementary figure 6. Acinar sensitivity to cerulein is unaltered by NHERF-1 expression. To determine the sensitivity of dispersed acinar cells (see supplementary methods) of WT (black line) and NHERF-1-KO (grey line) mice to cerulein, amylase secretion was determined in response to various concentrations (10^{-12}-10^{-8} M) of cerulein for 30 min. Amylase secretion was calculated as the percent of total release (medium/medium+cells). a: $P<0.05$ vs. 0 M cerulein, n=4-6 animals.

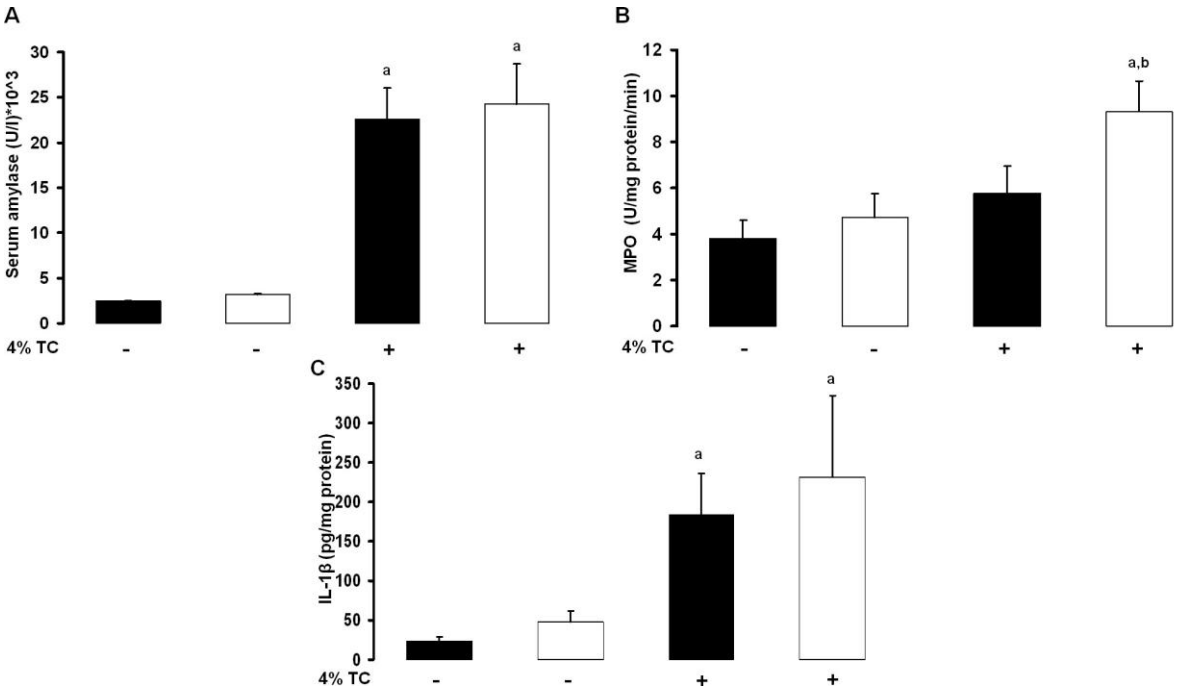

Supplementary figure 7. Severity of sodium-taurocholate-induced acute pancreatitis in wild-type and NHERF-1-knock-out mice. WT and NHERF-1-KO mice were treated as described in Figure 8. The mice were sacrificed by exsanguination through the inferior vena cava 24 h after the infusion. There were no significant differences in serum amylase (**A**) and pancreatic MPO (**B**) activities between Na^+-taurocholate-treated WT (closed columns) and NHERF-1-KO (open columns) mice. There was no significant difference in the levels of pancreatic IL-1β (**C**) of Na^+-taurocholate-treated WT and NHERF-1-KO mice. Data are shown as means ± SEM, n=4-6. $P<0.05$ vs. a: the respective control group or b: vs. the WT 4% TC+ group.

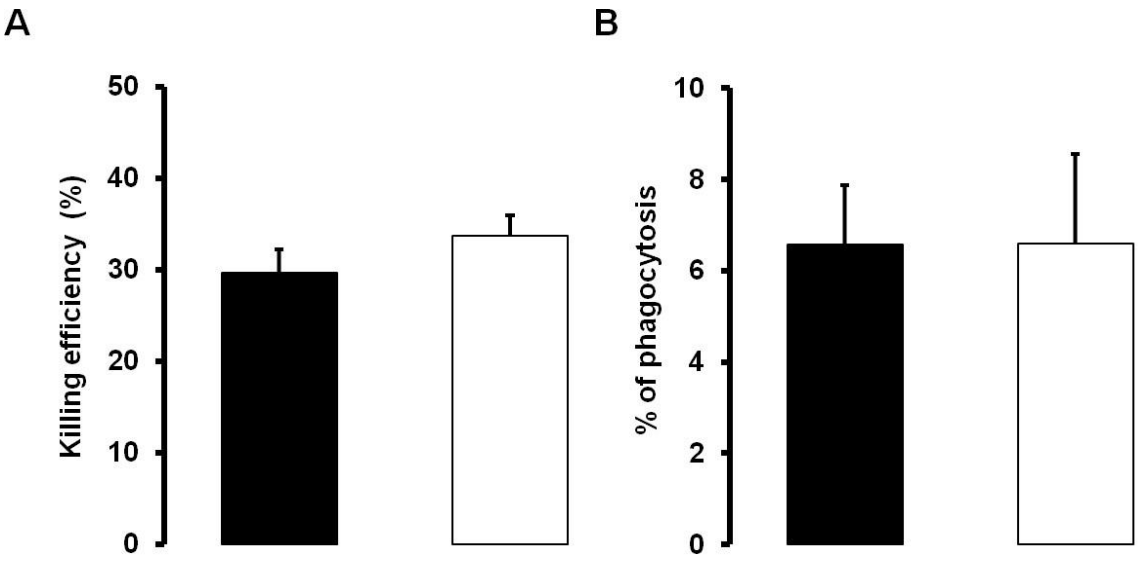

Supplementary figure 8. Functions of inflammatory cells are unaltered by deletion of NHERF-1. Blood polymorphonuclear cells and peritoneal macrophages were isolated from WT and NHERF-1-KO mice. (**A**) Bacterial killing efficiency of polymorphonuclear cells (PMNs) after a 1 h incubation period with *E. coli* was deduced from the number of colony forming units from control wells (without PMNs) and co-cultured wells (containing PMNs). (**B**) Phagocytosis by macrophages was determined on FITC-labeled, heat-killed *E. coli*. Data are shown as means ± SEM. WT (closed columns), NHERF-1-KO (open columns).

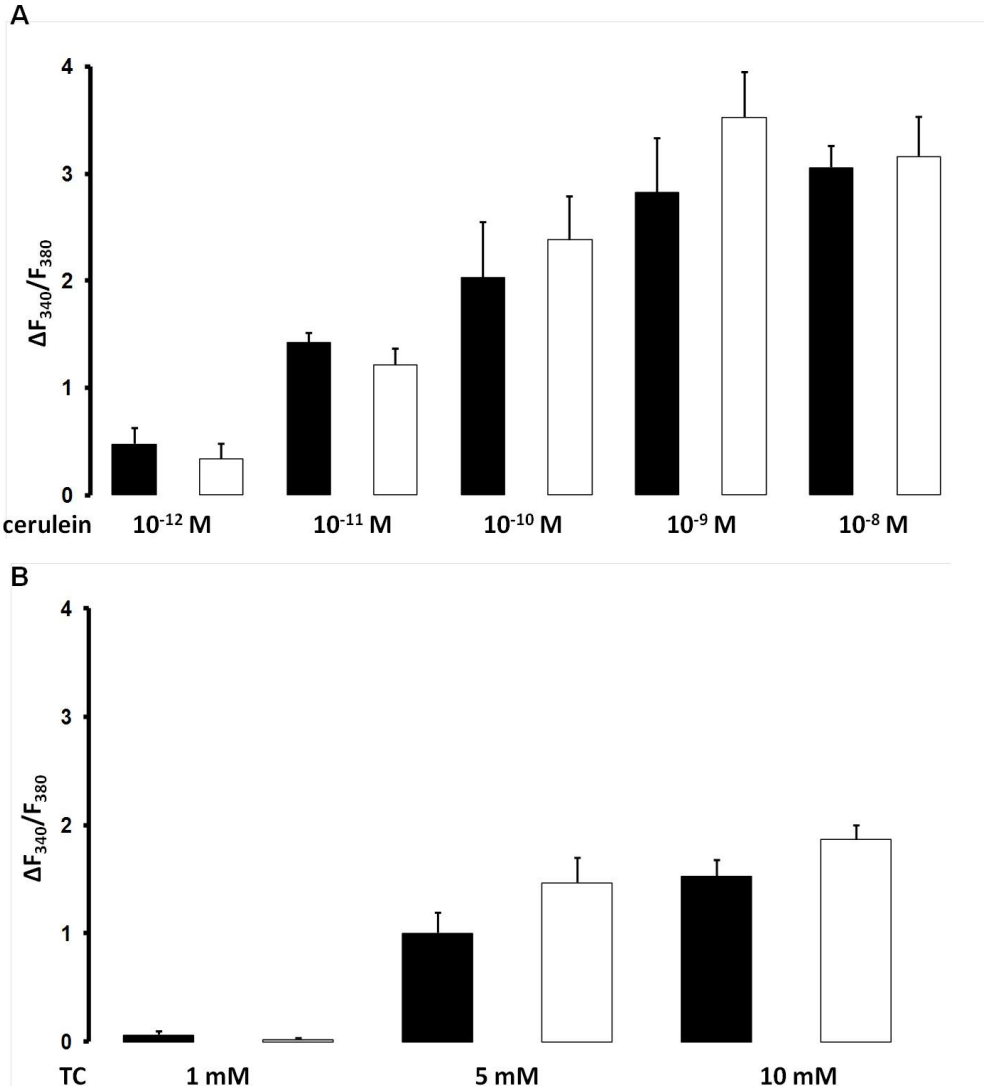

Supplementary figure 9. NHERF-1 expression does not influence the changes in intracellular Ca^{2+} concentration caused by cerulein or sodium-taurocholate in isolated acinar cells. Acinar cells were isolated from WT and NHERF-1-KO mice by collagenase digestion. Summary data show the maximal changes of $[Ca^{2+}]_i$ induced by administration of cerulein or Na^+-taurocholate (TC). There were no significant differences between WT and NHERF-1 KO mice in the changes of $[Ca^{2+}]_i$ on isolated acinar cell in response to different concentrations of cerulein (10^{-8}-10^{-12} M) (**A**) or TC (1-10 mM) (**B**). Data are shown as means ± SEM, n=5-8. WT (closed columns), NHERF-1-KO (open columns).

SUPPLEMENTARY REFERENCES

1. Alvarez BV, Kieller DM, Quon AL, Markovich D, Casey JR: Slc26a6: a cardiac chloride-hydroxyl exchanger and predominant chloride-bicarbonate exchanger of the mouse heart. *J Physiol* 2004, 561:721-734.
2. Hillesheim J, Riederer B, Tuo B, Chen M, Manns M, Biber J, Yun C, Kocher O, Seidler U: Down regulation of small intestinal ion transport in PDZK1-(CAP70/NHERF3) deficient mice. *Pflugers Arch* 2007, 454(4):575-586.
3. Giulietti A, Overbergh L, Valckx D, Decallonne B, Bouillon R, Mathieu C: An overview of real-time quantitative PCR: applications to quantify cytokine gene expression. *Methods* 2001, 25(4):386-401.
4. Weinman EJ, Steplock D, Tate K, Hall RA, Spurney RF, Shenolikar S: Structure-function of recombinant Na/H exchanger regulatory factor (NHE-RF). *J Clin Invest* 1998, 101(10):2199-2206.
5. Hegyi P, Rakonczay Z, Jr., Tiszlavicz L, Varró A, Tóth A, Rácz G, Varga G, Gray MA, Argent BE: Protein kinase C mediates the inhibitory effect of substance P on HCO_3^- secretion from guinea pig pancreatic ducts. *Am J Physiol Cell Physiol* 2005, 288(5):C1030-1041.
6. Fernandez-Salazar MP, Pascua P, Calvo JJ, Lopez MA, Case RM, Steward MC, San Roman JI: Basolateral anion transport mechanisms underlying fluid secretion by mouse, rat and guinea-pig pancreatic ducts. *J Physiol* 2004, 556(Pt 2):415-428.
7. Pandol SJ, Jensen RT, Gardner JD: Mechanism of [Tyr4]bombesin-induced desensitization in dispersed acini from guinea pig pancreas. *J Biol Chem* 1982, 257(20):12024-12029.
8. Zhang X, Goncalves R, Mosser DM: The isolation and characterization of murine macrophages. *Current protocols in immunology / edited by John E Coligan [et al]* 2008, Chapter 14:Unit 14 11.
9. Perides G, van Acker GJ, Laukkarinen JM, Steer ML: Experimental acute biliary pancreatitis induced by retrograde infusion of bile acids into the mouse pancreatic duct. *Nat Protoc* 2010, 5(2):335-341.